

A New Spatio-Temporal Model Exploiting Hamiltonian Equations

¹, Satyaki Mazumder^{*1}, Sayantan Banerjee², and Sourabh Bhattacharya³

¹DMS, IISER Kolkata, Mohanpur

²Operations Management & Quantitative Techniques Area, IIM Indore

³Interdisciplinary Statistical Research Unit, ISI Kolkata

Abstract

The solutions of Hamiltonian equations are known to describe the underlying phase space of a mechanical system. In this article, we propose a novel spatio-temporal model using a strategic modification of the Hamiltonian equations, incorporating appropriate stochasticity via Gaussian processes. The resultant spatio-temporal process, continuously varying with time, turns out to be nonparametric, non-stationary, non-separable, and non-Gaussian. Additionally, the lagged correlations converge to zero as the spatio-temporal lag goes to infinity. We investigate the theoretical properties of the new spatio-temporal process, including its continuity and smoothness properties. We derive methods for complete Bayesian inference using MCMC techniques in the Bayesian paradigm. The performance of our method has been compared with that of a non-stationary Gaussian process (GP) using two simulation studies, where our method shows a significant improvement over the non-stationary GP. Further, applying our new model to two real data sets revealed encouraging performance.

Keywords: Continuously varying time and space, Hamiltonian dynamics, Markov Chain Monte Carlo, Non-stationarity, Non-Gaussianity, Spatio-temporal modeling

Contents

1	Introduction	4
2	Modified Hamiltonian equations and the proposed model	6
2.1	Modification, the new leap-frog algorithm and the proposed model	7
2.2	Remaining specification and analysis of the proposed model	8
2.3	Connection to traditional Hamiltonian systems with Gaussian Process potentials	10
2.4	Connection to Modified Parameterized Leapfrog HMC	11
3	Calculation of likelihood functions	11
3.1	Joint conditional density of the observed data	12
3.2	Joint conditional density of latent data	12
3.3	Complete likelihood combining observed and latent data	13

*email: satyaki@iiserkol.ac.in

4	Prior distributions	13
5	Full conditional distributions	14
6	Simulation studies	15
6.1	Mixture of three Gaussian Processes	16
6.1.1	Data generation	16
6.1.2	Results from our model	17
6.2	Comparative study with nonstationary GP model	18
6.3	Mixture of two GQNs	19
6.3.1	Data generation	19
6.3.2	Results from our model	19
6.3.3	Comparative study with non-stationary GP model	20
7	Real data analyses	21
7.1	Alaska temperature data	21
7.1.1	Prior choices for the Alaska temperature data	22
7.1.2	Results of the Alaska temperature data	23
7.2	Sea surface temperature data	24
7.2.1	Prior choices for sea surface temperature data	27
7.2.2	Controlling M_s	27
7.2.3	Results of the sea surface temperature data	28
8	Summary and conclusion	30
A	Derivation of equations 3 and 4	31
B	Correlation analysis of GQN model	32
C	Spatial correlation plots	32
D	Proofs of our results	36
E	Calculation of joint conditional density of the observed data	46
F	Calculation of the conditional joint density of latent data	47
G	Calculation of full conditional distributions of the parameters and the latent variables, given the observed data	48
G.1	Full conditional distribution of β_*	48
G.2	Full conditional distribution of α_*	48
G.3	Full conditional distribution of σ_θ^2	48
G.4	Full conditional distribution of σ_p^2	49
G.5	Full conditional distribution of σ^2	49
G.6	Full conditional distributions of η_1^* , η_2^* , and η_3^*	49
G.7	Full conditional distribution of \mathbf{x}_0	50
H	Algorithm for temporal prediction	50

- I Algorithm for prediction of time series at a spatial point** **51**
- J Modification for irregularly spaced data** **52**
- K Supplementary plots for 3 component mixture of GPs** **53**
 - K.1 Trace plots 53
 - K.2 Posterior densities of the complete time series of latent variables 54
- L Supplementary plots for mixture of GQNs** **55**
 - L.1 Trace plots 55
 - L.2 Posterior densities of the complete time series of the latent variables 56
- M Supplementary plots for Alaska temperature data** **57**
 - M.1 Trace plots 57
- N Supplementary plots for sea temperature data** **58**
 - N.1 Trace plots 58
- O Stationarity, convergence of lagged correlations to zero and non-Gaussianity of the detrended Alaska data process** **59**
 - O.1 Stationarity of the detrended Alaska data process 59
 - O.2 Convergence of lagged spatio-temporal correlations to zero for the Alaska data 59
 - O.3 Non-Gaussianity of the Alaska data 61

1 Introduction

The modeling of spatial and spatio-temporal data has gained significant attention in the statistics community over the past few decades. Various scientific fields, including meteorology, environmental science, and ecology, generate spatio-temporal data, necessitating robust analytical methods. Significant research has been carried out on spatial modeling, with a particular focus on hierarchical Bayesian methods for climate applications (e.g., Jun et al. [2008], Furrer and Sain [2009], Tebaldi and Sansó [2009], Sain et al. [2011]). Results of different climate models concerning the increase in temperature for 22 different regions have been combined by Smith et al. [2009] using Bayesian methods, and Sang et al. [2011] built a hierarchical statistical model to integrate multiple climate errors. Numerous spatio-temporal models are available for analyzing climate data. To provide a few examples, spatio-temporal models aiming at analyzing rainfall data have been proposed by Cox and Isham [1988], Sanso and Guenni [1999], and Sahu et al. [2010] proposed a hierarchical Bayesian space-time model for wet deposition analysis.

Extensive research has applied spatial and spatio-temporal models to the analysis of environmental data, including ozone, particulate matter, sulfur dioxide, and nitrogen oxide. Notable works include Guttorp et al. [1994] on ground-level ozone, Huerta et al. [2004] on ozone concentration in Mexico City. Bruno et al. [2009] worked on a non-stationary, non-separable model for ozone data analysis. Dou et al. [2010] compared two models for hourly ozone concentration, while Paciorek et al. [2009] contributed fundamentally to particulate matter analysis using a spatio-temporal model. Studies on sulfur dioxide concentration include Holland et al. [2000] and Giannitrapani et al. [2006]. Modeling of nitrogen oxide concentration has been explored by Beelen et al. [2013] and Amini et al. [2016], among others. Beyond air pollution, Deng et al. [2009] and Chakraborty et al. [2010] applied spatio-temporal models to ecological data. These references represent only a fraction of the extensive work in this field.

Spatio-temporal data analysis often relies on two key assumptions: (i) separability of the covariance function in space and time (see Chapter 11 of Banerjee et al. [2014]) and (ii) covariance stationarity, meaning the covariance between two observations depends on their separation vector in space and time (Chapters 2 and 11 of Banerjee et al. [2014]). A common special case, isotropic stationarity, assumes covariance is solely a function of the distance between locations and time points. However, stationarity assumptions can be artificial when local influences affect the correlation structure Sampson and Guttorp [1992]. Studies have shown nonstationarity in PM10 pollution Paciorek et al. [2009], Das and Bhattacharya [2023], Roy and Bhattacharya [2020] and sea temperature data Bhattacharya [2021]. Furthermore, Paciorek [2003] showed that assuming stationarity can lead to over- or under-smoothing. For a review on the importance of nonstationary modeling in spatio-temporal data, see Chapter 9 of Gelfand et al. [2010].

Recent efforts to incorporate nonstationarity in spatio-temporal processes have explored various approaches. Sampson and Guttorp [1992] introduced spatial deformation to model nonstationary covariance, later extended in Bayesian frameworks Damian et al. [2001], Schmidt and O'Hagan [2003]. Kernel convolution techniques were employed by Higdon [1998], Higdon et al. [1999], Fuentes and Smith [2001], Higdon [2002], Fuentes [2002], Paciorek and Schervish [2006] to model nonstationarity, while Wikle and Hooten [2010] developed a general nonlinear, non-stationary but parametric hierarchical Bayesian model with an application to ecological and oceanographic data. The stochastic partial differential equation (SPDE) approach, first proposed by Lindgren et al. [2011], represents Gaussian fields (GF) as Gaussian Markov random fields (GMRF), a discretely indexed spatial random field. The key ingredient was to use the fact that a GF with Matérn covariance kernel is the solution of a fractional SPDE (Chapter 6 of Blangiardo and Cameletti [2015]). In the SPDE framework, non-stationary covariance is modeled by varying Matérn kernel parameters with respect to location Lindgren et al. [2011], Bolin and Lindgren [2011], Ingebrigtsen et al. [2014], Blangiardo and Cameletti [2015]. A review of the SPDE approach for spatial and spatio-temporal modeling can be found in Lindgren et al. [2022]. A major advantage of SPDE is its implementation in R via

the INLA package Lindgren and Rue [2015], which efficiently handles large datasets using sparse matrices Blangiardo and Cameletti [2015], Gómez-Rubio [2020]. Also see the website r-inla.org/home for further details on INLA. Alternative nonstationary models include a Dirichlet process-based Bayesian approach for conditional nonstationarity Gelfand et al. [2005], a kernel process mixing method Fuentes and Reich [2013], and a discretized stochastic differential equation model Duan et al. [2009]. More recently, Driver and Voelkle [2018] proposed a hierarchical Bayesian method for dynamic parametric models via stochastic differential equations.

In the above-mentioned works, the following aspects can be noticed. The underlying process is Gaussian (may be non-stationary) or parametric, or the correlation between the two spatio-temporal points does not converge to zero as the distance between the two points (locations and/or time points) increases to infinity or both. For example, our simulation from the general quadratic nonlinear model Wikle and Hooten [2010] reveals that the correlation does not vanish as the distance increases indefinitely (see Figures 10 and 11 in Appendix B). Moreover, spatio-temporal data may not always be Gaussian Fuentes and Reich [2013], Das and Bhattacharya [2023], Bhattacharya [2021]. Furthermore, in many real-life cases, sample correlation often approaches zero with increasing spatial or temporal distance Bhattacharya [2021], a property naturally following from the covariance structure of ergodic stationary processes but not necessarily for non-stationary ones. Thus, when modeling non-stationary spatio-temporal processes, ensuring correlation convergence to zero at large distances is crucial.

Recently, Das and Bhattacharya [2023] proposed a nonparametric, non-separable, non-stationary, and non-Gaussian spatio-temporal model based on an order-based dependent Dirichlet process, ensuring the covariance function converges to zero as spatial or temporal distance increases. Their model assumes continuous variation in time and space. However, while achieving desirable covariance properties, it lacks dynamic temporal evolution, a crucial aspect of modeling temporal variability (Chapter 1 of Cressie and Wikle [2015]). In contrast, Guha [2017] introduced a nonparametric non-stationary spatio-temporal model that incorporates a dynamic latent process to induce temporal dynamics. However, in their model time does not vary continually.

In summary, no existing model meets all the criteria of being nonparametric, non-stationary, non-separable, non-Gaussian, and dynamic, while ensuring continuity in time and space, incorporating a structured latent process, and guaranteeing correlation decay to zero at infinite spatial/temporal lags. To address this gap, we propose a dynamic, nonparametric, non-Gaussian spatio-temporal model with a non-stationary underlying process. Our model integrates a structured latent process, allows continuous variation in time and space, and ensures convergence of covariance to zero at large spatial/temporal distances.

We construct our model using Hamiltonian dynamics, a concept from physics also applied in Bayesian statistics for Hamiltonian Monte Carlo Betancourt [2017], Cheung and Beck [2009]. The solutions of Hamiltonian equations define a mechanical system’s phase-space and vary continuously over time, motivating their use in our spatio-temporal model. While deterministic Hamiltonian equations have been generalized to stochastic forms, ordinary or partial (Lázaro-Camí and Ortega [2007], Hong et al. [2022] and references therein), no temporal or spatio-temporal modeling has been attempted. These equations remain parametric, assuming known functional forms. Typically, a Brownian motion is added to deterministic equations to create stochastic Hamiltonian differential equations and partial differential equations are generalizations of the stochastic Hamiltonian ordinary differential equations. Since it is difficult to see how these stochastic equations with deterministic functional forms and (finite or infinite-dimensional) Brownian motions may be useful for constructing realistic temporal or spatio-temporal models with desirable properties, we do not pursue these in this work.

The use of Hamiltonian dynamics with the leap-frog algorithm Young [2014] in spatio-temporal modeling has not been explored earlier. Adaptation and exploitation of the leap-frog algorithm with appropriate choice of Gaussian process priors make the proposed model non-parametric. Specifically, we propose a

modified leap-frog algorithm alongside modified Hamiltonian equations to construct a spatio-temporal model incorporating latent and observed processes that continuously depend on time t . Since the leap-frog algorithm leverages derivatives, our model exhibits dynamic behavior through dependence on the previous time point $t - \delta t$. The Bayesian nonparametric nature arises from modeling unknown functions in Hamiltonian equations via Gaussian processes, *ensuring non-stationarity, non-separability, and non-Gaussianity*. Further analysis confirms that the covariance function converges to zero at large spatial/temporal lags. Additionally, under regularity conditions, we establish that the proposed process has continuous paths in both almost sure and mean square senses, along with almost sure and mean square differentiability. Moreover, we prove a lemma providing sufficient conditions for the mean square differentiability of a composition of a random spatial process and a Gaussian spatial process, a result of independent significance.

The article is structured as follows: Section 2 introduces a new spatio-temporal process using modified Hamiltonian equations and a leap-frog algorithm, along with key properties of the observed and latent processes. Proofs of related lemmas, theorems, and corollaries are in Appendix D. Section 3 derives the likelihood function, first obtaining the joint conditional density of data given latent variables and parameters (Subsection 3.1, Appendix E), followed by the joint density of latent variables (Subsection 3.2, Appendix F), and then the complete likelihood (Subsection 3.3). Section 4 discusses prior distributions and their justification. Section 5 derives full conditional densities for Gibbs sampling, with detailed calculations in Appendix G. Section 6 presents two simulation studies comparing our model with a non-stationary Gaussian process fitted using the SPDE approach Lindgren et al. [2011], Lindgren and Rue [2015]. Section 7 analyzes two real datasets—one non-stationary and non-Gaussian, the other stationary and non-Gaussian, to evaluate model performance. Finally, Section 8 summarizes contributions and concludes the study.

2 Modified Hamiltonian equations and the proposed model

We begin with a brief overview of Hamiltonian dynamics and its equations before linking them to our proposed spatio-temporal model. Let $(\mathcal{M}, \mathcal{L})$ be a mechanical system, where \mathcal{M} is the configuration space and \mathcal{L} is the smooth Lagrangian. The coordinate system of \mathcal{M} is determined by $(\theta, \dot{\theta})$, where θ is the position of a particle at time t and the $\dot{\theta}$ is the derivative vector with respect to time, thus representing the velocity. The partial derivative of \mathcal{L} with respect to $\dot{\theta}$, known as momenta, is denoted by p , which is a function of time t , the position θ , and velocity $\dot{\theta}$. Now the Hamiltonian, a function of p , θ and t , is defined as

$$H(p, \theta, t) = \sum_i p_i \dot{\theta}_i - \mathcal{L}(\theta, \dot{\theta}, t),$$

which is the energy function of the mechanical system. Here p_i and $\dot{\theta}_i$ are the i th component of p and $\dot{\theta}$. The pair (θ, p) corresponds to phase space coordinates. Now assume that $H(p, \theta, t) = V(\theta, t) + W(p, t)$, where $V(\theta, t)$ is the potential energy, $W(p, t)$ is the kinetic energy given as $W(p, t) = p^T M^{-1} p / 2$, with M being a chosen matrix (mass), and (θ, p) are phase space coordinates (depend on time t) Cheung and Beck [2009]. The Hamiltonian equations are given by

$$\frac{d\theta}{dt} = \frac{\partial H}{\partial p} = M^{-1} p, \text{ and } \frac{dp}{dt} = -\frac{\partial H}{\partial \theta} = -\nabla V(\theta),$$

where $\nabla V(\theta)$ represents gradient of V with respect to θ . Thus, the phase-space coordinates satisfy the Hamiltonian equations, where the solution θ , representing a particle's position at time t , depends on p , and varies continuously with time. Similarly, p depends on θ and also evolves continuously over time. To

get the solution (p, θ) numerically, leap-frog algorithm is employed and is given by

$$\begin{aligned}\theta(t + \delta t) &= \theta(t) + \delta t M^{-1} \left[p(t) - \frac{1}{2} \delta t \nabla V(\theta(t)) \right] \text{ and} \\ p(t + \delta t) &= p(t) - \frac{1}{2} \delta t \left[\nabla V(\theta(t)) + \nabla V(\theta(t + \delta t)) \right].\end{aligned}$$

2.1 Modification, the new leap-frog algorithm and the proposed model

We modify the original Hamiltonian equations so that the rate of change of p and θ with respect to t depends on both p and θ . One way to do so is to incorporate p and θ linearly in the equation of $\frac{d\theta}{dt}$ and $\frac{dp}{dt}$, respectively. That is, the Hamiltonian equations are modified to

$$\frac{d\theta}{dt} = \beta^* \theta + M^{-1} p, \text{ and } \frac{dp}{dt} = \alpha^* p - \nabla V(\theta). \quad (1)$$

In our proposal of spatio-temporal process, we introduce $p(\cdot)$ as the latent process, X , say, and $\theta(\cdot)$ as the data-generating spatio-temporal process, Y , say, in equation 1 with the hope that the solution to the modified Hamilton's equations will best describe the underlying state-space as the original Hamiltonian equations model the phase-space of the mechanical space. That is, at every location, say $s \in S$ with S being a non-empty subset of \mathbb{R}^2 containing a rectangle of positive volume, we have

$$\frac{dY(s, t)}{dt} = \beta^* Y(s, t) + M_s^{-1} X(s, t) \text{ and } \frac{dX(s, t)}{dt} = \alpha^* X(s, t) - \nabla V(Y(s, t)), \quad (2)$$

where by $\nabla V(Y(s, t))$ we mean $\left. \frac{d}{dx} V(x) \right|_{x=Y(s, t)}$, and M_s is a constant given a location s , equivalent to the mass in the original Hamiltonian equation. The function $V(\cdot)$ is assumed to be a random function. Stochasticity of $X(\cdot, \cdot)$ depends on the stochasticity of $V(\cdot)$ and stochasticity of $Y(\cdot, \cdot)$ depends on the stochasticity of $X(\cdot, \cdot)$. Therefore, stochasticity of both $Y(\cdot, \cdot)$ and $X(\cdot, \cdot)$, in turn, depend on the stochasticity of $V(\cdot)$.

The reason for choosing p as latent is that we believe that the latent process evolves compositely with respect to a unknown stochastic function; however, the data-generating process is a simple function of the underlying latent process. This philosophy has been followed in other works as well, see for example, Ghosh et al. [2014], Mazumder and Bhattacharya [2016, 2017] and the references therein. the proposed model is obtained by discretizing equations 2 via the Leap-frog algorithm (Hockney 1970, Verlet 1967, Young 2014) as

$$y(s, t + \delta t) = \beta y(s, t) + \delta t M_s^{-1} \left(\alpha x(s, t) - \nabla V(y(s, t)) \frac{\delta t}{2} \right), \text{ and} \quad (3)$$

$$x(s, t + \delta t) = \alpha^2 x(s, t) - \frac{\delta t}{2} \{ \alpha \nabla V(y(s, t)) + \nabla V(y(s, t + \delta t)) \}, \quad (4)$$

where $y(s, t)$ and $x(s, t)$ are realizations of the stochastic processes $\{Y(s, t) : s \in S, t \geq 0\}$ and $\{X(s, t) : s \in S, t \geq 0\}$, respectively. Further, α and β are defined as $\alpha = 1 + \alpha^* \frac{\delta t}{2}$ and $\beta = 1 + \beta^* \frac{\delta t}{2}$, respectively. The derivation of equations (3) and (4) are provided in Appendix A. Here we assume that $y(s, t)$ is the potential observation while $x(s, t)$ is unobserved.

Generally, Hamiltonian equations are numerically handled using Leap-frog algorithm, since it preserves the energy. Energy preservation is also important for ensuring good acceptance rates for HMC [Cheung

and Beck, 2009]. In our case, the new, modified Leap-frog algorithm is not directly related to energy conservation, rather, the use of Leap-frog algorithm leads to mean and covariance non-stationarity of the derived processes (see Section 2.2), which was one of the main goals of our work.

Equation (3) may be regarded as the observation equation while (4) deals with the dynamics of the latent process. The parameters α, β are such that $|\alpha| < 1$ and $|\beta| < 1$. We will see subsequently, the restriction on β is necessary for the lagged correlations between the observations to tend to zero as the space-time lag tends to infinity, and the restriction on α led to good MCMC mixing in our Bayesian applications. Note that equation (4) is not the latent equation *per se*, since it involves the observed variable as well. Integrating the conditional distribution of the latent variable (equation (4)) over the observed variable would give us the latent distribution.

To fully specify our spatio-temporal process, we model the function $V(\cdot)$ as a Gaussian process. Under suitable assumptions, this choice ensures that $V'(\cdot)$ is also Gaussian Stein [1999a], Rasmussen and Williams [2006], allowing the conditional likelihoods to be expressed in closed form (see Section 3). Additionally, specifying the proposed process requires an appropriate form for M_s . The next subsection provides further details on these aspects and explores the theoretical properties of our spatio-temporal processes.

2.2 Remaining specification and analysis of the proposed model

Let $s \in S$, a compact subset of \mathbb{R}^2 , and $\|\cdot\|$ denote the Euclidean norm. We consider the following assumptions on the processes $X(s, 0), Y(s, 0)$, $s \in S$ and the random function $V(\cdot)$.

- A1. $X(s, 0)$ and $Y(s, 0)$, $s \in S$, are assumed to be centered Gaussian processes with symmetric, positive definite covariance functions having bounded partial derivatives. In particular, due to reasons of popularity, the covariance functions for $X(s, 0)$ and $Y(s, 0)$ are taken to be squared exponential of the form $\text{cov}(X(s_1, 0), X(s_2, 0)) = \sigma_p^2 \exp\{-\eta_1 \|s_1 - s_2\|^2\}$ and $\text{cov}(Y(s_1, 0), Y(s_2, 0)) = \sigma_\theta^2 \exp\{-\eta_2 \|s_1 - s_2\|^2\}$, for $s_1, s_2 \in S$, respectively. However, the Matérn covariance function with $\nu > 1$ also has bounded partial derivatives and could be employed.
- A2. The function $V(\cdot)$ is assumed to be a Gaussian random function with zero mean and covariance function $c_v(x_1, x_2) = \sigma^2 \exp\{-\eta_3 \|x_1 - x_2\|^2\}$. Other covariance structures can be considered, provided the covariance function is twice continuously differentiable with Lipschitz continuous mixed partial derivatives. If it has bounded third-order partial derivatives, it is inherently Lipschitz. In our case, the chosen covariance function is infinitely differentiable with bounded derivatives. Alternative choices include the rational quadratic covariance function or the Matérn covariance function with $\nu > 2$, among others.

The above assumptions need well-behaved covariance functions in the sense of smoothness. For a list of such covariance functions, one may see Banerjee et al. [2014]. Smoothness properties along with other important properties of Matérn covariance functions have been covered in Stein [1999b] (Chapter 2).

Remark 1 *Assumption A1 implies that the covariance functions of $X(s, 0)$ and $Y(s, 0)$ are symmetric, positive definite, and Lipschitz continuous, and thus $X(s, 0)$ and $Y(s, 0)$ will have continuous sample paths with probability 1. If the covariance functions are taken to be the Matérn covariance function with $\nu > 1$ or the squared exponential covariance function, then $X(s, 0)$ and $Y(s, 0)$ will have differentiable sample paths in s .*

Remark 2 *Assumption A2 implies that the derivative process of $V(\cdot)$ is also a Gaussian process with continuous sample paths almost surely. If the squared exponential covariance function is used, then all the derivatives of $V(\cdot)$ remain Gaussian processes. In particular, the differential of $V(\cdot)$ will have differentiable*

sample paths. Similarly, for the Matérn covariance function with $\nu > 2$, $V(\cdot)$ is differentiable, and its covariance function corresponds to the mixed partial derivative of the original covariance function. As $\nu > 2$, the differential of $V(\cdot)$ also has differentiable sample paths (see Rasmussen and Williams [2006] and Stein [1999b]).

Now we propose a form of M_s which is continuous and infinitely differentiable when defined on a compact set $S \subset \mathbb{R}^2$.

Definition 1 (Definition of M_s) Let S be a compact subset of \mathbb{R}^2 . Define $M_s = \exp(\max\{\|s^2 - u^2\|^2 : u \in S\})$, where by \mathbf{v}^2 we mean $\mathbf{v}^2 = (v_1^2, v_2^2)^T$, for $\mathbf{v} \in S$.

Remark 3 We observe that with the choice of M_s , for a fixed s' (or for fixed s), as $\|s - s'\| \rightarrow \infty$, $M_s \rightarrow \infty$ (or $M_{s'} \rightarrow \infty$). This is a technical requirement for showing the lagged covariance to go to 0 (Theorem 2.1). Essentially, it means that as the spatial distance increases to infinity, the constant M_s also escapes to infinity. The proof can be argued in the following fashion.

When $\|s - s'\| \rightarrow \infty$, S also grows in the sense $S_1 \subset S_2 \subset \dots$, such that at each stage i , S_i remains compact. Under this limiting situation, $M_s = \exp(\max\{\|s^2 - u^2\|^2 : u \in S\}) \geq \exp(\|s^2 - s'^2\|^2) \rightarrow \infty$ and $M_{s'} = \exp(\max\{\|s'^2 - u^2\|^2 : u \in S\}) \geq \exp(\|s'^2 - s^2\|^2) \rightarrow \infty$.

Further, it can be shown that M_s is infinitely smooth in S . The following lemma proves the claim. We provide the proof in Appendix D.

Lemma 2.1 M_s is infinitely differentiable in $s \in S$.

The next results show that the covariance function of $Y(s, t)$ goes to 0 as the distance between two time points and two spatial locations increases to infinity. The distances between any two time points and any two spatial locations are measured with respect to their corresponding distance metrics.

Theorem 2.1 Under the assumptions A1 and A2, $\text{cov}(Y(s, h\delta t), Y(s', h'\delta t))$ converges to 0, as $\|s - s'\| \rightarrow \infty$ and/or $|h - h'| \rightarrow \infty$.

In Theorem 2.1, δt in $h\delta t$ and $h'\delta t$ make the time points continuous for continuous δt . However, discrete values of δt are also allowed.

Remark 4 The closed form of the covariance function of our proposed process $Y(s, t)$ is unavailable. However, we can argue in the following way that the covariance is non-stationary. Conditional on the latent variables, the covariance depends upon the latent variable. For simplicity, let us assume that the latent process is supported on a compact set. Then, by the mean value theorem for integrals, the unconditional covariance is a function of a specific value of the latent variables. Moreover, the latent variables are almost surely nonlinear in locations and times, implying that the unconditional covariance is a nonlinear function of space and time. Therefore, it must be non-stationary. In this context, it is important to note that even if we assume stationary covariance kernel for $V(\cdot)$, the proposed spatio-temporal process is rendered mean and covariance non-stationary.

To complete the discussion on correlation analysis, we provide an illustration to give us an idea regarding the spatial correlation matrix of our model and how it is different from the squared exponential or Matérn covariance. In particular, this illustration shows that the spatial correlation of the proposed model can be negative, whereas the correlation of squared exponential or Matérn will always be positive. The details of these simulation studies and the correlation plots (Figure 12) are provided in Appendix C.

Next we show that $Y(s, t)$ and $X(s, t)$ are continuous in s with probability 1 and in the mean square sense. Since the (modified) Hamiltonian equations already imply that $Y(s, t)$ and $X(s, t)$ are path-wise differentiable with respect to t , we focus on their smoothness properties with respect to s . The following theorems (except Lemma 2.2) are established under the assumption that A1 and A2 hold.

Theorem 2.2 $Y(s, h\delta t)$ and $X(s, h\delta t)$ are continuous in s , for all $h \geq 1$, with probability 1.

Theorem 2.3 $Y(s, h\delta t)$ and $X(s, h\delta t)$ are continuous in s in the mean square sense, for all $h \geq 1$.

The next two results deal with differentiability of the processes $Y(s, t)$ and $X(s, t)$.

Theorem 2.4 $Y(s, h\delta t)$ and $X(s, h\delta t)$ have differentiable sample paths with respect to s , almost surely.

Remark 5 Theorem 2.4 is about once differentiability, however, it can be extended to k times differentiability depending on the structure of the covariances assumed on the processes $Y(s, 0)$, $X(s, 0)$ and the random function $V(\cdot)$. For example, if we assume squared exponential covariance functions on each process, then $Y(s, h\delta t)$ and $X(s, h\delta t)$ will have k times differentiable sample paths in s , for any $k \in \mathbb{N}$.

To prove that the processes $Y(s, t)$ and $X(s, t)$ are mean square differentiable in s , we need a lemma, stated below, which may be of independent interest.

Lemma 2.2 Let $f : \mathbb{R} \rightarrow \mathbb{R}$ be a zero mean Gaussian random function with covariance function $c_f(x_1, x_2)$, $x_1, x_2 \in \mathbb{R}$, which is four times continuously differentiable. Let $\{Z(s) : s \in S\}$ be a random process with the following properties

1. $E(Z(s)) = 0$,
2. The covariance function $c_Z(s_1, s_2)$, $s_1, s_2 \in S$, where S is a compact subspace of \mathbb{R}^2 , is four times continuously differentiable, and
3. $\frac{\partial Z(s)}{\partial s_i}$ has finite fourth moment.

Then the process $\{g(s) : s \in S\}$, where $g(s) = f(Z(s))$, is mean square differentiable in s .

Theorem 2.5 Let A1 and A2 hold true, with the covariance functions of all the assumed Gaussian processes being squared exponential. Then $Y(s, h\delta t)$ and $X(s, h\delta t)$ are mean square differentiable in s , for every $h \geq 1$.

Therefore, we prove that for our choice of the random function $V(\cdot)$, there exist valid stochastic processes $Y(s, t)$ and $X(s, t)$ with continuity and smoothness properties. It is not difficult to check that the finite dimensional distributions satisfy Kolmogorov's consistency theorem and thus, by Kolmogorov's theorem, there exists a probability measure for our stochastic process. Almost surely all paths of our stochastic processes satisfy the modified Hamiltonian equations.

2.3 Connection to traditional Hamiltonian systems with Gaussian Process potentials

Although (3) and (4) have been proposed as a numerical solution to the equations given by (2), the modified stochastic Hamiltonian system driven by Gaussian process potentials, the mathematical analysis presented in [Bhattacharya, 2026a] revealed a deeper and more fundamental connection: the stochastic parameterized leapfrog scheme actually solves, in an appropriate mean-square sense, the *traditional* Hamiltonian equations with Gaussian process potentials. This mathematical result has significant implications for both the theoretical interpretation and practical application of our method.

From a theoretical perspective, this connection establishes that our parameterized framework does not deviate from the classical Hamiltonian structure that underlies phase-space dynamics in physical systems.

Rather, it represents an enriched version where the deterministic potential energy function is replaced by a Gaussian process potential, introducing stochasticity while preserving the fundamental symplectic geometry. The parameterization through α and β then emerges naturally as a flexible discretization scheme that accommodates this stochastic extension while maintaining numerical stability and convergence properties.

Practically, the Gaussian process potential introduces a remarkable flexibility that aligns with the nonparametric nature of many modern statistical models. Instead of assuming a specific parametric form for the potential energy, the Gaussian process formulation allows adaptation to complex, high-dimensional energy landscapes, making the approach particularly suitable for problems where the target spatio-temporal process exhibits intricate geometry or unknown structure. This nonparametric enhancement, combined with the parameterized discretization, creates a powerful synergy: the Gaussian process handles model complexity while the parameterized leapfrog provides computational control over the integration process.

The convergence analysis in Bhattacharya [2026a] establishes that this hybrid approach maintains $\mathcal{O}(\delta t)$ mean-square convergence, validating its numerical robustness. This theoretical guarantee, coupled with the empirical demonstrations in Sections 6 and 7 position our method not as an arbitrary modification of the standard Hamiltonian system, but as a principled stochastic extension that preserves the Hamiltonian foundation while introducing valuable flexibility for practical, nonparametric spatio-temporal modeling.

2.4 Connection to Modified Parameterized Leapfrog HMC

The parameterized leapfrog scheme introduced in this spatio-temporal context serves as the mathematical progenitor of the Modified Parameterized Leapfrog Hamiltonian Monte Carlo (MPL-HMC) method developed in our companion work Bhattacharya [2026b]. Indeed, the deterministic counterpart of equations (3)–(4)—obtained by removing the spatial index s and treating V as a fixed potential—yields exactly the MPL-HMC integrator:

$$\begin{cases} q_{n+1} = \beta(\delta t)q_n + \delta t M^{-1}(\alpha p_n - \frac{\delta t}{2}\nabla V(q_n)), \\ p_{n+1} = \alpha(\delta t)^2 p_n - \frac{\delta t}{2}(\alpha\nabla V(q_n) + \nabla V(q_{n+1})), \end{cases}$$

where $\alpha(\delta t)$ and $\beta(\delta t)$ are appropriate parameterized in terms of δt . The stochastic version studied here thus provides a rigorous foundation for the deterministic integrator: the mean-square convergence analysis of Bhattacharya [2026a] ensures that the discrete MPL-HMC map approximates the continuous Hamiltonian flow with $\mathcal{O}(\delta t)$ global error. Importantly, the parameters α and β —originally introduced to induce spatial non-stationarity and damping/anti-damping in the spatio-temporal model—translate into tunable knobs for controlling numerical stability, exploration, and damping behavior in MPL-HMC. This transfer of ideas exemplifies how innovations in stochastic ordinary differential equations and numerical analysis for spatio-temporal processes can directly inspire advances in Monte Carlo methodology, enriching both fields with cross-fertilized techniques and theoretical insights.

3 Calculation of likelihood functions

In this section, we will derive the data and process models under assumptions A1-A2. We assume here that the random function $V(\cdot)$ is a Gaussian process with mean 0 and squared exponential function as covariance function for simplicity of calculations (Matérn covariance kernel could be another choice but that will lead to very high computational complexity, so we avoid such a choice). In particular, we assume that the covariance function of $V(\cdot)$ takes the form $\text{cov}(V(x), V(y)) = k(h) = \sigma^2 e^{-\eta_3 h^2}$, where $h = \|x - y\|$. Then

$V'(\cdot)$ will be a Gaussian random function with mean 0 and covariance function (Stein [1999b], Chapter 2)

$$\text{cov}(V'(x), V'(y)) = 2\eta_3\sigma^2 e^{-\eta_3 h^2} (1 - 2\eta_3 h^2). \quad (5)$$

Before moving forward, we introduce a few notations that will be used for calculations of different distributions. Suppose s_1, \dots, s_n denote the n locations, where $s_i \in \mathbb{R}^2$, for $i = 1, \dots, n$. Let the observed data and the corresponding latent variables be denoted by $\mathbb{D} = \{\mathbf{y}_1^T, \mathbf{y}_2^T, \dots, \mathbf{y}_T^T\}$, and $\mathbb{L} = \{\mathbf{x}_1^T, \mathbf{x}_2^T, \dots, \mathbf{x}_T^T\}$, respectively, where, for $t = 1, \dots, T$, $\mathbf{y}_t = (y(s_1, t), y(s_2, t), \dots, y(s_n, t))^T$ and $\mathbf{x}_t = (x(s_1, t), x(s_2, t), \dots, x(s_n, t))^T$. By \mathbf{a}^T and f' , we mean transpose of a vector \mathbf{a} and derivative of a function f , respectively. Assuming $i, k \in \{1, \dots, n\}$, $m \in \{0, \dots, T\}$ and $r \in \{1, \dots, T\}$, we define

$$h_{ij}(m) = |y(s_i, m) - y(s_j, m)|, \mu_i(m) = \beta y(s_i, m) + \frac{\alpha x(s_i, m)}{M_{s_i}}, \boldsymbol{\mu}_m = (\mu_i(m), 1 \leq i \leq n)^T$$

$$\mathbf{W}_r = (V'(y(s_i, r)), 1 \leq i \leq n)^T, \mathbb{W}_{r-1} = \begin{pmatrix} \alpha \mathbf{W}_{r-1} \\ \mathbf{W}_r \end{pmatrix}, \ell_{ik}(r-1, r) = |y(s_i, r-1) - y(s_k, r)|.$$

3.1 Joint conditional density of the observed data

The joint conditional density of the data given the latent variables $\mathbf{x}_0, \mathbf{x}_1, \dots, \mathbf{x}_T$ and the parameter vector $\Theta = (\alpha, \beta, \sigma^2, \sigma_\theta^2, \sigma_p^2, \eta_1, \eta_2, \eta_3)$. is given by

$$\begin{aligned} [\mathbb{D} | \mathbf{x}_0; \dots; \mathbf{x}_{T-1}; \mathbf{y}_0; \Theta] &\propto [\mathbf{y}_1 | \mathbf{y}_0; \mathbf{x}_0; \Theta] \dots [\mathbf{y}_T | \mathbf{y}_{T-1}, \dots, \mathbf{y}_0; \mathbf{x}_{T-1}, \dots, \mathbf{x}_0; \Theta] \\ &\propto \frac{(\sigma^2)^{-nT/2}}{\prod_{t=1}^T |\Sigma_{t-1}|^{1/2}} \exp \left\{ -\frac{2}{\sigma^2} \sum_{t=1}^T (\mathbf{y}_t - \boldsymbol{\mu}_{t-1})^T \Sigma_{t-1}^{-1} (\mathbf{y}_t - \boldsymbol{\mu}_{t-1}) \right\}, \end{aligned} \quad (6)$$

where, for $j = 1, 2, \dots, T$, the (k, ℓ) th element of Σ_{j-1} is $2\eta_3 e^{-\eta_3 h_{k\ell}^2(j-1)} (1 - 2\eta_3 h_{k\ell}^2(j-1)) / (M_{s_k} M_{s_\ell})$. It is to be noted that due to the use of the Leap-frog algorithm, the randomness of \mathbb{D} given the latent variables is driven by the randomness of $V(\cdot)$. The details of the calculation of the joint density are provided in Appendix E. It has to be noted that although the conditional joint density of the data is Gaussian but unconditionally the joint density is not Gaussian and not even tractable.

3.2 Joint conditional density of latent data

It can be shown that (see Appendix F for the detailed calculation)

$$\begin{aligned} [\mathbb{L} | \mathbf{y}_0; \dots; \mathbf{y}_T; \mathbf{x}_0; \Theta] &\propto [\mathbf{x}_1 | \mathbf{x}_0; \mathbf{y}_0; \mathbf{y}_1; \Theta] \dots [\mathbf{x}_T | \mathbf{x}_{T-1}; \dots; \mathbf{x}_0; \mathbf{y}_0; \dots; \mathbf{y}_T; \Theta] \\ &\propto \frac{(\sigma^2)^{-nT/2}}{\prod_{t=1}^T |\Omega_t|^{1/2}} \exp \left\{ -\frac{2}{\sigma^2} \sum_{t=1}^T (\mathbf{x}_t - \alpha^2 \mathbf{x}_{t-1})^T \Omega_t^{-1} (\mathbf{x}_t - \alpha^2 \mathbf{x}_{t-1}) \right\}, \end{aligned} \quad (7)$$

where, for $m \in \{1, 2, \dots, T\}$, $\Omega_t = \alpha^2 \Sigma_{t-1, t-1} + \alpha \Sigma_{t-1, t} + \alpha \Sigma_{t, t-1} + \Sigma_{t, t}$, where the (i, k) th element of Σ_{jj} , for $j = t-1, t$, is $2\eta_3 e^{-\eta_3 h_{ik}^2(j)} (1 - 2\eta_3 h_{ik}^2(j))$, and the (i, k) th element of $\Sigma_{t-1, t} = \Sigma_{t, t-1}^T$ is $2\eta_3 e^{-\eta_3 \ell_{ik}^2(t-1, t)} (1 - 2\eta_3 \ell_{ik}^2(t-1, t))$.

3.3 Complete likelihood combining observed and latent data

Next we will find the joint distribution of Data and Latent observations given \mathbf{x}_0 , \mathbf{y}_0 and Θ . Finally, using the prior distributions on $Y(s, 0)$ and $X(s, 0)$ as mentioned in A1-A2, we shall obtain the complete joint distribution of $(\mathbf{y}_T, \dots, \mathbf{y}_1, \mathbf{y}_0)$ and $(\mathbf{x}_T, \dots, \mathbf{x}_1, \mathbf{x}_0)$, given the parameter Θ . The joint distribution of $(\mathbf{y}_T, \dots, \mathbf{y}_1)$ and $(\mathbf{x}_T, \dots, \mathbf{x}_1)$ given $(\mathbf{x}_0, \mathbf{y}_0, \Theta)$, using equations (6) and (7), is given by

$$\begin{aligned} \left[\mathbb{D}, \mathbb{L} \middle| \mathbf{y}_0, \mathbf{x}_0, \Theta \right] &= \prod_{t=1}^T \left[\mathbf{y}_t \middle| \mathbf{x}_{t-1}, \mathbf{y}_{t-1}, \Theta \right] \left[\mathbf{x}_t \middle| \mathbf{x}_{t-1}, \mathbf{y}_{t-1}, \mathbf{y}_t, \Theta \right] \propto \frac{(\sigma^2)^{-nT}}{\prod_{t=1}^T |\Sigma_{t-1}|^{1/2} |\Omega_t|^{1/2}} \times \\ &\exp \left\{ -\frac{2}{\sigma^2} \sum_{t=1}^T \left((\mathbf{y}_t - \boldsymbol{\mu}_{t-1})^T \Sigma_{t-1}^{-1} (\mathbf{y}_t - \boldsymbol{\mu}_{t-1}) + (\mathbf{x}_t - \alpha^2 \mathbf{x}_{t-1})^T \Omega_t^{-1} (\mathbf{x}_t - \alpha^2 \mathbf{x}_{t-1}) \right) \right\}. \end{aligned} \quad (8)$$

Let $\text{cov}(Y(s_1, 0), Y(s_2, 0)) = \sigma_\theta^2 \exp\{-\eta_2 k^2\}$ (see assumption A2), and $\text{cov}(X(s_1, 0), X(s_2, 0)) = \sigma_p^2 \exp\{-\eta_1 k^2\}$ (see assumption A1), where $k = \|s_1 - s_2\|$. Therefore, $[\mathbf{y}_0 | \Theta] \sim N_n(\mathbf{0}, \sigma_\theta^2 \Delta_0)$ and $[\mathbf{x}_0 | \Theta] \sim N_n(\mathbf{0}, \sigma_p^2 \Omega_0)$, where the (i, j) th element of Δ_0 and Ω_0 are $\exp\{-\eta_2 k_{ij}^2\}$ and $\exp\{-\eta_1 k_{ij}^2\}$, respectively, with $k_{ij} = \|s_i - s_j\|$. Thus,

$$\begin{aligned} \left[\mathbf{y}_T, \mathbf{x}_T, \dots, \mathbf{y}_1, \mathbf{x}_1, \mathbf{y}_0, \mathbf{x}_0 \middle| \Theta \right] &\propto \left[\mathbb{D}, \mathbb{L} \middle| \mathbf{y}_0, \mathbf{x}_0, \Theta \right] \frac{(\sigma_\theta^2)^{-n/2} (\sigma_p^2)^{-n/2}}{|\Delta_0|^{1/2} |\Omega_0|^{1/2}} \exp \left\{ -\frac{1}{2\sigma_\theta^2} \mathbf{y}_0^T \Delta_0^{-1} \mathbf{y}_0 \right\} \\ &\exp \left\{ -\frac{1}{2\sigma_p^2} \mathbf{x}_0^T \Omega_0^{-1} \mathbf{x}_0 \right\}, \end{aligned} \quad (9)$$

where $\left[\mathbb{D}, \mathbb{L} \middle| \mathbf{y}_0, \mathbf{x}_0, \Theta \right]$ is obtained from (8).

It is important to note that, thanks to our Gaussian process assumption for the random function $V(\cdot)$, we could obtain the conditional likelihoods as Gaussian; however, the unconditional distributions are non-Gaussian.

4 Prior distributions

In this section, we will specify the prior distributions of the components of $\Theta = (\alpha, \beta, \sigma^2, \sigma_\theta^2, \sigma_p^2, \eta_1, \eta_2, \eta_3)^T$. The parameter spaces of each component of Θ are the following: $|\alpha| < 1$, $|\beta| < 1$, and $\sigma^2, \sigma_\theta^2, \sigma_p^2, \eta_i > 0$, $i = 1, 2, 3$. We make the following transformations on α , β , η_i , for $i = 1, 2, 3$ for better MCMC mixing. Define $\alpha_* = \log\left(\frac{1+\alpha}{1-\alpha}\right)$, $\beta_* = \log\left(\frac{1+\beta}{1-\beta}\right)$, and $\eta_i^* = \log(\eta_i)$, for $i = 1, 2, 3$, so that $\alpha_*, \beta_*, \eta_i^* \in \mathbb{R}$, for $i = 1, 2, 3$.

This implies $\alpha = 1 - \frac{2e^{\alpha_*}}{1+e^{\alpha_*}}$, $\beta = 1 - \frac{2e^{\beta_*}}{1+e^{\beta_*}}$, $\eta_i = e^{\eta_i^*}$, $i = 1, 2, 3$, respectively. We assume that the prior distributions are independent. Since the parameter spaces of α_* and β_* are \mathbb{R} , and they are involved in the mean function of our proposed model, the prior for α_* and β_* are taken as normal with mean 0 and large variances (of the order 100). Particular choices of the prior variances are discussed in Sections 6 and 7. Moreover, the parameter spaces of η_i^* , $i = 1, 2, 3$ are also \mathbb{R} and they are involved in the covariance structure of our proposed model in the sense that they determine the amount of correlations between spatial and temporal points. So, we take the priors for η_i^* , $i = 1, 2, 3$, as normal with means μ_{η_i} and variances 1. Larger variance of the η_i^* made the variances of their posterior distributions unreasonably large due to huge data variability. The exact values of the hyper-prior means depend upon the data under consideration, and is discussed in Sections 6 and 7. Finally, the prior distributions of variance parameters are taken to be

inverse-gamma, as they are the conjugate priors, conditionally. It is expected that the variability of the spatio-temporal data is very large, which might possibly render the posterior means and variances of σ_θ^2 , σ_p^2 and σ^2 very large (especially for σ^2). So we decided to choose the hyper-parameters in such a way that the prior means (with exceptions in a few cases) and the variances are both close to zero. The exact choices of the hyper-parameters of priors of σ_p^2 , σ_θ^2 and σ^2 are mentioned in Sections 6 and 7.

The general forms of the prior distributions of α_* , β_* , σ^2 , σ_θ^2 , σ_p^2 , η_i^* , $i = 1, 2, 3$, are taken as follows:

$$[\alpha_*] \propto N(0, \sigma_\alpha), [\beta_*] \propto N(0, \sigma_\beta^2), [\sigma^2] \propto IG(\alpha_v, \gamma_v/2), [\sigma_\theta^2] \propto IG(\alpha_\theta, \gamma_\theta/2) \\ [\sigma_p^2] \propto IG(\alpha_p, \gamma_p/2), [\eta_1^*] \propto N(\mu_{\eta_1}, 1), [\eta_2^*] \propto N(\mu_{\eta_2}, 1), [\eta_3^*] \propto N(\mu_{\eta_3}, 1),$$

where IG stands for inverse gamma distribution.

5 Full conditional distributions

In this section, we provide the full conditional distributions of the parameters, which will be used for generating samples from posterior distributions of the parameters using Gibbs or Metropolis-Hastings steps. The detailed calculations are provided in Appendix G.

Full conditional distribution of β_*

The full conditional density of β_* , is given by $[\beta_* | \dots] \propto \exp\{-\beta_*^2/2\sigma_\beta^2\}g_1(\beta_*)$, where

$$g_1(\beta_*) = \exp \left\{ -\frac{2\tilde{\beta}^2}{\sigma^2} \sum_{t=1}^T \mathbf{y}_{t-1}^T \Sigma_{t-1}^{-1} \mathbf{y}_{t-1} + \frac{4\tilde{\beta}}{\sigma^2} \sum_{t=1}^T \mathbf{y}_t^T \Sigma_{t-1}^{-1} \mathbf{y}_{t-1} \right\},$$

with $\tilde{\beta} = 1 - 2e^{\beta_*}/(1 + e^{\beta_*})$.

Full conditional distribution of α_*

The full conditional density of α_* is given by $[\alpha_* | \dots] \propto \exp\{-\alpha_*^2/2\sigma_\alpha^2\}g_2(\alpha_*)$, where

$$g_2(\alpha_*) = \frac{1}{\prod_{t=1}^T |\Omega_t|^{1/2}} \exp \left\{ -\frac{2}{\sigma^2} \sum_{t=1}^T [(\mathbf{x}_t - \tilde{\alpha}^2 \mathbf{x}_{t-1})^T \Omega_t^{-1} (\mathbf{x}_t - \tilde{\alpha}^2 \mathbf{x}_{t-1})] - \right. \\ \left. \frac{2\tilde{\alpha}}{\sigma^2} \sum_{t=1}^T [\tilde{\alpha} \mathbf{x}_{t-1}^T D \Sigma_{t-1}^{-1} D \mathbf{x}_{t-1} - 2 \mathbf{y}_t^T \Sigma_{t-1}^{-1} D \mathbf{x}_{t-1}] \right\},$$

and $\tilde{\alpha} = 1 - 2e^{\alpha_*}/(1 + e^{\alpha_*})$. The closed forms of the full conditionals of α_* and β_* are not available, and hence will be updated using random walk Metropolis.

Full conditional distribution of σ_θ^2 , σ_p^2 and σ^2

The full conditional distribution of σ_θ^2 , σ_p^2 and σ^2 are $IG(\alpha_\theta + n/2, \gamma_\theta + \mathbf{y}_0^T \Delta_0^{-1} \mathbf{y}_0/2)$, $IG(\alpha_p + n/2, \gamma_p + \mathbf{x}_0^T \Delta_0^{-1} \mathbf{x}_0/2)$ and $IG(\alpha_v + Tn, \gamma_v/2 + 2\zeta)$, respectively, where

$$\zeta = \sum_{t=1}^T [(\mathbf{y}_t - \boldsymbol{\mu}_t)^T \Sigma_{t-1}^{-1} (\mathbf{y}_t - \boldsymbol{\mu}_t) + (\mathbf{x}_t - \alpha^2 \mathbf{x}_{t-1})^T \Omega_t^{-1} (\mathbf{x}_t - \alpha^2 \mathbf{x}_{t-1})].$$

Thus, $\sigma_\theta^2, \sigma_p^2$ and σ^2 updated using a Gibbs sampling step.

Full conditional distributions of η_i^* , $i = 1, 2, 3$

The full conditional distributions of η_1^* , η_2^* and η_3^* are $[\eta_1^* | \dots] \propto \pi(\eta_1^*)g_3(\eta_1^*)$, $[\eta_2^* | \dots] \propto \pi(\eta_2^*)g_4(\eta_2^*)$, and $[\eta_3^* | \dots] \propto \pi(\eta_3^*)g_5(\eta_3^*)$, where $\eta_j = \exp\{\eta_j^*\}$, $\pi(\eta_j^*) = \exp\{\eta_j^{*2}/2\}$, for $j = 1, 2, 3$. Here $g_3(\cdot)$, $g_4(\cdot)$ and $g_5(\cdot)$ are defined as the following:

$$g_3(\eta_1^*) = \frac{1}{|\Omega_0|^{1/2}} \exp \left\{ -\frac{1}{2\sigma_p^2} \mathbf{x}_0^T \Omega_0^{-1} \mathbf{x}_0 \right\}, g_4(\eta_2^*) = \frac{1}{|\Delta_0|^{1/2}} \exp \left\{ -\frac{1}{2\sigma_\theta^2} \mathbf{y}_0^T \Delta_0^{-1} \mathbf{y}_0 \right\}, \text{ and}$$

$$g_5(\eta_3^*) = \frac{1}{\prod_{t=1}^T |\Sigma_{t-1}|^{1/2} |\Omega_t|^{1/2}} \exp \left\{ -\frac{2}{\sigma^2} \sum_{t=1}^T [(\mathbf{y}_t - \boldsymbol{\mu}_t)^T \Sigma_{t-1}^{-1} (\mathbf{y}_t - \boldsymbol{\mu}_t) + (\mathbf{x}_t - \alpha^2 \mathbf{x}_{t-1})^T \Omega_t^{-1} (\mathbf{x}_t - \alpha^2 \mathbf{x}_{t-1})] \right\}.$$

None of the full conditional distributions of η_1^* , η_2^* or η_3^* has closed form and hence they will be updated using random walk Metropolis. The detailed calculations of the full conditionals for η_i^* , for $i = 1, 2, 3$, are provided in Appendix G.

Full conditional distributions of \mathbf{x}_t , $t = 1, 2, \dots, T$ and \mathbf{x}_0

From equation (7), we immediately see that $[\mathbf{x}_t | \dots] \sim N_n \left(\alpha^2 \mathbf{x}_{t-1}, \frac{\sigma^2}{4} \Omega_t \right)$, for $t = 1, \dots, T$. With $A = \Omega_0^{-1} + 4\sigma_p^2 \alpha^4 \sigma^{-2} \Omega_1^{-1} + 4\sigma_p^2 \alpha^2 \sigma^{-2} D \Sigma_0^{-1} D$, $B = 4\sigma_p^2 \alpha^2 \sigma^{-2} \Omega_1^{-1}$ and $C = 4\sigma_p^2 \alpha \sigma^{-2} D \Sigma_0^{-1}$, the full conditional density of \mathbf{x}_0 is found to be a n -variate normal with mean $A^{-1}(B\mathbf{x}_1 + C(\mathbf{y}_1 - \beta\mathbf{y}_0))$ and the variance-covariance matrix $\sigma_p^2 A^{-1}$. Hence, \mathbf{x}_t , for $t = 0, 1, \dots, T$ are updated using a Gibbs sampling step.

Remark 6 We add ridge parameters to the diagonals of all the dispersion matrices while performing the MCMC runs to make the matrices non-singular. Note that the ridge parameter for Σ_{t-1} , for $t = 1, \dots, T$ works as nugget in the model. The ridge parameter is fixed to a small value, which is chosen based on cross-validation with several pilot runs of MCMC.

Remark 7 Within the Bayesian framework, missing observations can be addressed by initializing the MCMC chain with pseudo-values at the missing locations and time points, and then updating them using predictive densities within MCMC runs. After burn-in, we can obtain the posterior predictive densities at those locations and time points. This approach was applied in one of our real data analysis (see 7.1). If needed, any measure of central tendency can be used for imputation.

6 Simulation studies

To evaluate the performance of our model and compare our results with those of a well-known non-stationary Gaussian process model (described below), we conduct two extensive simulation studies. The first data set is generated from a mixture of three Gaussian process models, while the second is generated from a mixture of two general quadratic nonlinear (GQN) models. The data generation algorithms are outlined in Sections 6.1 and 6.3. We begin by describing the model, whose results are compared with the findings from our model applied to the simulated data sets. The model is as follows:

Letting s and s' denote the locations, and t, t' denote the time points, we have

$$y_{s,t} | \omega_{s,t} \sim N(\eta_{s,t}, \sigma_\epsilon^2), \quad \eta_{s,t} = b_0 + \omega_{s,t},$$

$$\omega_{s,t} = a\omega_{s,(t-1)} + \xi_{s,t}, \quad \text{with } |a| < 1, \text{ and } \xi_{s,t} \sim NGP(0, C(\cdot, \cdot)),$$

where *NGP* stands for non-stationary Gaussian process and

$$C(\xi_{s,t}, \xi_{s',t'}) = \begin{cases} 0 & \text{if } t \neq t' \\ \text{cov}(\xi_s, \xi_{s'}) & \text{if } t = t', \end{cases}$$

with $\text{cov}(\xi_s, \xi_{s'})$ being a Matérn covariance kernel with smoothness parameter 2. The other parameters of the Matérn covariance kernel vary with location s , making the model non-stationary (Lindgren et al. [2011], Bolin and Lindgren [2011], Ingebrigtsen et al. [2014], and Blangiardo and Cameletti [2015]). For future reference, we will denote this model as the NGP model. The NGP model is fitted using the SPDE approach, as outlined in Chapter 6 of Blangiardo and Cameletti [2015] (also see Lindgren et al. [2022] for a review on the SPDE approach).

In all simulation experiments, we set the number of locations to $n = 50$ and the number of time points to $T = 20$. The data vector corresponding to the last time point, which contains observations at the 50 locations, is kept aside for model performance evaluation (algorithm to generate from predictive density at a future time point is provided in Appendix H). Therefore, the observed data set is $\mathbb{D} = \{y(s_1, 1), \dots, y(s_{50}, 1), \dots, y(s_1, 19), \dots, y(s_{50}, 19)\}$ and the corresponding latent data is $\mathbb{L} = \{x(s_1, 1), \dots, x(s_{50}, 1), \dots, x(s_1, 19), \dots, x(s_{50}, 19)\}$. The validation set contains $\mathbf{y}_{20} = (y(s_1, 20), \dots, y(s_{50}, 20))^T$ and $\mathbf{x}_{20} = (x(s_1, 20), \dots, x(s_{50}, 20))^T$.

We run our MCMC sampler for 1,75,000 iterations with a burn-in of 1,50,000 for simulation examples. The MCMC computations were carried out in MATLAB R2018a. For each model-fitting it took about 3 hours 49 minutes on a desktop computer having 8GB RAM, 1 TB Hard Drive and 3.8 GHz core_i5.

6.1 Mixture of three Gaussian Processes

6.1.1 Data generation

A data set is simulated from a mixture of three Gaussian process models. Given the number of locations n and the number of time points T , we obeyed the following steps to simulate the data set.

- a. Generate n locations, s_1, \dots, s_n , uniformly from $[0, 1] \times [0, 1]$.
- b. For $j = 1, 2, 3$, simulate an $n \times T$ matrix ξ_j , where each column is independently simulated from n -variate normal with mean $\mathbf{0}$ and covariance C_j . The $n \times n$ matrix C_j is determined by Matérn covariance kernel (2) with parameters κ_j and σ_j^2 .
- c. Calculate $\omega_j(s, t) = a_j \omega_j(s, t-1) + \xi_j(s, t)$, for $t = 1, \dots, T$, $s = s_1, \dots, s_n$, and $j = 1, 2, 3$. Here we set $\omega(s, 0) = 0$, for $s = s_1, \dots, s_n$.
- d. Set $\mathbf{p} = (1/3, 1/3, 1/3)$, which defines a partition of $[0, 1]$ as $\mathbb{P}_1 = [0, 1/3)$, $\mathbb{P}_2 = [1/3, 2/3)$ and $\mathbb{P}_3 = [2/3, 1]$.
- e. For $s = s_1, \dots, s_n$, simulate $u \sim (0, 1)$. If $u \in \mathbb{P}_j$, generate T -variate observation vector $\mathbf{y}(s) = (y(s, 1), \dots, y(s, T))^T$ from a T -variate normal distribution with mean $b_{0_j} \mathbf{1}_T + \boldsymbol{\omega}_j(s)$ and covariance $\sigma_{\epsilon_j}^2 \mathbb{I}_T$, where $\boldsymbol{\omega}_j(s)^T = (\omega_j(s, r), 1 \leq r \leq T)$. Finally, set $\omega_j(s, t) = x(s, t)$, for $t = 1, \dots, T$.

The following values of parameters are provided for the purpose of simulation: $b_{0_1} = 0$, $b_{0_2} = 10$, $b_{0_3} = 20$, $\sigma_{\epsilon_1}^2 = 1.0$, $\sigma_{\epsilon_2}^2 = 0.01$, $\sigma_{\epsilon_3}^2 = 2.0$, $a_1 = -0.75$, $a_2 = 0.75$, $a_3 = 0.25$, $\kappa_1 = 1$, $\kappa_2 = 1.5$, $\kappa_3 = 2$, $\sigma_1^2 = 1$, $\sigma_2^2 = 2$ and $\sigma_3^2 = 0.2$.

6.1.2 Results from our model

With the observed data set \mathbb{D} , we run MCMC iterations for the proposed model. Based on MCMC iterations, observations from the predictive densities of \mathbf{y}_{20} and \mathbf{x}_{20} given the data set \mathbb{D} are simulated using the algorithm given in Appendix H. For running MCMC iterations, one needs to provide the prior parameters. Although we have chosen a finite prior variance for η_3^* , the posterior variance of η_3 turned out to be very large, which is probably due to huge variability present in the spatio-temporal data. This large posterior variance of η_3 makes the complete system unstable, so, we fix the value of η_3 at its maximum likelihood estimate (MLE) 2.6889 computed by simulated annealing. Note that it is not very uncommon to fix the decay parameter in Bayesian inference of spatial data analysis, see for example Zhang [2004] and Banerjee [2020]. We give a complete prior specification for the other parameters in the following.

Choice of prior parameters:

The particular choices of the hyper-prior parameters have been chosen using the leave-one-out cross-validation technique. Specifically, for $t = 1, \dots, 20$, we leave \mathbf{y}_t in turn and compute its posterior predictive distribution using relatively short MCMC runs. We then selected those hyperparameters that yielded the minimum average length of the 95% prediction intervals. The final specifications are as follows:

$$\alpha_* \sim N(0, \sqrt{500}), \beta_* \sim N(0, \sqrt{300}), [\sigma^2] \propto IG(170000, 2/2), [\sigma_\theta^2] \propto IG(5500, 780/2),$$

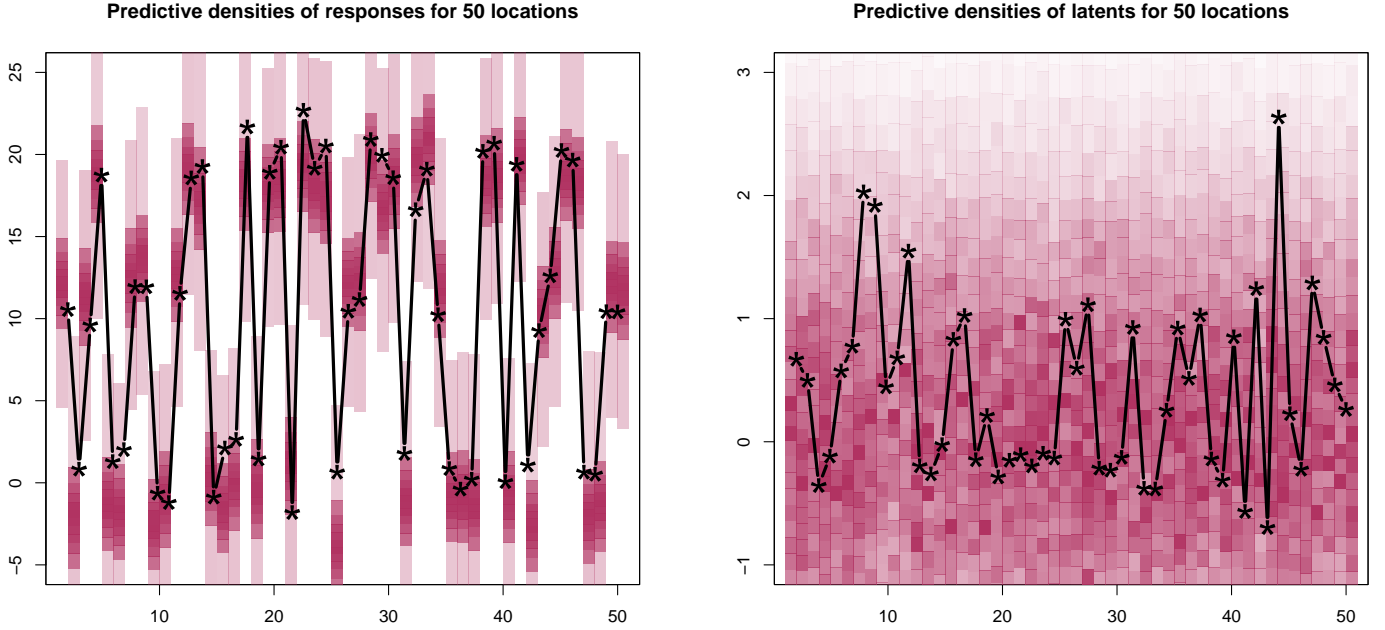
$$[\sigma_p^2] \propto IG(800, 20/2), [\eta_1^*] \propto N(-3, 1), [\eta_2^*] \propto N(-5, 1).$$

Large values of the shape parameters of the variance parameters are used, otherwise the posterior variance explodes and makes the complete model unstable. The plausible reason for such behaviour is the inherent large data variability. To control such large posterior variance, we restrict the prior of variance parameters very close to 0, with a very narrow variance (see Bhattacharya [2021] also for similar choices).

Trace plots and posterior analysis:

The trace plots of the parameters are given in Figure 13 of Appendix K. The plots do not exhibit lack of convergence of the MCMC runs. The posterior probability densities of the latent variables at randomly selected 6 locations for 19 time points are shown in Figures 14 of Appendix K, where higher probability densities are depicted by progressively intense colors. We observe that true latent time series at all the 50 locations always lie in the high probability density regions.

We provide a high probability density (HPD) plot for the predictive densities of response vector \mathbf{y}_{20} and latent vector \mathbf{x}_{20} based on our model in Figure 1. Figure 1a shows the HPD plot for the predictive density of \mathbf{y}_{20} . It can be seen that the majority of the observations fall in high density regions, which, in turn, follow the pattern of the observed data values. The corresponding HPD plot for the latent vector \mathbf{x}_{20} is provided in Figure 1b. We have not provided the individual posterior predictive densities for the response vector \mathbf{y}_{20} and the latent vector \mathbf{x}_{20} for brevity. However, it is observed that the predictive densities for the responses capture the true values within the 95% predictive intervals in all but one location (25th location). The lengths of the predictive intervals vary between 7.49 to 8.83 with mean being 8.0219 and standard deviation 0.304879. For the latent vector \mathbf{x}_{20} , all the true values fall within the 95% predictive intervals of the predictive densities. The lengths of the intervals, in this case, range from 9.44 to 9.69 with mean 9.55808 and standard deviation (sd) 0.0582219.



(a) HPD color plot of predictive densities of the elements of \mathbf{y}_{20} . (b) HPD plot of the posterior predictive of the elements of \mathbf{x}_{20} .

Figure 1: Higher the intensity of the color higher is the density. Black stars denote the true values. Most of the true values lie in the high density regions.

6.2 Comparative study with nonstationary GP model

Using the generated data set, we fit the NGP model with the SPDE technique, implemented through the INLA package in the statistical software R. The posterior predictive densities of \mathbf{y}_{20} and \mathbf{x}_{20} , given \mathbb{D} , are computed for comparison with the performance of our model. The 95% predictive intervals for each component of \mathbf{y}_{20} contain the true values, with lengths ranging from 1894 to 3364, a mean of 2378.483, and a standard deviation of 259.3669. A similar pattern is observed for the latent vector \mathbf{x}_{20} , with interval lengths ranging from 1764 to 3053, a mean of 2371.798, and a standard deviation of 217.7212. Our model outperforms the NGP model in terms of shorter predictive intervals for both \mathbf{y}_{20} and \mathbf{x}_{20} (see Table 1).

	Mean		Std		% of locations misses	
	INLA	Prop Model	INLA	Prop Model	INLA	Prop Model
\mathbf{y}_{20}	2378.483	8.021	259.3669	0.30487	0	2
\mathbf{x}_{20}	2371.798	9.55808	217.7212	0.0582219	0	0

Table 1: The table contains the summary of the lengths of 95% predictive intervals for \mathbf{y}_{20} and \mathbf{x}_{20} obtained using INLA and the proposed model for the 3-component mixture of GPs. The columns named “Mean” and “Std” contain the mean length and the standard deviation of the 95% posterior predictive intervals across the locations.

6.3 Mixture of two GQNs

For a second comparison study, we choose to simulate from a mixture of two nonlinear models, called general quadratic nonlinear (GQN) models. The GQN model has been widely used in the literature of spatial and spatio-temporal modeling, see, for example, Wikle and Hooten [2010], Cressie and Wikle [2015], and Bhattacharya [2021] for a significant overview of the GQN model. We define the GQN model as

$$Y(s_i, t_k) = \phi_1(t_k, s_i) + \phi_2(t_k, s_i) \tan(X(s_i, t_k)) + \epsilon(s_i, t_k), \quad (10)$$

$$X(s_i, t_k) = \sum_{j=1}^n a_{ij} X(s_j, t_{k-1}) + \sum_{j=1}^n \sum_{l=1}^n b_{ijl} X(s_j, t_{k-1}) [X(s_l, t_{k-1})]^2 + \eta(s_i, t_k), \quad (11)$$

where $i \in \{1, \dots, n\}$ and $k \in \{1, \dots, T\}$. The coefficients $\phi_1(t_k, \cdot)$, $\phi_2(t_k, \cdot)$, random errors $\epsilon(t_k, \cdot)$, $\eta(t_k, \cdot)$ and the initial latent variable $X(t_0, \cdot)$ are assumed to be independent zero-mean Gaussian processes having covariance structure $c(\mathbf{s}_1, \mathbf{s}_2) = \exp(-\|\mathbf{s}_1 - \mathbf{s}_2\|)$, for $\mathbf{s}_1, \mathbf{s}_2 \in \mathbb{R}^2$, with $\|\cdot\|$ being the Euclidean norm. Moreover, it is assumed that for $i, j, l \in \{1, \dots, n\}$, a_{ij} and b_{ijl} have independent univariate 0 mean normal distributions with variance 0.001^2 .

6.3.1 Data generation

Here, a step-by-step description is provided for generating observations from the mixture of two GQNs. Let n and T denote the number of locations and time points.

- a. Generate n locations s_1, \dots, s_n from $[0, 1] \times [0, 1]$.
- b. Generate $n \times T$ matrix X using equation (11) by taking the coefficients as described above.
- c. $\phi_1(t)$, $\phi_2(t)$ and $\epsilon(t)$ are generated independently for $t = 1, \dots, T$ from zero-mean m -variate Gaussian with variance-covariance matrix \mathbb{S} , whose (i, j) th element is $\exp(-\|s_i - s_j\|)$. Let the i th element of $\phi_j(t)$, $j = 1, 2$, and $\epsilon(t)$ be $\phi_j(t, s_i)$ and $\epsilon(t, s_i)$, respectively.
- d. Let $u \sim \text{unif}(0, 1)$. Given all the parameters and latent variables, generate $Y(s_i, t)$, for $i = 1, \dots, n$ and $t = 1, \dots, T$, as

$$Y(s_i, t) = \begin{cases} \phi_1(t, s_i) + \phi_2(t, s_i) \tan(X(s_i, t)) + \epsilon(t, s_i) & \text{if } u < 0.6, \\ 5 + \phi_1(t, s_i) + \phi_2(t, s_i) \tan(X(s_i, t)) + \epsilon(t, s_i) & \text{if } u \geq 0.6. \end{cases}$$

6.3.2 Results from our model

For this data set as well, we run MCMC iterations for simulating observations from the posterior densities of the parameters involved in our model. These MCMC iterations and Monte Carlo averages provide simulated observations from the posterior densities of \mathbf{y}_{20} and \mathbf{x}_{20} , given the data set \mathbb{D} (for the algorithm, see Appendix H). To complete the model, one needs to specify the prior parameters. The specific choices of the hyperparameters are mentioned below, except for η_3 , which is kept fixed at its MLE 5.5042, obtained by simulated annealing.

Choice of prior parameters:

Using the same cross-validation technique as before, we obtain the following prior specifications:

$$\alpha_* \sim N(0, \sqrt{500}), \beta_* \sim N(0, \sqrt{300}), [\sigma^2] \propto IG(780000, 2/2), [\sigma_\theta^2] \propto IG(58900, 770/2),$$

$$[\sigma_p^2] \propto IG(385, 20/2), [\eta_1^*] \propto N(-3, 1), [\eta_2^*] \propto N(-5, 1).$$

As earlier, here also the shape parameters of the variance parameters are taken large because of the huge inherent data-variability. Unless we restrict the prior mean and variance very close to 0, the posterior variances of the variance parameters become extremely high, making the complete system unstable.

Trace plots and posterior analysis:

The trace plots of the parameters are provided in Figure 15, and the posterior density plot of $\mathbf{x}_t, t = 1, \dots, 19$ are displayed in Figures 16 and 16 of Appendix L. The trace plots do not show any evidence of non-convergence of MCMC runs.

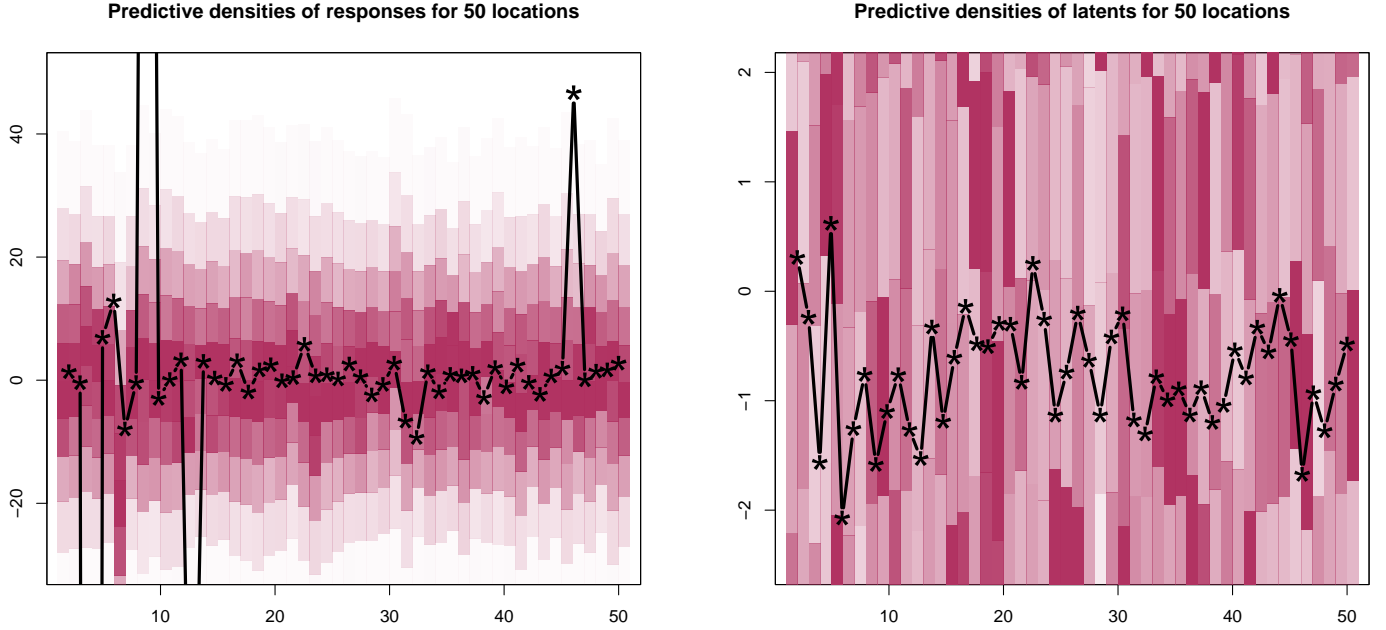
The HPD plot of the posterior predictive densities of the elements of latent vector \mathbf{x}_{20} and response vector \mathbf{y}_{20} are provided in Figure 2. Apart from a few true values of \mathbf{y}_{20} , the rest lie well within the high density region (Figure 2a). The high probability region of the predictive densities of \mathbf{x}_{20} could not satisfactorily capture the true values, as seen in Figure 2b. This may possibly be attributed to the complicated structure of the simulation model, making the latent variables non-identifiable, and also possibly to large variability of the data, rendering the densities of the latent variables wide, leading to much sparser HPD regions. For the sake of brevity, we have not included component-wise density plots of \mathbf{x}_{20} and \mathbf{y}_{20} . Out of 50 locations, except for 3 places (at locations 3, 8 and 13), the true response values are captured by the 95% predictive intervals of the response variable \mathbf{y}_{20} . The lengths of the intervals vary from 99 to 141 units. The mean length of intervals turned out to be 112 with standard deviation 7.9680. In the case of the latent vector, \mathbf{x}_{20} , all the true values are captured by the respective 95% predictive intervals. The lengths of the intervals vary from 138 to 142.5 with mean 140.4856 and standard deviation 0.8524.

6.3.3 Comparative study with non-stationary GP model

Similar to the analysis of the mixture of GP models, we fitted the NGP model to the current data set using INLA in R. The same SPDE technique was applied for model fitting. The 95% predictive intervals of the components of \mathbf{y}_{20} capture the true values except for the 3rd, 8th and 12th components. The interval lengths range from 172 to 233.5 units, with a mean of 200.79 and a standard deviation of 10.1872. Notably, the mean predictive interval length exceeds that of our proposed model. In contrast, none of the true values fall within the 95% predictive intervals for \mathbf{x}_{20} , and the intervals are extremely narrow, in the order of 10^{-4} . This analysis indicates that our model significantly outperforms the NGP model for the mixture of GQN data. A summary of the comparison is provided in Table 2.

	Mean		Std		% of locations misses	
	INLA	Prop Model	INLA	Prop Model	INLA	Prop Model
\mathbf{y}_{20}	200.79	112	10.1872	7.9680	6	6
\mathbf{x}_{20}	$\sim 10^{-4}$	140.4856	$\sim 10^{-4}$	0.8524	100	0

Table 2: The table contains the summary of the lengths of the 95% predictive intervals for \mathbf{y}_{20} and \mathbf{x}_{20} obtained using INLA and the proposed model for mixture of two GQNs. The columns named “Mean” and “Std” contain the mean length and the standard deviation of the 95% posterior predictive intervals across the locations.



(a) HPD color plot of predictive densities of the elements of \mathbf{y}_{20} . (b) HPD plot of the posterior predictive of the elements of \mathbf{x}_{20} .

Figure 2: Higher the intensity of the color higher is the density. Black stars denote the true values. Most of the true values lie in the high density regions.

7 Real data analyses

We evaluate our model’s performance on two real temperature datasets. The first is a spatio-temporal dataset of temperature measurements recorded in Alaska over 65–70 years. The second consists of sea surface temperatures collected over a wide range of areas for 100 months. Details of these datasets are provided in Sections 7.1 and 7.2, respectively.

Before applying our model to these datasets, we first transform the locations using the Lambert projection (Guha [2017]) to ensure that Euclidean distances are meaningful. Let ϕ be longitude and ψ be latitude in radian. Then the following transformation is made:

$$s_1 = 2 \sin \left(\frac{\pi}{4} - \frac{\psi}{2} \right) \sin \phi, \text{ and } s_2 = -2 \sin \left(\frac{\pi}{4} - \frac{\psi}{2} \right) \cos \phi. \quad (12)$$

7.1 Alaska temperature data

We conduct a real data analysis on temperature data from Alaska and its surroundings. The dataset is collected from <https://www.metoffice.gov.uk/hadobs/crutem4/data/download.html> by selecting the `CRUTEM.4.6.0.0.station_files.zip` link under the **Station data** section. The details on the dataset can be found at <https://crudata.uea.ac.uk/cru/data/temperature/crutem4/station-data.htm>.

For the analysis, we consider 30 locations, using annual average temperature data from 1950 to 2015 after detrending. At four locations, a significant amount of data was missing, so we reconstructed the complete time series for these locations. Among the 30 locations, data were available up to 2021 for 16

locations, allowing us to make multiple time predictions for these sites. Figure 3 shows the 26 spatial points in red, while the four locations with reconstructed time series are marked in blue. The latitudes and longitudes are listed in Table 3.

Sl. No.	Lat.	Long.	Sl. No.	Lat.	Long.	Sl. No.	Lat.	Long.
1	71.3N	156.8W	11	64.8N	147.9W	21	62.2N	145.5W
2	60.6N	151.3W	12	60.1N	149.5W	22	66.9N	162.6W
3	59.5N	139.7W	13	63N	155.6W	23	58.4N	134.6W
4	55.2N	162.7W	14	63N	141.9W	24	63.7N	149W
5	61.2N	150W	15	55N	131.6W	25	68.2N	135W
6	70.1N	143.6W	16	61.6N	149.3W	26	59.6N	133.7W
7	64.5N	165.4W	17	64N	145.7W	27	62.8N	137.4W
8	66.9N	151.5W	18	60.8N	161.8W	28	64.1N	139.1W
9	59.6N	151.5W	19	57.8N	152.5W	29	67.4N	134.9W
10	60.5N	145.5W	20	58.7N	156.7W	30	60.7N	135.1W

Table 3: Latitude and Longitude (in degrees) of 30 locations in and around Alaska. The locations corresponding to the serial numbers, indicated in bold, are used for multiple predictions. The serial numbers which are denoted in blue, for the corresponding spatial locations, complete time series are reconstructed. These blue serial numbers are indicated by L_{25}, L_{26}, L_{28} and L_{30} for future references.

Thus, the dataset considered here consists of 26 locations and 65 time points from 1950 to 2014, with the final time point set aside for single-time-point prediction. We denote the dataset as $\mathbb{D} = \{\mathbf{y}_1, \dots, \mathbf{y}_{65}\}$, where \mathbf{y}_t , for $t \in \{1, \dots, 65\}$, is a 26-dimensional vector. In this analysis, we perform both temporal and spatial predictions after detrending the data. At these 26 locations, we obtain predictive densities for the year 2015.

For 16 locations (indicated by $L_1, \dots, L_7, L_{11}, \dots, L_{13}, L_{18}, \dots, L_{20}, L_{22}, L_{27}, L_{29}$ for references hereafter), we make multiple time-point predictions (see Appendix H). Additionally, we construct 95% predictive intervals for the complete time series at four locations with missing data (the spatial prediction algorithm is detailed in Appendix I). To achieve this, we augment the dataset \mathbb{D} with initial values for the 65 time points at these four locations and iteratively update them by computing conditional densities given \mathbb{D} . That is, we define an augmented dataset $\mathbb{D}^* = \{\mathbf{y}_1^*, \dots, \mathbf{y}_{65}^*\}$, where each \mathbf{y}_t^* is a 30-dimensional vector, with the last four values initialized. The parameters of our model, including the latent variables, are updated given \mathbb{D}^* , and then the last four values of \mathbf{y}_t^* are updated given the parameter values and latent variables. This process continues throughout the entire MCMC run. In Appendix O, we validate that the underlying spatio-temporal process generating the Alaska data is non-Gaussian, strictly stationary, and exhibits lagged correlations that converge to zero as lag increases. Moreover, there is no justification for assuming separability in the spatio-temporal covariance structure. While our spatio-temporal process is non-stationary, it retains other desirable properties, and the analysis results demonstrate that it is well-suited for modeling this dataset.

7.1.1 Prior choices for the Alaska temperature data

With the same cross-validation technique as in the simulation experiments, the complete specification of the priors are obtained as follows:

$$\alpha^* \sim N(0, \sqrt{500}), \beta^* \sim N(0, \sqrt{300}), [\sigma^2] \propto IG(550000, 2/2), [\sigma_\theta^2] \propto IG(700, 780/2),$$

$$[\sigma_p^2] \propto IG(1000, 100/2), [\eta_1^*] \propto N(-3, 1), [\eta_2^*] \propto N(-5, 1).$$

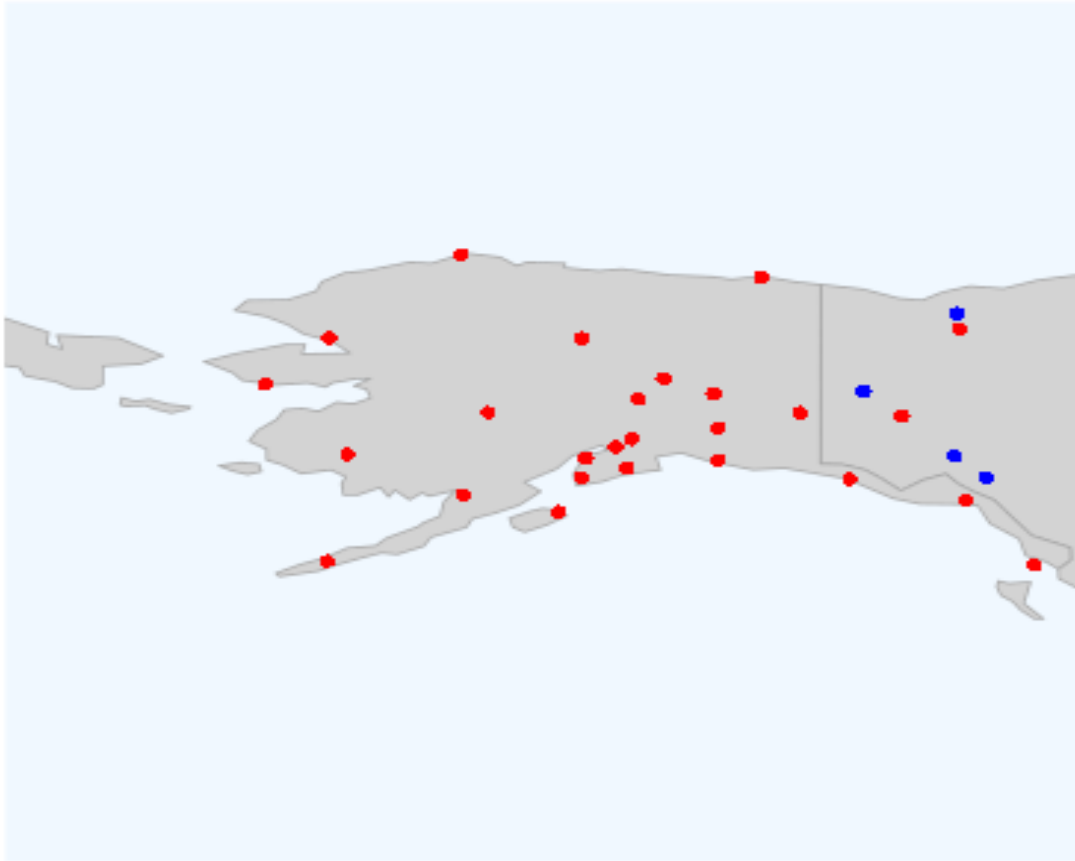


Figure 3: The map of Alaska and its surroundings. The red dots indicate the locations at which the data for the year 1950-2015 are considered. The positions indicated by the blue dots are those at which spatial predictions are made for the complete time series.

As before, we fix η_3 at its MLE of 4.5579. Similar to the simulation studies, the shape parameters for the prior distribution of the variance parameters are set to large values to ensure that the posterior variances of the variance parameters remain finite; see Bhattacharya [2021] for a similar strategy.

7.1.2 Results of the Alaska temperature data

For this study, we run 250,000 MCMC iterations, discarding the first 125,000 iterations as burn-in. Additionally, we apply a thinning of width 5 to improve mixing of the MCMC samples. The total computation time was approximately 8 hours and 12 minutes on our desktop computer.

The trace plots for all parameters except η_3 are shown in Figure 17 in Appendix M.1. These plots do not indicate any sign of non-convergence. The HPD plots of the predictive densities for \mathbf{y}_{66} (detrended temperatures of the Alaska temperature data for the year 2015) at 26 locations are shown in Figure 4. The color intensity is proportional to the density of the predictive distributions of \mathbf{y}_{66} . The plot indicates that most true values fall within the highest density regions. We have not provided the predictive density plots of the individual components of \mathbf{y}_{66} for brevity, however, it is observed that except for one location (at 2nd location), all true values lie well within the 95% predictive intervals. The mean length of the predictive interval is 10.6387 (standard deviation=0.1).

The predictive densities, along with the highest density regions (where higher color intensity indicates

Predictive densities for 26 locations

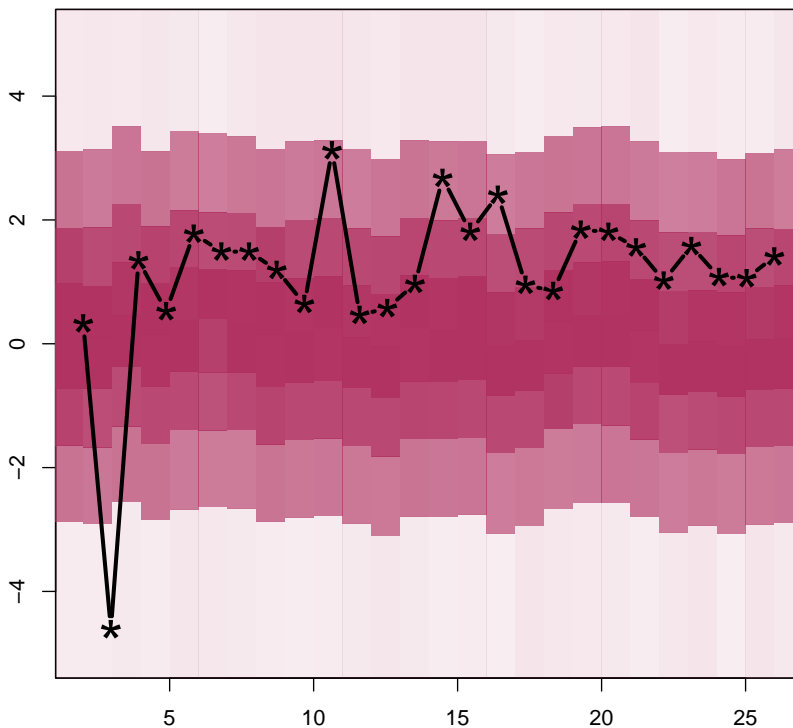


Figure 4: The highest probability density regions of the predictive densities and the true values of detrended temperatures (Alaska temperature data) for the year 2015 at 26 locations are depicted in this figure. The x-axis of the figure indicates the locations, and at each location, color-coded densities are plotted in the vertical axis. The intensity of the color is proportional to the density. The true values are indicated by the black stars. Majority of the true values fall in the high density regions.

higher density), for the years 2016–2021 at the 16 locations $L_1, \dots, L_7, L_{11}, L_{12}, L_{13}, L_{18}, L_{19}, L_{20}, L_{22}, L_{27},$ and L_{28} are shown in Figure 5. Apart from a few observations, the true values fall within high density regions.

The complete time series for the four locations, represented as blue dots in Figure 3, are reconstructed using our model. The Bayesian predictive densities at each time point for these locations are visualized in Figure 6 using probability plots, where higher color intensity indicates higher density. The available true detrended temperature values at these locations are overlaid as black stars in Figure 6. With only a few exceptions, the true detrended values fall well within the high-density regions. Overall, our model demonstrates strong performance on this dataset.

7.2 Sea surface temperature data

The sea surface temperature data is taken from <http://iridl.ldeo.columbia.edu/SOURCES/.CAC/>. For illustration, we use spatio-temporal observations from the first 40 locations and the first 100 time points. These locations range from 56°W to 110°E and 19°S to 25°N , as listed in Table 4. The dataset consists of 100 monthly average temperatures starting from January 1970. Among these, observations from the first

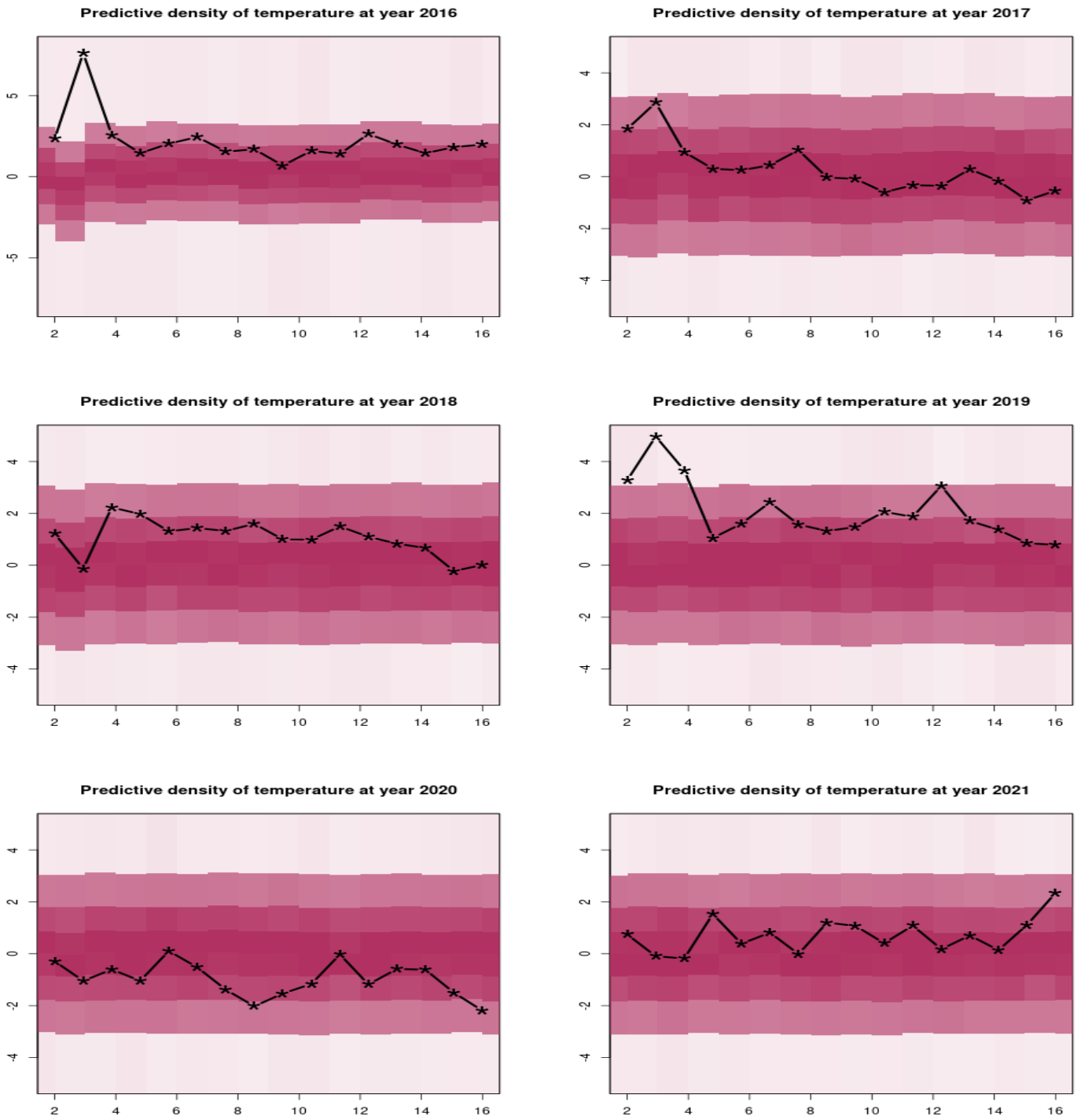


Figure 5: The highest probability density regions of the predictive densities and the true values of detrended temperatures (Alaska temperature data) for the years 2016 to 2021 at 16 locations are depicted in this figure. The x-axis of the figure indicates the locations, and at each location, color-coded densities are plotted in the vertical axis. The intensity of the color is proportional to the density. The true values are indicated by the black stars. Majority of the true values for all the 6 years fall in the high density regions.

30 locations and 99 time points form the learning set, while the last 10 locations and the final time point

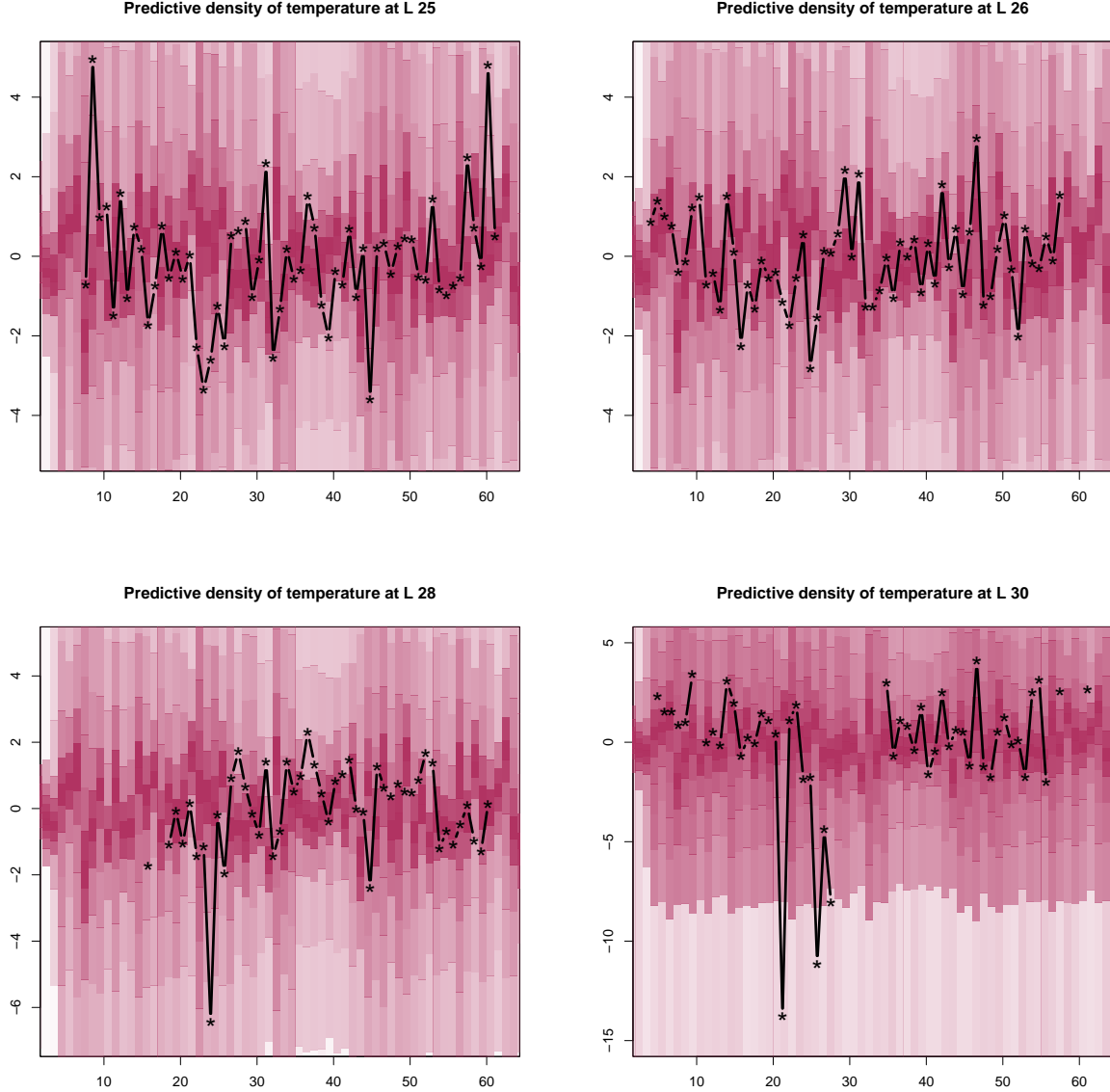


Figure 6: Posterior predictive densities of the reconstructed detrended temperature data of Alaska and its surroundings at 4 locations. Higher the intensity of the color, higher is the probability density. The black stars represent the available true temperature values (detrended). Except for a few points, majority of the true values at each location fall within the high probability density regions.

are reserved for prediction. For computational convenience, each location’s time series is mean-referenced by subtracting its mean from the original data.

Similar to the Alaska temperature data analysis, we denote the learning data set by $\mathbb{D} = \{\mathbf{y}_1, \dots, \mathbf{y}_{99}\}$, where \mathbf{y}_t is a 30 dimensional spatial observation at time point t . At these 30 locations, we obtain the posterior predictive densities for the 100th time point (see Appendix H for temporal predictive density) and find out the high probability density regions for the entire time series of the locations corresponding to the serial numbers indicated in bold within Table 4. These locations are referred to as L_{31}, \dots, L_{40} hereafter. To compute the posterior predictive densities of the entire time series for these 10 spatial locations, we follow the similar path as in the Alaska temperature data analysis. We skip the details here to avoid repetitive

Sl. No.	Lat.	Long.	Sl. No.	Lat.	Long.	Sl. No.	Lat.	Long.	Sl. No.	Lat.	Long.
1	19S	108E	11	1N	84E	21	13N	30E	31	25N	4E
2	19N	20W	12	19S	14E	22	7S	36E	32	7N	52E
3	19S	42E	13	13N	48E	23	29N	104E	33	11N	18E
4	17N	58E	14	27N	18W	24	15S	24W	34	5N	16W
5	7N	2W	15	5S	110E	25	1N	72E	35	7N	56W
6	11S	76E	16	17S	46W	26	1S	46W	36	19S	106E
7	3S	2E	17	7S	10W	27	13S	64E	37	1S	20W
8	25S	28W	18	23S	14E	28	9N	12E	38	17S	28W
9	25N	100E	19	21S	36W	29	15N	24E	39	19S	0
10	7N	26W	20	1S	28W	30	25S	52E	40	29N	48W

Table 4: Latitude and Longitude (in degrees) of 40 locations for the sea surface temperature data. The locations corresponding to the serial numbers, indicated in bold, are used for complete time series prediction. These bold serial numbers are indicated as L_{31}, \dots, L_{40} for future reference.

description. The detailed algorithm can be found in Appendix I. Notably, this sea surface temperature data originates from a non-stationary (both weakly and strongly), non-Gaussian spatio-temporal process with lagged correlations tending to zero (see Bhattacharya [2021] for further details).

7.2.1 Prior choices for sea surface temperature data

We completely specify the priors as follows:

$$\alpha_* \sim N(0, \sqrt{500}), \beta_* \sim N(0, \sqrt{300}), [\sigma^2] \propto IG(45000, 2/2), [\sigma_\theta^2] \propto IG(1000, 780/2),$$

$$[\sigma_p^2] \propto IG(100, 100/2), [\eta_1^*] \propto N(-3, 1), [\eta_2^*] \propto N(-3, 1).$$

The hyperparameters are determined by cross-validation, similar to the previous analyses. As before, we fixed η_3 at its MLE, which in this case is 5.8879, and to ensure finite posterior variances for the variance parameters, we set large shape parameters for their prior distributions.

A total of 250,000 MCMC iterations were performed, discarding the first 100,000 as burn-in. To improve mixing, a thinning interval of 5 was applied. The entire computation took approximately 12 hours and 53 minutes on our desktop computer.

7.2.2 Controlling M_s

Since the locations are widely distributed in space, the value of M_s becomes excessively large for a given s in this dataset. As M_s appears in the denominator of the variance-covariance matrix of the predictive densities of the time series at a given location (see Equation (6)), this leads to an unrealistically low variability. To address this, we redefine M_s as $M_s = \exp(c \max \{ \|s^2 - u^2\|^2 : u \in S \})$, where c is a small positive constant. This modification preserves all theoretical properties of M_s , ensuring the process characteristics remain unchanged. The constant c serves as a spatial variability control parameter, acting as a distance scaling factor. The optimal choice of c was determined via cross-validation, with $c = 0.25$ yielding reasonable performance for the sea surface temperature data.

7.2.3 Results of the sea surface temperature data

Figure 18 of Appendix N.1, representing the MCMC trace plots of the parameters, exhibits no evidence of non-convergence of our MCMC algorithm.

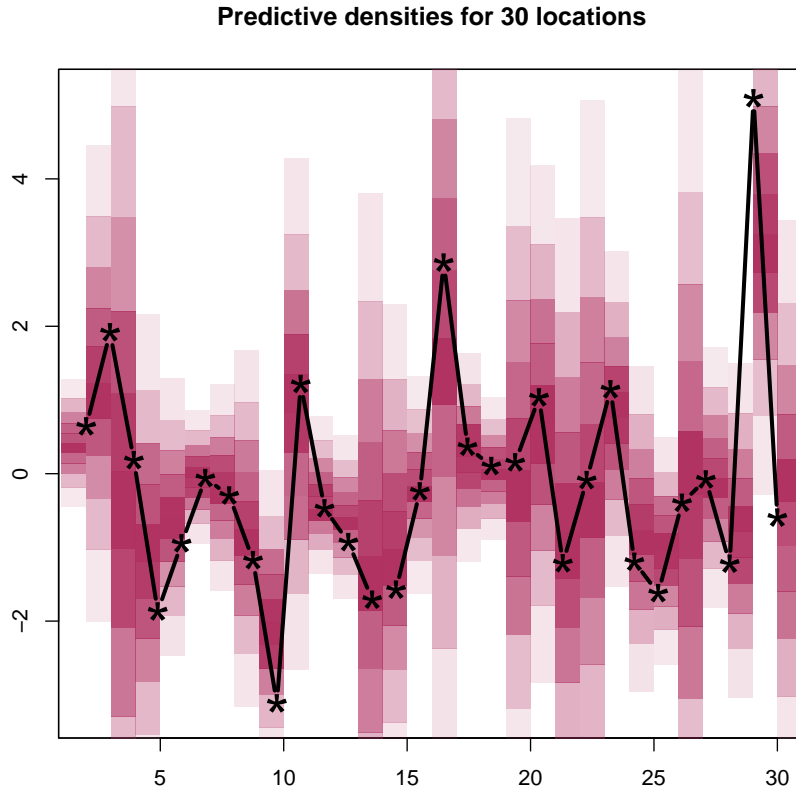


Figure 7: The highest probability density regions of the predictive densities and the true values of sea surface temperature data for the 100th month at 30 locations are depicted in this figure. The x-axis of the figure indicates the locations, and at each location, color-coded densities are plotted in the vertical axis. The intensity of the color is proportional to the density. The true values are indicated by the black stars. Majority of the true values (average referenced) fall in the high density regions.

Next, we provide the posterior predictive densities at the 100th month for each of the 30 locations, following the algorithm of temporal predictive densities given in the Appendix H. The highest predictive density regions for these 30 locations are shown in Figure 7, where most of the true values fall in the high probability density regions. The individual predictive densities along with the 95% predictive intervals indicate the posterior predictive densities correctly contain the true values at all locations (plots are not shown for brevity). The average length of the 95% predictive intervals is 8.3161 (standard deviation = 4.8172).

Similar to previous real data analyses, we perform spatial predictions in this study. As outlined in Section 7.2, we set aside the complete temporal observations for ten locations to evaluate our model's performance. For each of these locations, we obtained the posterior predictive densities for all 99 time points (see Appendix I for the algorithm). The highest density regions of the predictive densities are depicted in Figures 8 and 9. As evident from the figure, most of the true values fall in the high probability

density regions, further validating the effectiveness of our model.

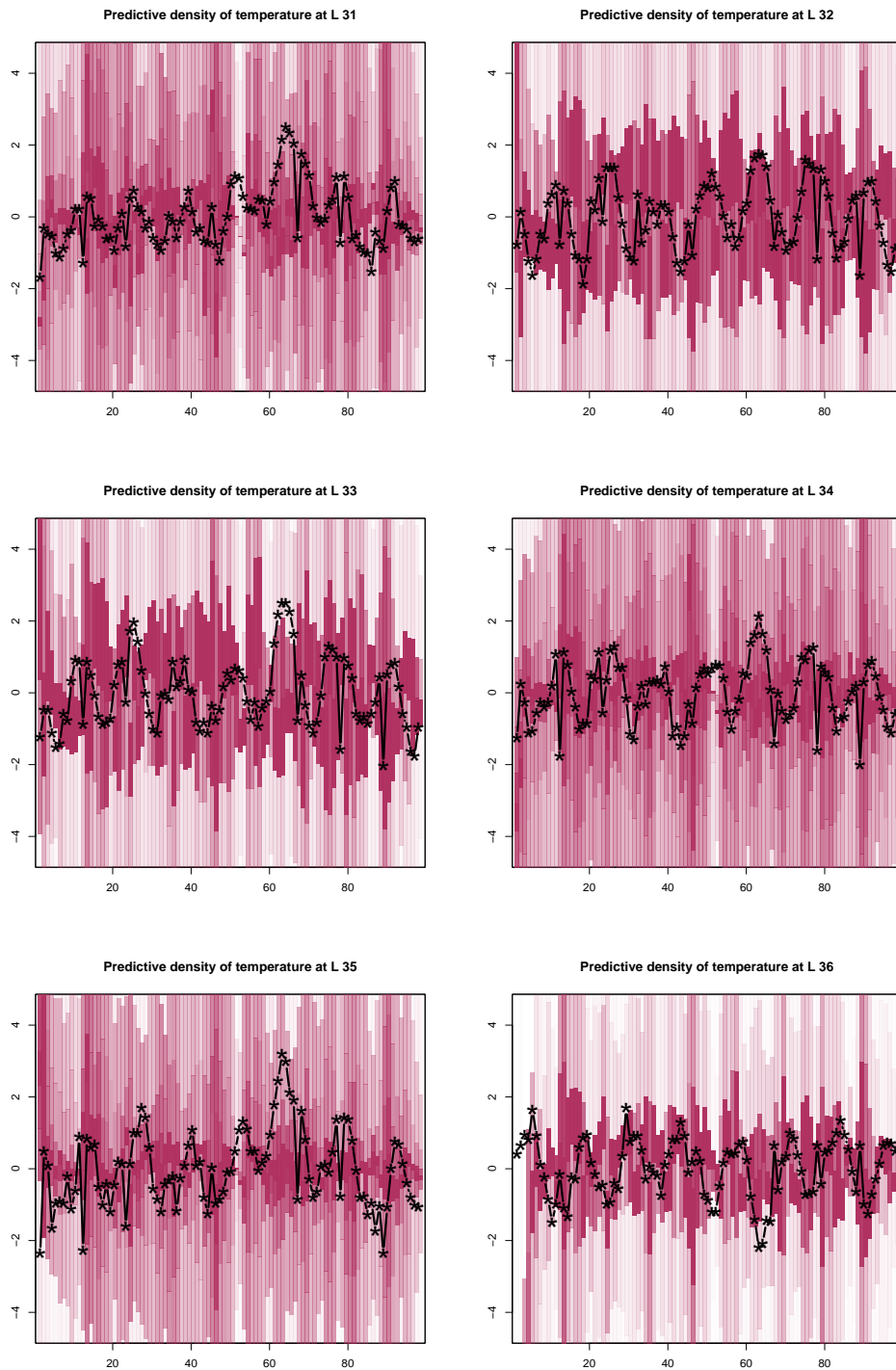


Figure 8: Posterior predictive densities of the reconstructed time series of sea surface temperature data (average referenced) at 6 locations. Higher the intensity of the color, higher is the probability density. The black stars represent the true temperature values (average referenced). Most of the true values fall within the high density regions.

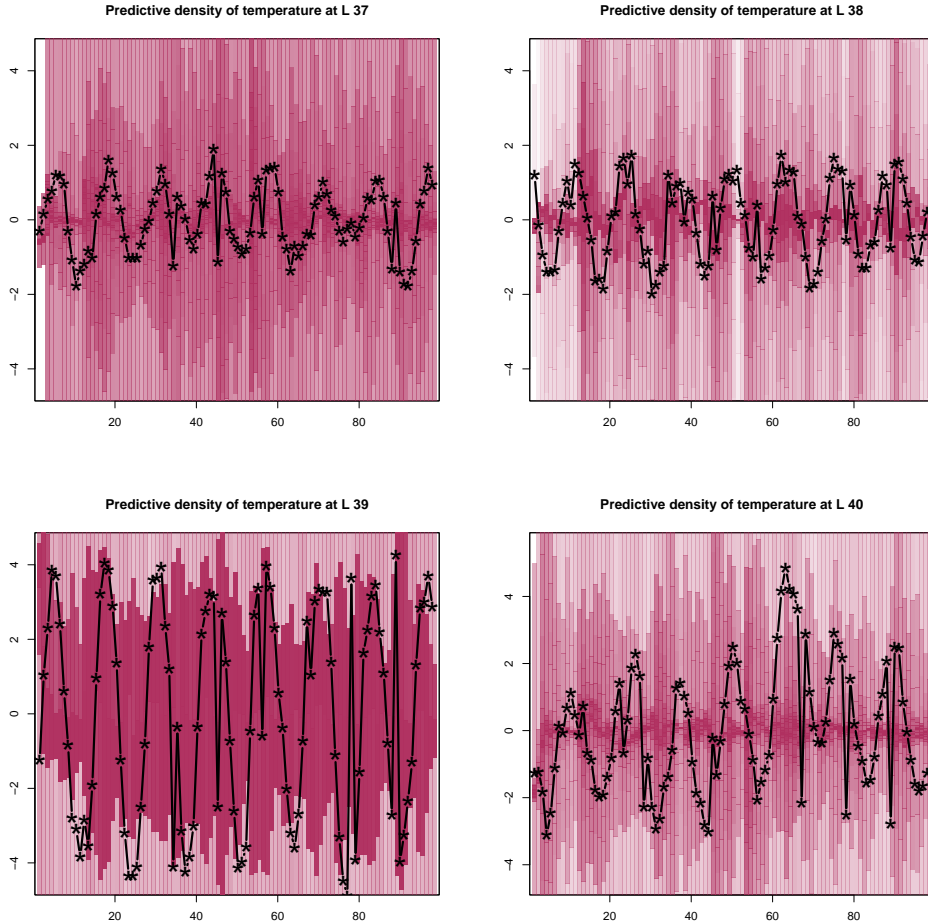


Figure 9: Posterior predictive densities of the reconstructed time series of sea surface temperature data (average referenced) at another 4 locations. Higher the intensity of the color, higher is the probability density. The black stars represent the true temperature values (average referenced). Most of the true values fall within the high density regions.

8 Summary and conclusion

Although Hamiltonian equations are well-known in physics, their role in statistics has primarily been limited to Hamiltonian Monte Carlo for approximate posterior simulations. However, given their success in phase-space modeling, it is natural to anticipate their potential in spatio-temporal statistics if properly utilized. This key insight motivated us to develop a novel spatio-temporal model based on the leap-frog algorithm applied to a suitably modified set of Hamiltonian equations, where stochasticity is induced through appropriate Gaussian processes.

Our marginal stochastic process is *nonparametric, non-Gaussian, non-stationary, and non-separable*, with a well-structured dynamic temporal component and continuous-time treatment. Additionally, the lagged correlations between observations decay to zero as the space-time lag approaches infinity, making our process more realistic compared to existing spatio-temporal non-stationary models. Simulation studies demonstrate that our model consistently outperforms the widely used latent process spatio-temporal modeling approach based on non-stationary Gaussian processes. Furthermore, the model’s flexibility and applicability are confirmed by its strong performance on two real datasets. The continuity and smoothness

properties further enhance the elegance of our proposed process.

In all simulations and real data analyses, we assume evenly spaced time points. However, our model can be readily adapted to unevenly spaced time points with minimal modifications. We propose such a modification in Section J of Appendix. We shall elaborate with simulation and real data analyses in a later work.

In this study, we have not focused on analyzing particularly large datasets. In future work, we plan to extend our approach to massive datasets using basis function representations and a transdimensional MCMC technique known as TTMC, introduced by Das and Bhattacharya [2019].

Acknowledgment

The authors are thankful to Dr. Moumita Das and Dr. Suman Guha for their valuable remarks, which significantly improved the presentation of the manuscript. During the preparation of this work the authors used ChatGPT in order to improve the English writing solely. After using this tool, the authors reviewed and edited the content as needed and take full responsibility for the content of the publication.

A Derivation of equations 3 and 4

Here we show how the equations 3 and 4 are obtained using Leap-frog algorithm on modified Hamiltonian equation 2. From equation 2 we have $\frac{dy(s,t)}{dt} = \beta^*y(s,t) + M_s^{-1}x(s,t)$ and applying Leap-frog (Young [2014]) on $y(s, \cdot)$, we get

$$\begin{aligned} y(s, t + \delta t) &= y(s, t) + \beta^*y(s, t)\delta t + \delta t M_s^{-1}x(s, t + \delta t/2) \\ &= y(s, t) (1 + \beta^*\delta t) + \delta t M_s^{-1}x(s, t + \delta t/2) \\ &= \beta y(s, t) + \delta t M_s^{-1}x(s, t + \delta t/2), \end{aligned} \tag{13}$$

where $\beta = (1 + \beta^*\delta t)$. We set $|\beta| < 1$, which implies $-2 < \beta^*\delta t < 0$. From equation 2, we obtain $\frac{dx(s,t)}{dt} = \alpha^*x(s,t) - \nabla V(y(s,t))$, and a numerical approximation for $x(s, \cdot)$ is given as:

$$\begin{aligned} x\left(s, t + \frac{\delta t}{2}\right) &= x(s, t) + \alpha^*x(s, t)\frac{\delta t}{2} - \nabla V(y(s, t))\frac{\delta t}{2} \\ &= x(s, t) \left(1 + \alpha^*\frac{\delta t}{2}\right) - \nabla V(y(s, t))\frac{\delta t}{2} \\ &= \alpha x(s, t) - \nabla V(y(s, t))\frac{\delta t}{2}, \end{aligned} \tag{14}$$

where $\alpha = (1 + \alpha^*\delta t/2)$. We set $|\alpha| < 1$ implying $-2 < \alpha^*\delta t/2 < 0$. Replacing equation (14) into equation (13), we obtain equation 3 of Section 2.1 as

$$\theta(t + \delta t) = \beta\theta(t) + \delta t M^{-1} \left(\alpha p(t) - \nabla V(\theta(t))\frac{\delta t}{2} \right).$$

Again, invoking leap-frog algorithm for $x(s, \cdot)$ [Young, 2014], we get 4 of Section 2.1 as

$$x(s, t + \delta t) = x\left(s, t + \frac{\delta t}{2}\right) + \alpha^*x\left(s, t + \frac{\delta t}{2}\right)\frac{\delta t}{2} - \nabla V(y(s, t + \delta t))\frac{\delta t}{2}$$

$$\begin{aligned}
&= x \left(s, t + \frac{\delta t}{2} \right) \left(1 + \alpha^* \frac{\delta t}{2} \right) - \nabla V(y(s, t + \delta t)) \frac{\delta t}{2} \\
&= \alpha x \left(s, t + \frac{\delta t}{2} \right) - \nabla V(y(s, t + \delta t)) \frac{\delta t}{2} \\
&= \alpha \left(\alpha x(s, t) - \nabla V(y(s, t)) \frac{\delta t}{2} \right) - \nabla V(y(s, t + \delta t)) \frac{\delta t}{2} \text{ (using equation 14)} \\
&= \alpha^2 x(s, t) - \frac{\delta t}{2} \{ \alpha \nabla V(y(s, t)) + \nabla V(y(s, t + \delta t)) \}.
\end{aligned}$$

B Correlation analysis of GQN model

We performed two simulation studies on the GQN model, taking large temporal and spatial lags, which shows no evidence of correlation going to zero. To obtain the lagged spatial correlations, we simulated 100 spatio-temporal observations from the GQN model independently with five time points and 100 locations; to obtain lagged temporal correlations, we simulated spatio-temporal observations from the same model with 100 time points and 5 locations. We provide five lagged spatial correlation plots corresponding to five time points, each containing five locations (10). Similarly, we provide five lagged temporal correlation plots corresponding to five locations containing five different time points (11).

C Spatial correlation plots

We compared the spatial correlations of our model with that of squared exponential and Matérn spatial correlation using simulations. We simulated spatio-temporal observations 1000 times from our model taking $\eta_1 = \eta_2 = \eta_3 = 1$, $\sigma^2 = \sigma_\theta^2 = \sigma_p^2 = 1$, $\alpha = \beta = 0.9$. The number of locations and time points are taken to be 10 and 4, respectively. Based on 1000 simulations we calculated the sample spatial correlation matrix. Similarly, we simulated spatio-temporal observations from a Gaussian process with zero mean and squared exponential kernel with variance and decaying parameter 1. The corresponding sample spatial correlation matrix is calculated based on the 1000 repetitions. The same exercise has been performed by replacing the squared exponential kernel with two Matérn covariance kernels, namely, Matérn(3/2) and Matérn(5/2), respectively. The range parameter for the Matérn covariance kernel is taken as 1 for both the cases. The sample spatial correlations are provided in Figure 12.

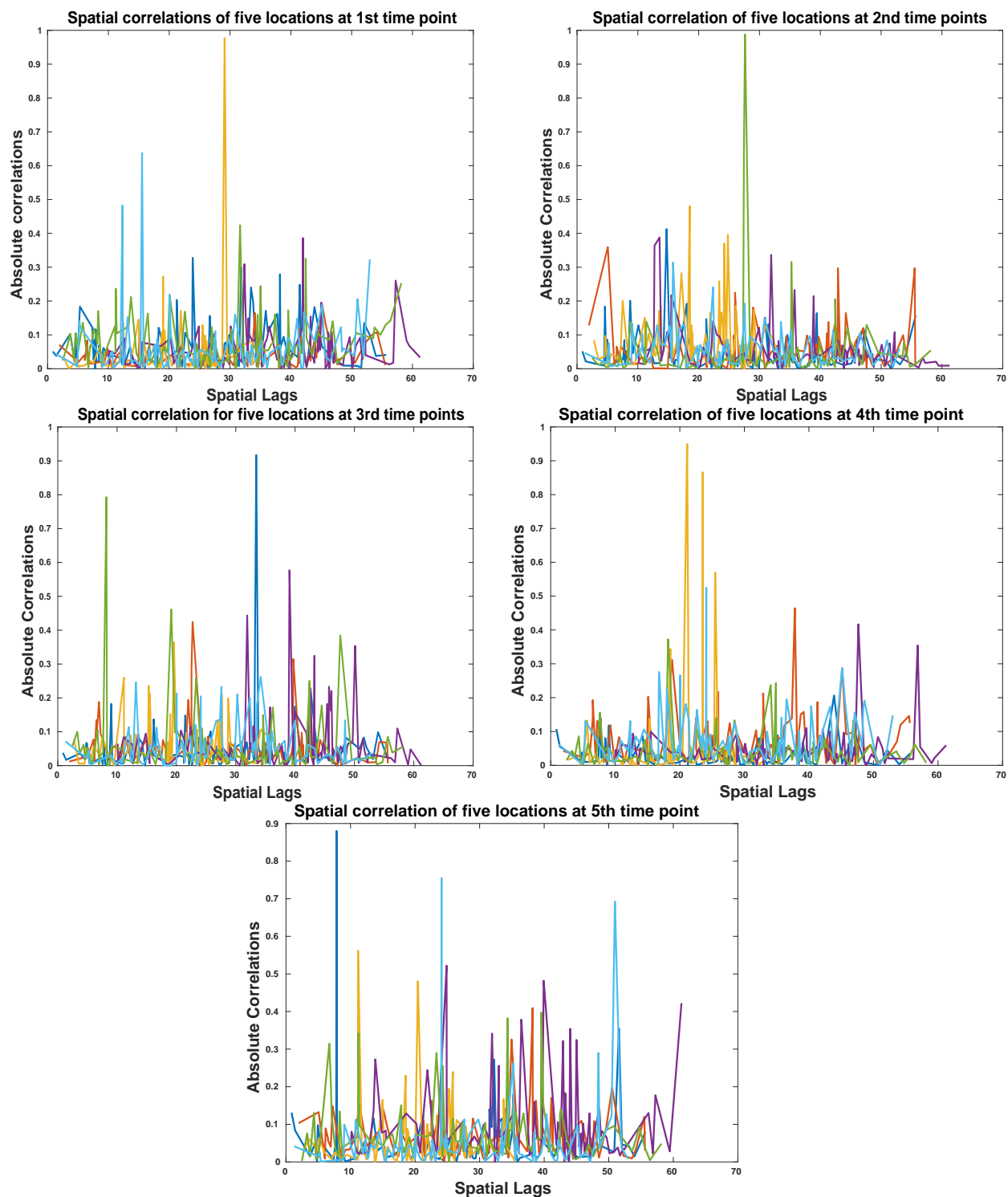


Figure 10: Spatial correlation plots at 5 times points using observations simulated from the GQN model are depicted. x-axis and y-axis denote the spatial lags and the correlations, respectively. The five different colors indicate 5 locations in each plot.

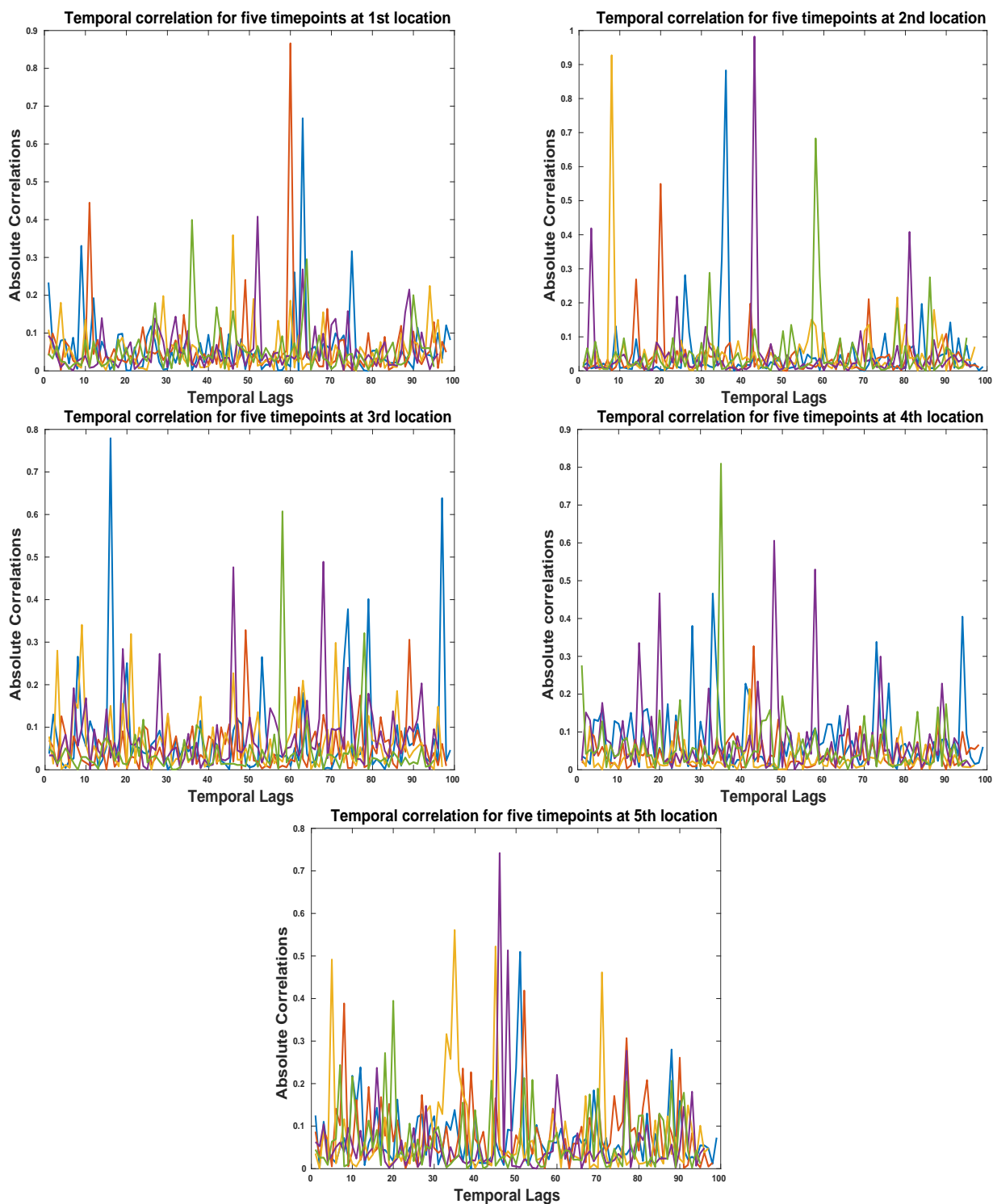
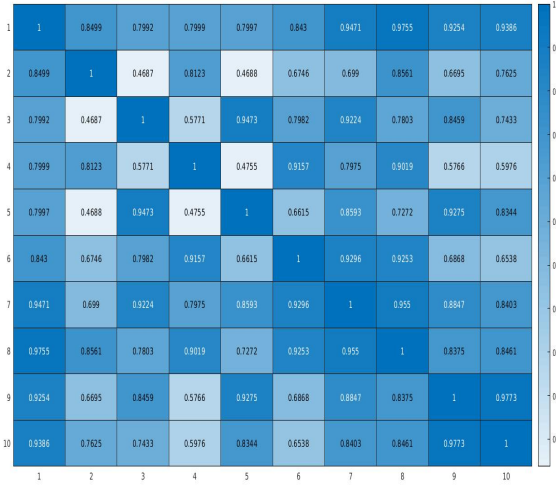
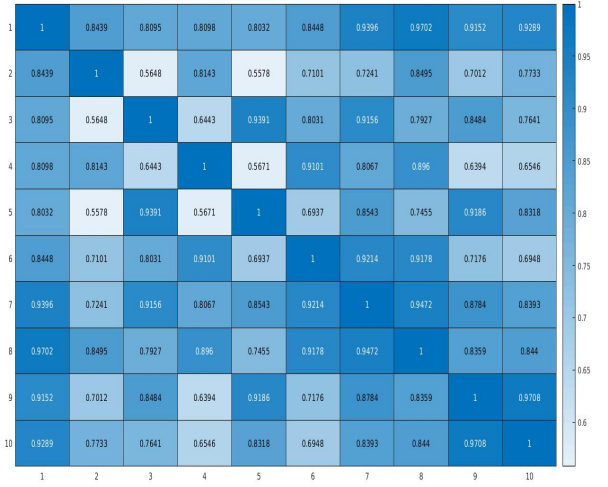


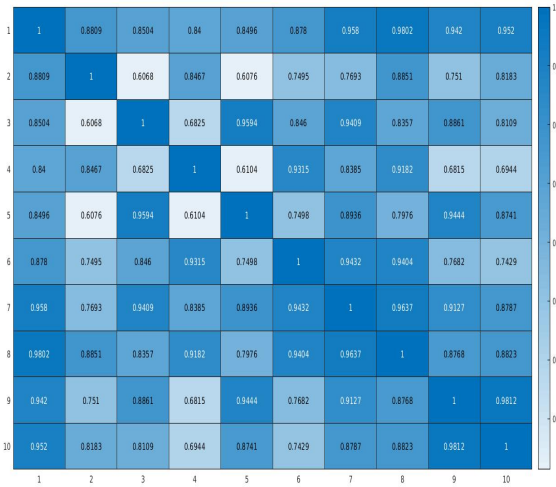
Figure 11: Temporal correlation plots at 5 locations using the observations simulated from GQN model are depicted. x-axis and y-axis denote the temporal lags and the correlations, respectively. The five different colors denote 5 time points in each plots.



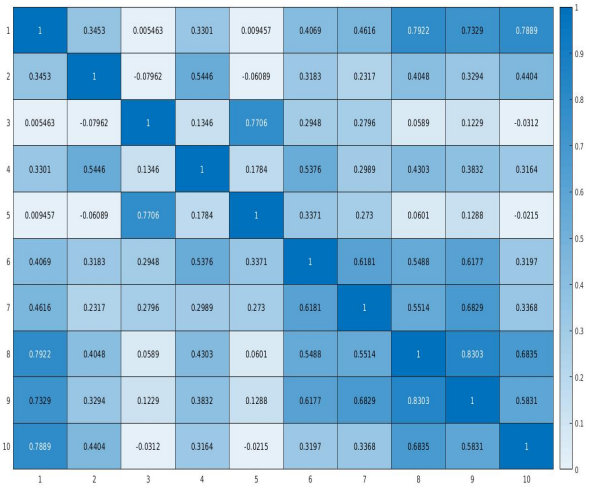
(a)



(b)



(c)



(d)

Figure 12: The figure depicts examples of spatial correlation matrices for four different models. The x-axis and the y-axis represent the indices of the locations. Higher color intensity represents larger correlation. Plot (a) shows spatial correlations obtained from a squared exponential covariance kernel with variance and decay parameter 1, abbreviated as SE(1,1). Plots (b) and (c) depict spatial correlations for Matérn(3/2) and Matérn(5/2) with range parameter 1. Finally plot (d) shows spatial correlations for the proposed model, with $\eta_1 = \eta_2 = \eta_3 = 1$, $\sigma^2 = \sigma_\theta^2 = \sigma_p^2 = 1$, $\alpha = \beta = 0.9$. Our model can have negative entries in a correlation matrix whereas the correlation matrices for the other models are always positive.

D Proofs of our results

This appendix contains proofs of all the relevant results presented in Section 2.2.

Lemma D.1 M_s is infinitely differentiable in $s \in S$.

Proof: Since the exponential function is infinitely differentiable, it is sufficient to show that $\max\{|s^2 - u^2|^2 : u \in S\}$ is infinitely differentiable with respect to s . We first prove the result in one dimension and then will generalize to higher dimension. Let S be a compact set in \mathbb{R} . We consider different cases as follows.

Case 1: Let $S = [a, b]$, where $0 < a < b$. Then $\max\{|s^2 - u^2|^2 : u \in [a, b]\} = s^4 + \max(a^4, b^4) - 2s^2a^2$, which is an infinitely smooth function of s .

Case2: Let $S = [a, b]$, where $a < b < 0$. Then $\max\{|s^2 - u^2|^2 : u \in [a, b]\} = s^4 + \max(a^4, b^4) - 2s^2b^2$, which is also infinitely differentiable function of s .

Case 3: Let $S = [-a, b]$, where $a, b > 0$. Then

$$\max\{|s^2 - u^2|^2 : u \in [-a, b]\} = s^4 + \max(a^4, b^4) - 2s^2 \min(a^2, b^2) \quad (15)$$

Clearly, $\max\{|s^2 - u^2|^2 : u \in [-a, b]\}$ is infinitely differentiable function of s , for any $s \in [-a, b]$.

Now suppose that $S = [-a_1, b_1] \times [-a_2, b_2]$, where a_i, b_i are positive for each $i = 1, 2$. Let $s \in S$. Define $f_s : S \rightarrow \mathbb{R}$, such that $f_s(u) = |s^2 - u^2|^2 = (s_1^2 - u_1^2)^2 + (s_2^2 - u_2^2)^2$. Define $f_{1s}(u_1) = (s_1^2 - u_1^2)^2$ and $f_{2s}(u_2) = (s_2^2 - u_2^2)^2$. Therefore, $f_s(u) = f_{1s}(u_1) + f_{2s}(u_2)$ and $\max_{u \in S} f_s(u) = \max_{u \in S} [f_{1s}(u_1) + f_{2s}(u_2)] = \max_{u_1 \in [-a_1, b_1]} f_{1s}(u_1) +$

$\max_{u_2 \in [-a_2, b_2]} f_{2s}(u_2)$. The equality follows as $u = (u_1, u_2) \in S$, with $u_1 \in [-a_1, b_1]$ and $u_2 \in [-a_2, b_2]$. We have already proved that (Case 3, equation (15)) $\max_{u_i \in [-a_i, b_i]} f_{is}(u_i) = s_i^4 + \max(a_i^4, b_i^4) - 2s_i^2 \min(a_i^2, b_i^2)$ for $i = 1, 2$.

Hence $\max_{u \in S} f_s(u) = \sum_{i=1}^2 s_i^4 + \max(a_i^4, b_i^4) - 2s_i^2 \min(a_i^2, b_i^2)$, which is infinitely differentiable with respect to s_1 and s_2 .

If $S = [a_1, b_1] \times [a_2, b_2]$ where (i) $0 < a_1 < b_1$ and $0 < a_2 < b_2$ or (ii) $a_1 < b_1 < 0$ and $a_2 < b_2 < 0$ or (iii) $0 < a_1 < b_1$ and $a_2 < b_2 < 0$ or (iv) $a_1 < b_1 < 0$ and $0 < a_2 < b_2$, the proof goes in a similar manner as above except that now we have to use Case 1 and Case 2 for one dimension, instead of Case 3. \square

In the proofs of the theorems and lemmas that follow, we denote $Y(s, t)$ by $\theta_s(t)$ and $X(s, t)$ by $p_s(t)$, for any $s \in S$, and $t \in [0, \infty)$.

Theorem D.1 Under assumptions A1 to A3, $\text{cov}(Y(s, h\delta t), Y(s', h'\delta t))$ converges to 0 as $\|s - s'\| \rightarrow \infty$ and/or $|h - h'| \rightarrow \infty$.

Proof: First we shall show that

$$\text{cov}\left(\theta_s(h\delta t), \theta_{s'}(h'\delta t) \middle| p\right) \rightarrow 0,$$

as $\|s - s'\| \rightarrow \infty$ and/or $|h - h'| \rightarrow \infty$. Without loss of generality let us assume that $h > h'$. Now

$$\begin{aligned} & \text{cov}\left(\theta_s(h\delta t), \theta_{s'}(h'\delta t) \middle| p\right) \\ &= \text{cov}\left(\beta\theta_s((h-1)\delta t) + \frac{\delta t}{M_s} \left\{ \alpha p_s((h-1)\delta t) - \frac{\delta t}{2} \frac{\partial}{\partial \theta_s} V(\theta_s((h-1)\delta t)) \right\}, \theta_{s'}(h'\delta t) \middle| p\right) \\ &= \text{cov}(\beta\theta_s((h-1)\delta t), \theta_{s'}(h'\delta t) \middle| p) - \frac{1}{2} \frac{(\delta t)^2}{M_s} \text{cov}\left(\frac{\partial}{\partial \theta_s} V(\theta_s((h-1)\delta t)), \theta_{s'}(h'\delta t) \middle| p\right) \\ &= \dots \end{aligned}$$

$$= \beta^{h-h'} \text{cov}(\theta_s(h'\delta t), \theta_{s'}(h'\delta t)|p) - \frac{1}{2} \frac{(\delta t)^2}{M_s} \sum_{k=1}^{h-h'} \beta^{k-1} \text{cov} \left[\frac{\partial}{\partial \theta_s} V(\theta_s((h-k)\delta t)), \theta_{s'}(h'\delta t)|p \right]. \quad (16)$$

Since, for any $1 \leq \ell \leq h - h'$,

$$\begin{aligned} & \text{cov} \left(\frac{\partial}{\partial \theta_s} V(\theta_s((h-\ell)\delta t)), \theta_{s'}(h'\delta t) \middle| p \right) \\ &= \text{cov} \left(\frac{\partial}{\partial \theta_s} V(\theta_s((h-\ell)\delta t)), \beta \theta_{s'}((h'-1)\delta t) + \frac{\delta t}{M_{s'}} \left\{ \alpha p_s((h'-1)\delta t) - \frac{\delta t}{2} \frac{\partial}{\partial \theta_{s'}} V(\theta_s((h'-1)\delta t)) \right\} \middle| p \right) \\ &= \beta \text{cov} \left(\frac{\partial}{\partial \theta_s} V(\theta_s((h-\ell)\delta t)), \theta_{s'}((h'-1)\delta t) \middle| p \right) - \frac{(\delta t)^2}{2M_{s'}} \text{cov} \left(\frac{\partial}{\partial \theta_s} V(\theta_s((h-\ell)\delta t)), \frac{\partial}{\partial \theta_{s'}} \right. \\ & \quad \left. V(\theta_{s'}((h-1)\delta t)) \middle| p \right) \\ &= \dots \\ &= \beta^{h'} \text{cov} \left(\frac{\partial}{\partial \theta_s} V(\theta_s((h-\ell)\delta t)), \theta_{s'}(0) \middle| p \right) - \frac{(\delta t)^2}{2M_{s'}} \sum_{k=1}^{h'} \beta^{k-1} \text{cov} \left(\frac{\partial}{\partial \theta_s} V(\theta_s((h-\ell)\delta t)), \frac{\partial}{\partial \theta_{s'}} \right. \\ & \quad \left. V(\theta_{s'}((h-k)\delta t)) \middle| p \right), \end{aligned}$$

we have,

$$\begin{aligned} & \left| \text{cov} \left(\frac{\partial}{\partial \theta_s} V(\theta_s((h-\ell)\delta t)), \theta_{s'}(h'\delta t) \middle| p \right) \right| \\ & \leq \left| \beta^{h'} \text{cov} \left(\frac{\partial}{\partial \theta_s} V(\theta_s((h-\ell)\delta t)), \theta_{s'}(0) \middle| p \right) \right| + \frac{(\delta t)^2}{2M_{s'}} \sum_{k=1}^{h'} \left| \beta^{k-1} \text{cov} \left[\frac{\partial}{\partial \theta_s} V(\theta_s((h-\ell)\delta t)), \frac{\partial}{\partial \theta_{s'}} \right. \right. \\ & \quad \left. \left. V(\theta_{s'}((h-k)\delta t)) \right] \right| \\ & \leq |\beta|^{h'} \sigma_\theta \sigma + \frac{1 - |\beta|^{h'}}{1 - |\beta|} \frac{(\delta t)^2}{2M_{s'}} \sigma^2 = \epsilon, \text{ say,} \end{aligned} \quad (17)$$

where σ^2 and σ_θ^2 are the variance terms of the processes $\frac{\partial}{\partial \theta_s} V(\theta_s(h-1)\delta t)$ and $\theta_s(0)$, respectively (see A2 and A3). Therefore, from Equation (16) we obtain

$$\begin{aligned} & \left| \text{cov}(\theta_s(h\delta t), \theta_{s'}(h'\delta t)|p) - \beta^{h-h'} \text{cov}(\theta_s(h'\delta t), \theta_{s'}(h'\delta t)|p) \right| \\ & \leq \frac{1}{2} \frac{(\delta t)^2}{M_s} \sum_{k=1}^{h-h'} |\beta|^{k-1} \left| \text{cov} \left[\frac{\partial}{\partial \theta_s} V(\theta_s((h-k)\delta t)), \theta_{s'}(h'\delta t) \middle| p \right] \right| \\ & \leq \frac{1}{2} \frac{(\delta t)^2}{M_s} \frac{1 - |\beta|^{h-h'}}{1 - |\beta|} \epsilon, \end{aligned} \quad (18)$$

using equation (17). Now from the first term of the right hand side of equation (16), we obtain

$$\text{cov}(\theta_s(h'\delta t), \theta_{s'}(h'\delta t)|p)$$

$$\begin{aligned}
&= \text{cov} \left(\beta \theta_s((h' - 1)\delta t) + \frac{\delta t}{M_s} \left\{ \alpha p_s((h' - 1)\delta t) - \frac{\delta t}{2} \frac{\partial}{\partial \theta_s} V(\theta_s((h' - 1)\delta t)) \right\}, \right. \\
&\quad \left. \beta \theta_{s'}((h' - 1)\delta t) + \frac{\delta t}{M_{s'}} \left\{ \alpha p_{s'}((h' - 1)\delta t) - \frac{\delta t}{2} \frac{\partial}{\partial \theta_{s'}} V(\theta_{s'}((h' - 1)\delta t)) \right\} \middle| p \right) \\
&= \beta^2 \text{cov} \left(\theta_s((h' - 1)\delta t), \theta_{s'}((h' - 1)\delta t) \middle| p \right) - \beta \frac{1}{2} \frac{(\delta t)^2}{M_{s'}} \text{cov} \left(\theta_s((h' - 1)\delta t), \frac{\partial}{\partial \theta_{s'}} V(\theta_{s'}((h' - 1)\delta t)) \middle| p \right) \\
&\quad - \beta \frac{1}{2} \frac{(\delta t)^2}{M_s} \text{cov} \left(\theta_{s'}((h' - 1)\delta t), \frac{\partial}{\partial \theta_s} V(\theta_s((h' - 1)\delta t)) \middle| p \right) + \frac{1}{4} \frac{(\delta t)^4}{M_s M_{s'}} \text{cov} \left(\frac{\partial}{\partial \theta_s} V(\theta_s((h' - 1)\delta t)), \right. \\
&\quad \left. \frac{\partial}{\partial \theta_{s'}} V(\theta_{s'}((h' - 1)\delta t)) \middle| p \right) \\
&= \dots \\
&= \beta^{2h'} \text{cov} \left(\theta_s(0), \theta_{s'}(0) \middle| p \right) - \frac{(\delta t)^2}{2M_{s'}} \sum_{k=1}^{h'} \beta^{2k-1} \text{cov} \left(\theta_s((h' - k)\delta t), \frac{\partial}{\partial \theta_{s'}} V(\theta_{s'}((h' - k)\delta t)) \middle| p \right) \\
&\quad - \frac{(\delta t)^2}{2M_s} \sum_{k=1}^{h'} \beta^{2k-1} \text{cov} \left(\theta_{s'}((h' - k)\delta t), \frac{\partial}{\partial \theta_s} V(\theta_s((h' - k)\delta t)) \middle| p \right) + \frac{1}{4} \frac{(\delta t)^4}{M_s M_{s'}} \sum_{k=1}^{h'} \beta^{2(k-1)} \times \\
&\quad \text{cov} \left(\frac{\partial}{\partial \theta_s} V(\theta_s((h' - k)\delta t)), \frac{\partial}{\partial \theta_{s'}} V(\theta_{s'}((h' - k)\delta t)) \middle| p \right),
\end{aligned}$$

which in turn implies

$$\begin{aligned}
&\left| \text{cov} \left(\theta_s(h'\delta t), \theta_{s'}(h'\delta t) \middle| p \right) - \beta^{2h'} \text{cov} \left(\theta_s(0), \theta_{s'}(0) \middle| p \right) \right| \\
&\leq \frac{(\delta t)^2}{2M_{s'}} \sum_{k=1}^{h'} |\beta|^{2k-1} \left| \text{cov} \left(\theta_s((h' - k)\delta t), \frac{\partial}{\partial \theta_{s'}} V(\theta_{s'}((h' - k)\delta t)) \middle| p \right) \right| + \frac{(\delta t)^2}{2M_s} \sum_{k=1}^{h'} |\beta|^{2k-1} \times \\
&\quad \left| \text{cov} \left(\theta_{s'}((h' - k)\delta t), \frac{\partial}{\partial \theta_s} V(\theta_s((h' - k)\delta t)) \middle| p \right) \right| + \frac{1}{4} \frac{(\delta t)^4}{M_s M_{s'}} \sum_{k=1}^{h'} |\beta|^{2(k-1)} \left| \text{cov} \left(\frac{\partial}{\partial \theta_s} V(\theta_s((h' - k)\delta t)), \right. \right. \\
&\quad \left. \left. \frac{\partial}{\partial \theta_{s'}} V(\theta_{s'}((h' - k)\delta t)) \middle| p \right) \right| \leq \frac{(\delta t)^2}{2M_{s'}} \sum_{k=1}^{h'} |\beta|^{2k-1} \epsilon + \frac{(\delta t)^2}{2M_s} \sum_{k=1}^{h'} |\beta|^{2k-1} \epsilon + \frac{1}{4} \frac{(\delta t)^4}{M_s M_{s'}} \sum_{k=1}^{h'} |\beta|^{2(k-1)} \sigma^2 \\
&\leq \frac{(\delta t)^2}{2M_{s'}} |\beta| \frac{1 - |\beta|^{2h'}}{1 - |\beta|^2} \epsilon + \frac{(\delta t)^2}{2M_s} |\beta| \frac{1 - |\beta|^{2h'}}{1 - |\beta|^2} \epsilon + \frac{1}{4} \frac{(\delta t)^4}{M_s M_{s'}} \frac{1 - |\beta|^{2h'}}{1 - |\beta|^2} \sigma^2. \tag{19}
\end{aligned}$$

From equations (18) and (19), we get

$$\begin{aligned}
&\left| \text{Cov} \left[\theta_s(h\delta t), \theta_{s'}(h'\delta t) \middle| p \right] - \beta^{(h-h')+2h'} \text{cov} \left(\theta_s(0), \theta_{s'}(0) \middle| p \right) \right| \\
&\leq \left| \text{Cov} \left[\theta_s(h\delta t), \theta_{s'}(h'\delta t) \middle| p \right] - \beta^{h-h'} \text{Cov} \left[\theta_s(h'\delta t), \theta_{s'}(h'\delta t) \middle| p \right] \right| + |\beta|^{h-h'} \left| \text{Cov} \left[\theta_s(h'\delta t), \theta_{s'}(h'\delta t) \middle| p \right] - \right. \\
&\quad \left. \beta^{2h'} \text{cov} \left(\theta_s(0), \theta_{s'}(0) \middle| p \right) \right|
\end{aligned}$$

$$\leq \frac{1}{2} \frac{(\delta t)^2}{M_s} \frac{1 - |\beta|^{h-h'}}{1 - |\beta|} \epsilon + |\beta|^{h-h'} \left\{ \frac{(\delta t)^2}{2M_{s'}} |\beta| \frac{1 - |\beta|^{2h'}}{1 - |\beta|^2} \epsilon + \frac{(\delta t)^2}{2M_s} |\beta| \frac{1 - |\beta|^{2h'}}{1 - |\beta|^2} \epsilon + \frac{1}{4} \frac{(\delta t)^4}{M_s M_{s'}} \frac{1 - |\beta|^{2h'}}{1 - |\beta|^2} \sigma^2 \right\}, \quad (20)$$

which goes to 0 as $|h - h'| \rightarrow \infty$ and/or $\|s - s'\| \rightarrow \infty$, under assumptions A1-A3 in conjunction with Remark 3. Writing $\left| \text{Cov} \left[\theta_s(h\delta t), \theta_{s'}(h'\delta t) \middle| p \right] \right|$ as $\left| \text{Cov} \left[\theta_s(h\delta t), \theta_{s'}(h'\delta t) \middle| p \right] - \beta^{(h-h')+2h'} \text{Cov} \left[\theta_s(0), \theta_{s'}(0) \middle| p \right] + \beta^{(h-h')+2h'} \text{Cov} \left[\theta_s(0), \theta_{s'}(0) \middle| p \right] \right|$ and noting that $\left| \beta^{(h-h')+2h'} \text{Cov} \left[\theta_s(0), \theta_{s'}(0) \middle| p \right] \right|$ is $|\beta|^{(h-h')} |\beta|^{2h'} \sigma_\theta^2 \exp \{-\eta_2 \|s_1 - s_2\|^2\}$ (by assumption A2), we have

$$\text{cov} \left(\theta_s(h\delta t), \theta_{s'}(h'\delta t) \middle| p \right) \rightarrow 0,$$

as $\|s - s'\| \rightarrow \infty$ and/or $|h - h'| \rightarrow \infty$. Now the dominated convergence theorem indicates that the unconditional covariance $\text{cov} (Y(s, h\delta t), Y(s', h'\delta t)) \rightarrow 0$ as $\|s - s'\| \rightarrow \infty$ and $|h - h'| \rightarrow \infty$. \square

Theorem D.2 *If the assumptions A1-A3 hold true, then $Y(s, h\delta t)$ and $X(s, h\delta t)$ are continuous in s , for all $h \geq 1$, with probability 1.*

Proof: Note that, for $h \geq 1$,

$$\theta_s(h\delta t) = \beta \theta_s((h-1)\delta t) + \frac{\delta t}{M_s} \left\{ \alpha p_s((h-1)\delta t) - \frac{\delta t}{2} \frac{\partial}{\partial \theta_s} V(\theta_s((h-1)\delta t)) \right\} \quad \text{and} \quad (21)$$

$$p_s(h\delta t) = \alpha^2 p_s((h-1)\delta t) - \frac{\delta t}{2} \left\{ \alpha \frac{\partial}{\partial \theta_s} V(\theta_s((h-1)\delta t)) + \frac{\partial}{\partial \theta_s} V(\theta_s(h\delta t)) \right\}. \quad (22)$$

Putting $h = 1$ in equations (21) and (22), we get

$$\begin{aligned} \theta_s(\delta t) &= \beta \theta_s(0) + \frac{\delta t}{M_s} \left\{ \alpha p_s(0) - \frac{\delta t}{2} \frac{\partial}{\partial \theta_s} V(\theta_s(0)) \right\} \quad \text{and} \\ p_s(\delta t) &= \alpha^2 p_s(0) - \frac{\delta t}{2} \left\{ \alpha \frac{\partial}{\partial \theta_s} V(\theta_s(0)) + \frac{\partial}{\partial \theta_s} V(\theta_s(\delta t)) \right\}. \end{aligned}$$

Now $p_s(0)$ and $\theta_s(0)$ are Gaussian processes with continuous sample paths with probability 1 under assumptions A1 and A2 (also see Remark 1), and Lemma 2.1 shows that M_s is continuous in s . Furthermore, assumption A3 implies that the derivative of $V(\cdot)$ is also a Gaussian process with continuous sample paths (see Remark 2). Since composition of two continuous function is also a continuous function, therefore, $\frac{\partial}{\partial \theta_s} V(\theta_s(0))$ is also continuous in s with probability 1. This implies $\theta_s(\delta t)$ is continuous in s with probability 1 as it is a linear combination of three almost sure continuous functions in s . This immediately implies that $p_s(\delta t)$ is also continuous in s with probability 1.

Assume that $\theta_s(h\delta t)$ and $p_s(h\delta t)$ are continuous in s with probability 1, for $h = k + 1$. We will show that $\theta_s((k+2)\delta t)$ and $p_s((k+2)\delta t)$ are almost surely continuous in s for $h = k + 2$. Now

$$\begin{aligned} \theta_s((k+2)\delta t) &= \beta \theta_s((k+1)\delta t) + \frac{\delta t}{M_s} \left\{ p_s((k+1)\delta t) - \frac{\delta t}{2} \frac{\partial}{\partial \theta_s} V(\theta_s((k+1)\delta t)) \right\} \quad \text{and} \\ p_s((k+2)\delta t) &= \alpha^2 p_s((k+1)\delta t) - \frac{\delta t}{2} \left\{ \alpha \frac{\partial}{\partial \theta_s} V(\theta_s((k+1)\delta t)) + \frac{\partial}{\partial \theta_s} V(\theta_s((k+2)\delta t)) \right\}. \end{aligned}$$

Since $\theta_s((k+1)\delta t)$ and $p_s((k+1)\delta t)$ are assumed to be continuous in s with probability 1, derivative of a Gaussian process is also a Gaussian process, composition of two continuous functions is also a continuous function, and linear combinations of continuous functions is a continuous function, we have $\theta_s((k+2)\delta t)$ is continuous in s with probability 1. Similar arguments show that $p_s((k+2)\delta t)$ is also continuous in s with probability 1. Hence using the argument of induction, we claim that $\theta_s(h\delta t)$ and $p_s(h\delta t)$ are continuous in s for any $h \geq 1$, with probability 1. \square

Theorem D.3 *Under the assumptions A1-A3, $Y(s, h\delta t)$ and $X(s, h\delta t)$ are continuous in s in the mean square sense, for all $h \geq 1$.*

Proof: We follow similar steps as in Lemma 2.2. From equation (21) we have

$$\theta_s(\delta t) = \beta\theta_s(0) + \frac{\delta t}{M_s} \left\{ \alpha p_s(0) - \frac{\delta t}{2} \frac{\partial}{\partial \theta_s} V(\theta_s(0)) \right\}.$$

Under assumptions A1 and A2, $p_s(0)$ and $\theta_s(0)$ are continuous in s in the mean square sense, and by Lemma 2.1, M_s is continuous in s . Now since the random function $V(\cdot)$ is twice differentiable under assumption A3 (see also Remark 2), the partial derivative process of V is Lipschitz and hence the composition function $\frac{\partial}{\partial \theta_s} V(\theta_s(0))$ is also mean square continuous in s (see page 416 of Banerjee et al. [2015]). Now using the fact that the linear combination of mean square continuous processes is also mean-square continuous, we have $\theta_s(\delta t)$ is mean square continuous in s . This, in turn, implies that, $\frac{\partial}{\partial \theta_s} V(\theta_s(\delta t))$ is also mean square continuous in s using the same argument as above. Therefore,

$$p_s(\delta t) = \alpha^2 p_s(0) - \frac{\delta t}{2} \left\{ \alpha \frac{\partial}{\partial \theta_s} V(\theta_s(0)) + \frac{\partial}{\partial \theta_s} V(\theta_s(\delta t)) \right\}$$

is mean square continuous in s .

Now applying the similar argument of induction as in Lemma 2.2, we have the desired result. \square

Theorem D.4 *Under the assumptions A1-A3, $Y(s, h\delta t)$ and $X(s, h\delta t)$ have differentiable sample paths with respect to s , almost surely.*

Proof: The proof goes in the same line as that of Lemma 2.2. We start with $\theta_s(\delta t)$ which is a linear combination of $\theta_s(0)$, $p_s(0)$ and $\frac{\partial}{\partial \theta_s} V(\theta_s(0))$. Note that $\theta_s(0)$, $p_s(0)$ have differentiable sample paths in s by assumptions A1 and A2 (see Remark 1). Now using the fact that composition of two differentiable functions is also differentiable (see the Lemma 3.4 of Guha [2017]), $\frac{\partial}{\partial \theta_s} V(\theta_s(0))$ has differentiable sample paths in s (refer to assumption A3 and Remark 2). Moreover, since M_s is differentiable (Lemma 2.1) and since the linear combination of differentiable functions is a differentiable function, $\theta_s(\delta t)$ has differentiable sample paths in s . The existence of differentiable sample paths of $\theta_s(\delta t)$ implies that $p_s(\delta t)$ will have differentiable sample paths in s . The rest of the proof is similar to that of Lemma 2.2. \square

Lemma D.2 *Let $f : \mathbb{R} \rightarrow \mathbb{R}$ be a zero mean Gaussian random function with covariance function $c_f(x_1, x_2)$, $x_1, x_2 \in \mathbb{R}$, which is four times continuously differentiable. Let $\{Z(s) : s \in S\}$ be a random process with the following properties*

1. $E(Z(s)) = 0$,
2. The covariance function $c_Z(s_1, s_2)$, $s_1, s_2 \in S$, where S is a compact subspace of \mathbb{R}^2 , is four times continuously differentiable, and
3. $\frac{\partial Z(s)}{\partial s_i}$ has finite fourth moment.

Then the process $\{g(s) : s \in S\}$, where $g(s) = f(Z(s))$, is mean square differentiable in s .

Proof: To show that $\{g(s) : s \in S\}$ is mean square differentiable in s we have to show that, for any $p \in S$, there exists a function $L_s(p)$, linear in p , such that

$$g(s + p) = g(s) + L_s(p) + R(s, p),$$

where

$$\frac{R(s, p)}{\|p\|} \xrightarrow{L_2} 0.$$

Let $s_o \in S$ be any point in S . Using multivariate Taylor series expansion we have

$$g(s_o + p) = g(s_o) + p^T \nabla g(s_o) + R(s_o, p),$$

where $\nabla g(s_o) = \left(\frac{\partial f(Z(s))}{\partial s_1}, \frac{\partial f(Z(s))}{\partial s_2} \right)^T$, with $\frac{\partial f(Z(s))}{\partial s_i} = \frac{df(Z(s))}{d(Z(s))} \frac{\partial Z(s)}{\partial s_i}$, for $i = 1, 2$. Therefore, $L_{s_o}(p) = p^T \nabla g(s_o)$, a linear function in p . To complete the proof we note that, from multivariate Taylor series expansion, $|R(s_o, p)| \leq M^* \|p\|^2$, where

$$M^* = \max \left\{ \left| \frac{\partial^2 f(Z(s))}{\partial s_1^2} \right|, \left| \frac{\partial^2 f(Z(s))}{\partial s_1 \partial s_2} \right|, \left| \frac{\partial^2 f(Z(s))}{\partial s_2 \partial s_1} \right|, \left| \frac{\partial^2 f(Z(s))}{\partial s_2^2} \right| \right\},$$

with

$$\frac{\partial^2 f(Z(s))}{\partial s_i^2} = \frac{d^2 f(Z(s))}{d((Z(s)))^2} \left(\frac{\partial Z(s)}{\partial s_i} \right)^2 + \frac{df(Z(s))}{dZ(s)} \frac{\partial^2 Z(s)}{\partial s_i^2}, \text{ for } i = 1, 2,$$

and

$$\frac{\partial^2 f(Z(s))}{\partial s_1 \partial s_2} = \frac{\partial^2 f(Z(s))}{\partial s_2 \partial s_1} = \frac{d^2 f(Z(s))}{d(Z(s))^2} \frac{\partial Z(s)}{\partial s_1} \frac{\partial Z(s)}{\partial s_2} + \frac{df(Z(s))}{d(Z(s))} \frac{\partial^2 Z(s)}{\partial s_1 \partial s_2}.$$

Since we have assumed that $Z(\cdot)$ and $f(\cdot)$ have covariance functions which are four times continuously differentiable, $Z(\cdot)$ and $f(\cdot)$ are twice differentiable (in the mean square sense) and hence the above terms involving first and second derivatives of $f(\cdot)$ and $Z(\cdot)$ are well-defined.

We will now show that the second moment of $\frac{\partial^2 f(Z(s))}{\partial s_i^2}$, for $i = 1, 2$, and $\frac{\partial^2 f(Z(s))}{\partial s_1 \partial s_2}$ are finite. To prove the above fact, we first show that $\text{var} \left(\frac{d^2 f(Z(s))}{d((Z(s)))^2} \right) < \infty$. Note that

$$\text{var} \left(\frac{d^2 f(Z(s))}{d((Z(s)))^2} \right) = \text{var} \left(E \left\{ \frac{d^2 f(Z(s))}{d((Z(s)))^2} \middle| Z(s) \right\} \right) + E \left(\text{var} \left\{ \frac{d^2 f(Z(s))}{d((Z(s)))^2} \middle| Z(s) \right\} \right). \quad (23)$$

Moreover, since $f''(x)$ is a Gaussian function with 0 mean and constant variance, we have

$$E \left\{ \frac{d^2 f(Z(s))}{d((Z(s)))^2} \middle| Z(s) \right\} = 0 \text{ and } \text{var} \left\{ \frac{d^2 f(Z(s))}{d((Z(s)))^2} \middle| Z(s) \right\} = \text{constant} < \infty. \text{ Thus}$$

$$\text{var} \left(E \left\{ \frac{d^2 f(Z(s))}{d((Z(s)))^2} \middle| Z(s) \right\} \right) = 0 \text{ and} \quad (24)$$

$$E \left(\text{var} \left\{ \left. \frac{d^2 f(Z(s))}{d((Z(s)))^2} \right| Z(s) \right\} \right) = \text{constant}. \quad (25)$$

Therefore, combining equations (24) and (25), and using equation (23) we see that $\text{var} \left(\frac{d^2 f(Z(s))}{d((Z(s)))^2} \right) < \infty$. Similar argument shows that $\text{var} \left(\frac{df(Z(s))}{dZ(s)} \right) < \infty$. Now to show that $E \left(\frac{\partial^2 f(Z(s))}{\partial s_i^2} \right)^2 < \infty$, we use $(a+b)^2 \leq 2(a^2 + b^2)$ and have

$$\begin{aligned} E \left(\frac{\partial^2 f(Z(s))}{\partial s_i^2} \right)^2 &\leq 2 \left\{ E \left(\left[\frac{d^2 f(Z(s))}{d((Z(s)))^2} \right]^2 \left[\frac{\partial Z(s)}{\partial s_i} \right]^4 \right) + E \left(\left[\frac{df(Z(s))}{dZ(s)} \right]^2 \left[\frac{\partial^2 Z(s)}{\partial s_i^2} \right]^2 \right) \right\} \\ &= 2E \left(E \left(\left[\frac{d^2 f(Z(s))}{d((Z(s)))^2} \right]^2 \middle| Z(s) \right) \left[\frac{\partial Z(s)}{\partial s_i} \right]^4 \right) \\ &\quad + 2E \left(E \left(\left[\frac{df(Z(s))}{dZ(s)} \right]^2 \middle| Z(s) \right) \left[\frac{\partial^2 Z(s)}{\partial s_i^2} \right]^2 \right). \end{aligned} \quad (26)$$

Again using the fact that $f'(x)$ and $f''(x)$ are Gaussian with 0 mean and constant variance, we have $E \left(\left[\frac{d^2 f(Z(s))}{d((Z(s)))^2} \right]^2 \middle| Z(s) \right) = \text{constant}$ and $E \left(\left[\frac{df(Z(s))}{dZ(s)} \right]^2 \middle| Z(s) \right) = \text{constant}$.

Further, since the covariance function of $Z(s)$ is assumed to be four times continuously differentiable (2nd assumption of the lemma), the first two derivatives of $Z(s)$, $\frac{\partial Z(s)}{\partial s_i}, i = 1, 2$ and $\frac{\partial^2 Z(s)}{\partial s_i^2}, i = 1, 2, \frac{\partial^2 Z(s)}{\partial s_1 \partial s_2}$ will also exist in the mean square sense, with zero means. Thus, $E \left[\frac{\partial^2 Z(s)}{\partial s_1^2} \right]^2 = \text{constant}$. Also, by the 3rd assumption of the Lemma, the fourth moment of $\frac{\partial Z(s)}{\partial s_i}$, for $i = 1, 2$, are finite. That is, $E \left[\frac{\partial Z(s)}{\partial s_i} \right]^4 = \text{constant}$. Therefore, from equation (26) we see that $E \left(\frac{\partial^2 f(Z(s))}{\partial s_1^2} \right)^2 < M_1 < \infty$, for some $M_1 \in \mathbb{R}$.

Next we show that $E \left(\frac{\partial^2 f(Z(s))}{\partial s_1 \partial s_2} \right)^2 < \infty$. Using the same inequality, $(a+b)^2 \leq 2(a^2 + b^2)$, we have

$$\begin{aligned} E \left(\frac{\partial^2 f(Z(s))}{\partial s_1 \partial s_2} \right)^2 &\leq 2 \left[E \left\{ \frac{d^2 f(Z(s))}{d(Z(s))^2} \frac{\partial Z(s)}{\partial s_1} \frac{\partial Z(s)}{\partial s_2} \right\}^2 + E \left\{ \frac{df(Z(s))}{d(Z(s))} \frac{\partial^2 Z(s)}{\partial s_1 \partial s_2} \right\}^2 \right] \\ &= 2E \left[E \left(\left[\frac{d^2 f(Z(s))}{d((Z(s)))^2} \right]^2 \middle| Z(s) \right) \left(\frac{\partial Z(s)}{\partial s_1} \right)^2 \left(\frac{\partial Z(s)}{\partial s_2} \right)^2 \right] \\ &\quad + 2E \left[E \left\{ \left(\frac{df(Z(s))}{d(Z(s))} \right)^2 \middle| Z(s) \right\} \left(\frac{\partial^2 Z(s)}{\partial s_1 \partial s_2} \right)^2 \right]. \end{aligned} \quad (27)$$

Since $f'(x)$ and $f''(x)$ are Gaussian functions with mean 0 and constant variance, therefore,

$E \left(\left[\frac{d^2 f(Z(s))}{d((Z(s)))^2} \right]^2 \middle| Z(s) \right)$ and $E \left(\left(\frac{df(Z(s))}{d(Z(s))} \right)^2 \middle| Z(s) \right)$ are constants. Moreover, since by our assumption,

the fourth moment of $\frac{\partial Z(s)}{\partial s_i}$, for $i = 1, 2$, are finite, we have $E \left[\left(\frac{\partial Z(s)}{\partial s_1} \right)^2 \left(\frac{\partial Z(s)}{\partial s_2} \right)^2 \right] \leq \sqrt{E \left(\frac{\partial Z(s)}{\partial s_1} \right)^4 E \left(\frac{\partial Z(s)}{\partial s_2} \right)^4}$
 $= \text{constant}$. Since the covariance function of $Z(s)$ is four times continuously differentiable, $E \left(\frac{\partial^2 Z(s)}{\partial s_1 \partial s_2} \right)^2 =$

constant. Thus we have, from equation (27), $E \left(\frac{\partial^2 f(Z(s))}{\partial s_1 \partial s_2} \right)^2 < M_2$, for some $M_2 \in R$. Hence each term in $M^* = \max \left\{ \left| \frac{\partial^2 f(Z(s))}{\partial s_1^2} \right|, \left| \frac{\partial^2 f(Z(s))}{\partial s_1 \partial s_2} \right|, \left| \frac{\partial^2 f(Z(s))}{\partial s_2 \partial s_1} \right|, \left| \frac{\partial^2 f(Z(s))}{\partial s_2^2} \right| \right\}$ has bounded second moment.

Next we have to show that $E(M^*)^2 < \infty$. Denote $M^* = \max\{A, B, C, D\}$, where $A = \left| \frac{\partial^2 f(Z(s))}{\partial s_1^2} \right|$, $B = \left| \frac{\partial^2 f(Z(s))}{\partial s_1 \partial s_2} \right|$, $C = \left| \frac{\partial^2 f(Z(s))}{\partial s_2 \partial s_1} \right|$ and $D = \left| \frac{\partial^2 f(Z(s))}{\partial s_2^2} \right|$. Note that it is sufficient to show that $X = \max\{A, B\}$ has finite second moment, because then with the same argument $Y = \max\{C, D\}$ will have finite second moment, and finally $Z = \max\{X, Y\}$ ($= \max\{A, B, C, D\}$) will have finite second moment.

Now $X = \max\{A, B\} = \frac{A+B+|A-B|}{2} \leq \frac{A+B+|A|+|B|}{2}$. Therefore,

$$\begin{aligned} EX^2 &\leq \frac{1}{4} 2 [E \{(A+B)^2 + (|A| + |B|)^2\}] \\ &\leq E\{A^2 + B^2 + |A|^2 + |B|^2\} = 2E(A^2 + B^2). \end{aligned}$$

Since $EA^2 < \infty$ and $EB^2 < \infty$, therefore, $EX^2 < \infty$. Now exactly the same arguments imply that $EY^2 < \infty$ and $EZ^2 < \infty$. Hence, $\frac{R(s_0, p)}{\|p\|} \xrightarrow{L_2} 0$. Since s_0 is any point in S , the proof is complete. \square

Theorem D.5 *Let the assumptions A1-A3 hold true, with the covariance functions of all the assumed Gaussian processes being square exponentials. Then $Y(s, h\delta t)$ and $X(s, h\delta t)$ are mean square differentiable in s , for every $h \geq 1$.*

Proof: The proof will follow the similar argument of induction as done in Lemma 2.2. For $h = 1$, we have

$$\theta_s(\delta t) = \beta \theta_s(0) + \frac{\delta t}{M_s} \left\{ \alpha p_s(0) - \frac{1}{2} \delta t \frac{\partial}{\partial \theta_s} V(\theta_s(0)) \right\}.$$

Since, under the assumption A2 and the assumption of the theorem, $\theta_s(0)$ is a centered Gaussian process with squared exponential covariance function, the fourth moment of $\frac{\partial \delta_s(0)}{\partial s_i}$, $i = 1, 2$ are finite, and by assumption A3, $V(\cdot)$ is a zero-mean Gaussian random function with squared exponential covariance. Therefore, using Lemma 2.2, $\frac{\partial}{\partial \theta_s} V(\theta_s(0))$ is mean square differentiable. Under the assumptions A1 and A2, and using the fact that the covariance functions are assumed to squared exponential, $p_s(0)$ and $\theta_s(0)$ are mean squared differentiable. Using the fact that M_s is differentiable in s (see Lemma 2.1), $\theta_s(\delta t)$, being a linear combination of mean square differentiable functions, is also mean square differentiable.

Next we show that $E(\theta_s(\delta t)) = 0$ and $\text{cov}(\theta_{s_1}(\delta t), \theta_{s_2}(\delta t))$ is 4-times differentiable. Denoting the first derivative of V by V' , we obtain

$$E(\theta_s(\delta t)) = \beta E(\theta_s(0)) + \frac{\delta t}{M_s} \left\{ \alpha E(p_s(0)) - \frac{1}{2} \delta t E(V'(\theta_s(0))) \right\} = 0,$$

where we have used the fact that $E(V'(\theta_s(0))) = E[E(V'(\theta_s(0))) | \theta_s(0)] = E(0) = 0$.

Therefore, $\text{cov}(\theta_{s_1}(\delta t), \theta_{s_2}(\delta t)) = E(\theta_{s_1}(\delta t)\theta_{s_2}(\delta t))$. Since the processes are assumed to be independent, we have

$$E(\theta_{s_1}(\delta t)\theta_{s_2}(\delta t)) = \beta^2 \sigma_\theta^2 e^{-\eta_2 \|s_1 - s_2\|^2} + \frac{(\delta t)^2 \alpha^2}{M_{s_1} M_{s_2}} \sigma_p^2 e^{-\eta_1 \|s_1 - s_2\|^2} + \frac{(\delta t)^4}{4M_{s_1} M_{s_2}} E[V'(\theta_{s_1}(0))V'(\theta_{s_2}(0))]. \quad (28)$$

Now according to our assumption, $\text{cov}(V(x_1), V(x_2)) = \sigma^2 e^{-\eta_3 \|x_1 - x_2\|^2}$, that is, the covariance function of $V(\cdot)$ can be written as $\kappa(h) = \sigma^2 e^{-\eta_3 h^2}$, where $h = \|x_1 - x_2\|$. The second derivative of $\kappa(h)$ is given by $-2\sigma^2 \eta_3 e^{-\eta_3 h^2} (1 - 2\eta_3 h^2)$. Hence the covariance function of $V'(\cdot)$ will be $\text{cov}(V'(x_1), V'(x_2)) =$

$2\sigma^2\eta_3e^{-\eta_3h^2}(1 - 2\eta_3h^2)$ (see Stein [1999b], page 21). Therefore, the last term of the right hand side of equation (28) can be computed as

$$\begin{aligned} E[V'(\theta_{s_1}(0))V'(\theta_{s_2}(0))] &= EE[V'(\theta_{s_1}(0))V'(\theta_{s_2}(0))|\theta_{s_1}(0)\theta_{s_2}(0)] \\ &= E\left[2\sigma^2\eta_3e^{-\eta_3(\theta_{s_1}(0)-\theta_{s_2}(0))^2}(1 - 2\eta_3(\theta_{s_1}(0) - \theta_{s_2}(0))^2)\right] \\ &= 2\sigma^2\eta_3\left[Ee^{-\eta_3(\theta_{s_1}(0)-\theta_{s_2}(0))^2} - 2\eta_3E\left\{(\theta_{s_1}(0) - \theta_{s_2}(0))^2e^{-\eta_3(\theta_{s_1}(0)-\theta_{s_2}(0))^2}\right\}\right]. \end{aligned} \quad (29)$$

Since $(\theta_{s_1}(0), \theta_{s_2}(0))^T \sim N_2\left(\mathbf{0}, \begin{pmatrix} \sigma_\theta^2 & \sigma_\theta^2e^{-\eta_2\|s_1-s_2\|^2} \\ \sigma_\theta^2e^{-\eta_2\|s_1-s_2\|^2} & \sigma_\theta^2 \end{pmatrix}\right)$, therefore, $\theta_{s_1}(0) - \theta_{s_2}(0) \sim N(0, 2\sigma_\theta^2 - 2\sigma_\theta^2e^{-\eta_2\|s_1-s_2\|^2})$, which in turn implies that

$$\frac{(\theta_{s_1}(0) - \theta_{s_2}(0))^2}{\nu} \sim \chi_{(1)}^2,$$

where $\nu = 2\sigma_\theta^2 - 2\sigma_\theta^2e^{-\eta_2\|s_1-s_2\|^2}$. Using the fact that the moment generating function (mgf) of a $\chi_{(1)}^2$ random variable is $(1 - 2t)^{-1/2}$, we have

$$E\left[e^{-\eta_3(\theta_{s_1}(0)-\theta_{s_2}(0))^2}\right] = \left(1 + 4\eta_3\sigma_\theta^2\left(1 - e^{\eta_2\|s_1-s_2\|^2}\right)\right)^{-1/2}. \quad (30)$$

Differentiating equation (30) with respect to η_3 and cancelling the minus sign from both sides yield

$$E\left[(\theta_{s_1}(0) - \theta_{s_2}(0))^2e^{-\eta_3(\theta_{s_1}(0)-\theta_{s_2}(0))^2}\right] = 2\sigma_\theta^2(1 - e^{\eta_2\|s_1-s_2\|^2})\left(1 + 4\eta_3\sigma_\theta^2(1 - e^{\eta_2\|s_1-s_2\|^2})\right)^{-3/2}. \quad (31)$$

Combining equations (29), (30), (31), we get

$$E[V'(\theta_{s_1}(0))V'(\theta_{s_2}(0))] = 2\sigma^2\eta_3\left[\frac{1}{(1 + 4\eta_3\sigma_\theta^2(1 - e^{\eta_2\|s_1-s_2\|^2}))^{1/2}} - \frac{4\eta_3\sigma_\theta^2(1 - e^{\eta_2\|s_1-s_2\|^2})}{(1 + 4\eta_3\sigma_\theta^2(1 - e^{\eta_2\|s_1-s_2\|^2}))^{3/2}}\right]. \quad (32)$$

Then inserting the value of $E[V'(\theta_{s_1}(0))V'(\theta_{s_2}(0))]$ from equation (32) in equation (28) we obtain

$$\begin{aligned} E(\theta_{s_1}(\delta t)\theta_{s_2}(\delta t)) &= \beta^2\sigma_\theta^2e^{-\eta_2\|s_1-s_2\|^2} + \frac{(\delta t)^2\alpha^2}{M_{s_1}M_{s_2}}\sigma_p^2e^{-\eta_1\|s_1-s_2\|^2} + \frac{(\delta t)^4}{4M_{s_1}M_{s_2}}2\sigma^2\eta_3 \\ &\quad \left[\frac{1}{(1 + 4\eta_3\sigma_\theta^2(1 - e^{\eta_2\|s_1-s_2\|^2}))^{1/2}} - \frac{4\eta_3\sigma_\theta^2(1 - e^{\eta_2\|s_1-s_2\|^2})}{(1 + 4\eta_3\sigma_\theta^2(1 - e^{\eta_2\|s_1-s_2\|^2}))^{3/2}}\right]. \end{aligned}$$

Clearly, the covariance function of $\theta_s(\delta t)$ is four times differentiable, provided M_s is also four times differentiable. To apply Lemma 2.2 on $V'(\theta_s(\delta t))$ we have to show that the fourth moment of $\frac{\partial}{\partial s_1}\theta_s(\delta t)$ finitely exists. From

$$\theta_s(\delta t) = \beta\theta_s(0) + \frac{\delta t}{M_s}\left\{\alpha p_s(0) - \frac{\delta t}{2}\frac{\partial}{\partial\theta_s}V(\theta_s(0))\right\}$$

we obtain

$$\frac{\partial\theta_s(\delta t)}{\partial s_1} = \beta\frac{\partial\theta_s(0)}{\partial s_1} + \frac{\delta t}{M_s}\left\{\frac{\partial p_s(0)}{\partial s_1} - \frac{\delta t}{2}\frac{\partial}{\partial s_1}V'(\theta_s(0))\right\} - \frac{\delta t}{M_s^2}\frac{\partial M_s}{\partial s_1}\left\{p_s(0) - \frac{1}{2}\delta t\frac{\partial}{\partial\theta_s}V(\theta_s(0))\right\}$$

$$= \beta \frac{\partial \theta_s(0)}{\partial s_1} + \frac{\delta t}{M_s} \left\{ \frac{\partial p_s(0)}{\partial s_1} - \frac{\delta t}{2} V''(\theta_s(0)) \frac{\partial \theta_s(0)}{\partial s_1} \right\} - \frac{\delta t}{M_s^2} \frac{\partial M_s}{\partial s_1} \left\{ p_s(0) - \frac{1}{2} \delta t \frac{\partial}{\partial \theta_s} V(\theta_s(0)) \right\}. \quad (33)$$

Now the fourth moment of $\frac{\partial \theta_s(\delta t)}{\partial s_1}$ will be finite if individually each term of equation (33) has finite fourth moment, because

$$\begin{aligned} \left(\frac{\partial \theta_s(\delta t)}{\partial s_1} \right)^4 &\leq \kappa \left[\beta^4 \left(\frac{\partial \theta_s(0)}{\partial s_1} \right)^4 + \left(\frac{\delta t}{M_s} \right)^4 \left\{ \left(\frac{\partial p_s(0)}{\partial s_1} \right)^4 + \left(\frac{\delta t}{2} \right)^4 \left(V''(\theta_s(0)) \frac{\partial \theta_s(0)}{\partial s_1} \right)^4 \right\} + \right. \\ &\quad \left. \left(\frac{\delta t}{M_s^2} \frac{\partial M_s}{\partial s_1} \right)^4 \left\{ (p_s(0))^4 + \left(\frac{1}{2} \delta t \right)^4 \left(\frac{\partial}{\partial \theta_s} V(\theta_s(0)) \right)^4 \right\} \right], \end{aligned}$$

where κ is a suitable constant. Note that due to assumptions A1-A2 and squared exponential covariance functions, $\frac{\partial \theta_s(0)}{\partial s_1}$, $\frac{\partial p_s(0)}{\partial s_1}$, and $p_s(0)$ are Gaussian processes with 0 mean and constant variances. Hence they have finite fourth moments. Therefore, we just need to show that $V''(\theta_s(0)) \frac{\partial \theta_s(0)}{\partial s_1}$ and $\frac{\partial}{\partial \theta_s} V(\theta_s(0))$ have finite 4th moments. Observe that

$$\begin{aligned} E \left[V''(\theta_s(0)) \frac{\partial \theta_s(0)}{\partial s_1} \right]^4 &= E E \left\{ \left[V''(\theta_s(0)) \frac{\partial \theta_s(0)}{\partial s_1} \right]^4 \middle| \theta_s(0) \right\} \\ &= E \left[E \left\{ [V''(\theta_s(0))]^4 \middle| \theta_s(0) \right\} \left(\frac{\partial \theta_s(0)}{\partial s_1} \right)^4 \right] \end{aligned} \quad (34)$$

Now since $V''(\theta_s(0))$, given $\theta_s(0)$, is Gaussian with mean 0 and constant variance,

$E \left\{ [V''(\theta_s(0))]^4 \middle| \theta_s(0) \right\}$ is constant (independent of $\theta_s(0)$), say κ_1 . Hence from equation (34) we obtain

$$E \left[V''(\theta_s(0)) \frac{\partial \theta_s(0)}{\partial s_1} \right]^4 = \kappa_1 E \left(\frac{\partial \theta_s(0)}{\partial s_1} \right)^4. \quad (35)$$

Now note that $\frac{\partial \theta_s(0)}{\partial s_1}$ is also Gaussian with mean 0 and constant variance, so that $E \left(\frac{\partial \theta_s(0)}{\partial s_1} \right)^4$ is also constant. Thus, combining equations (34) and (35) we have

$$E \left[V''(\theta_s(0)) \frac{\partial \theta_s(0)}{\partial s_1} \right]^4 < \infty. \quad (36)$$

Next to show that $\frac{\partial}{\partial \theta_s} V(\theta_s(0))$ has finite 4th moment, we notice that

$$E(V'(\theta_s(0)))^4 = E \left[E(V'(\theta_s(0)))^4 \middle| \theta_s(0) \right] = \text{constant} = \kappa_2, \text{ say.}$$

The last equality follows because $V'(\theta_s(0))$, given $\theta_s(0)$, is a Gaussian process with 0 mean and constant variance.

Therefore, the fourth moment of $\frac{\partial}{\partial s_1} \theta_s(\delta t)$ exists finitely. So, by Lemma 2.2, $V'(\theta_s(\delta t))$ is mean square differentiable, and hence under assumptions A1, A2, for $h = 1$,

$$p_s(\delta t) = \alpha^2 p_s(0) - \frac{\delta t}{2} \left\{ \alpha \frac{\partial}{\partial \theta_s} V(\theta_s(0)) + \frac{\partial}{\partial \theta_s} V(\theta_s(\delta t)) \right\},$$

a linear combination of mean square differentiable function, is also mean square differentiable. Before applying the steps of induction, we show that $\frac{\partial p_s(\delta t)}{\partial s_i}$, $i = 1, 2$, have finite 4th moment as it has to be used for the next step of induction. Note that, for $i = 1, 2$,

$$\frac{\partial p_s(\delta t)}{\partial s_i} = \alpha^2 \frac{\partial p_s(0)}{\partial s_i} - \frac{\delta t}{2} \left\{ \alpha V'''(\theta_s(0)) \frac{\partial \theta_s(0)}{\partial s_i} + V'''(\theta_s(\delta t)) \frac{\partial \theta_s(\delta t)}{\partial s_i} \right\}.$$

From equation (36), $E \left(V'''(\theta_s(0)) \frac{\partial \theta_s(0)}{\partial s_i} \right)^4 < \infty$. We have already shown that $\frac{\partial \theta_s(\delta t)}{\partial s_i}$ has finite fourth moment, for $i = 1, 2$. Thus, each term in the expression of $\frac{\partial p_s(\delta t)}{\partial s_i}$ has finite fourth moment. Hence $E \left(\frac{\partial p_s(\delta t)}{\partial s_i} \right)^4 < \infty$.

Thereafter, using the argument of induction as in the proof of Lemma 2.2, we have the desired result. \square

E Calculation of joint conditional density of the observed data

Here we will find the data model, that is, the conditional distribution of Data given Latent, \mathbf{y}_0 , \mathbf{x}_0 and the parameter $\boldsymbol{\theta}$.

First, we will find the conditional distribution of \mathbf{y}_1 given \mathbf{y}_0 , \mathbf{x}_0 and the parameter $\boldsymbol{\theta}$. We have, for $i = 1, 2, \dots, n$,

$$y(s_i, 1) = \beta y(s_i, 0) + \frac{\alpha x(s_i, 0)}{M_{s_i}} - \frac{1}{2} \frac{V'(y(s_i, 0))}{M_{s_i}},$$

and

$$\frac{1}{2} \left[\frac{V'(y(s_1, 0))}{M_{s_1}}, \dots, \frac{V'(y(s_n, 0))}{M_{s_n}} \right]' \sim N_n \left(\mathbf{0}, \frac{\sigma^2}{4} \Sigma_0 \right),$$

where Σ_0 is the $n \times n$ covariance matrix with (i, j) th element $\frac{2\eta_3 e^{-\eta_3 h_{ij}^2(0)} (1 - 2\eta_3 h_{ij}^2(0))}{M_{s_i} M_{s_j}}$. Therefore,

$$\left[\mathbf{y}_1 \mid \mathbf{y}_0; \mathbf{x}_0; \boldsymbol{\theta} \right] \sim N_n \left(\boldsymbol{\mu}_0, \frac{\sigma^2}{4} \Sigma_0 \right). \quad (37)$$

Similarly,

$$\left[\mathbf{y}_2 \mid \mathbf{y}_1; \mathbf{x}_1; \mathbf{y}_0; \mathbf{x}_0; \boldsymbol{\theta} \right] \sim N_n \left(\boldsymbol{\mu}_1, \frac{\sigma^2}{4} \Sigma_1 \right), \quad (38)$$

where the (i, j) th element of the $n \times n$ covariance matrix Σ_1 is $\frac{2\eta_3 e^{-\eta_3 h_{ij}^2(1)} (1 - 2\eta_3 h_{ij}^2(1))}{M_{s_i} M_{s_j}}$. Following the same argument, we can write down the likelihood as

$$\begin{aligned} L &= [\mathbb{D} \mid \mathbf{x}_0; \dots; \mathbf{x}_{T-1}; \mathbf{y}_0; \boldsymbol{\theta}] \\ &\propto [\mathbf{y}_1 \mid \mathbf{y}_0; \mathbf{x}_0; \boldsymbol{\theta}] \dots [\mathbf{y}_T \mid \mathbf{y}_{T-1}, \dots, \mathbf{y}_0; \mathbf{x}_{T-1}, \dots, \mathbf{x}_0; \boldsymbol{\theta}] \\ &\propto \frac{(\sigma^2)^{-nT/2}}{\prod_{t=1}^T |\Sigma_{t-1}|^{1/2}} e^{-\frac{2}{\sigma^2} \sum_{t=1}^T (\mathbf{y}_t - \boldsymbol{\mu}_{t-1})^T \Sigma_{t-1}^{-1} (\mathbf{y}_t - \boldsymbol{\mu}_{t-1})}, \end{aligned}$$

where, for $j = 1, 2, \dots, T$, the (k, ℓ) th element of Σ_{j-1} is

$$\frac{2\eta_3 e^{-\eta_3 h_{k\ell}^2(j-1)} (1 - 2\eta_3 h_{k\ell}^2(j-1))}{M_{s_k} M_{s_\ell}}.$$

F Calculation of the conditional joint density of latent data

Here we will derive the conditional distribution of \mathbb{L} given \mathbb{D} , \mathbf{y}_0 , \mathbf{x}_0 and the parameter $\boldsymbol{\theta}$.

First, we shall find the conditional distribution of \mathbf{x}_1 given \mathbf{x}_0 , \mathbf{y}_0 , and \mathbf{y}_1 . For $i = 1, \dots, n$, we have

$$x(s_i, 1) = \alpha^2 x(s_i, 0) - \frac{1}{2} \{ \alpha V'(y(s_i, 0)) + V'(y(s_i, 1)) \}.$$

Since $V'(\cdot)$ is a random Gaussian function with zero mean and covariance function given in equation (5) and $\mathbb{W}_0 = (\mathbf{W}'_0 \mathbf{W}'_1)'$ is a $2n \times 1$ vector, $\mathbb{W}_0 \sim N_{2n}(\mathbf{0}, \sigma^2 \Sigma)$, where Σ is the $2n \times 2n$ covariance matrix partitioned as

$$\begin{pmatrix} \alpha^2 \Sigma_{00} & \alpha \Sigma_{01} \\ \alpha \Sigma_{10} & \Sigma_{11} \end{pmatrix},$$

where the (i, k) th element of Σ_{jj} is $2\eta_3 e^{-\eta_3 h_{ik}^2(j)} (1 - 2\eta_3 h_{ik}^2(j))$, for $j = 0, 1$, and the (i, k) th element of $\Sigma_{01} = \Sigma'_{10}$ is $2\eta_3 e^{-\eta_3 \ell_{ik}^2(0,1)} (1 - 2\eta_3 \ell_{ik}^2(0,1))$. Therefore,

$$\mathbf{W}_0 + \mathbf{W}_1 = [I_n : I_n] \mathbb{W}_0 \sim N_n(\mathbf{0}, \sigma^2 (\alpha^2 \Sigma_{00} + \alpha \Sigma_{01} + \alpha \Sigma_{10} + \Sigma_{11})).$$

Let $\Omega_1 = \alpha^2 \Sigma_{00} + \alpha \Sigma_{01} + \alpha \Sigma_{10} + \Sigma_{11}$. Then

$$[\mathbf{x}_1 | \mathbf{x}_0; \mathbf{y}_0; \mathbf{y}_1; \boldsymbol{\theta}] \sim N_n(\alpha^2 \mathbf{x}_0, \frac{\sigma^2}{4} \Omega_1). \quad (39)$$

Similarly,

$$[\mathbf{x}_2 | \mathbf{x}_1; \mathbf{x}_0; \mathbf{y}_0; \mathbf{y}_1; \mathbf{y}_2; \boldsymbol{\theta}] \sim N_n(\alpha^2 \mathbf{x}_1, \frac{\sigma^2}{4} \Omega_2), \quad (40)$$

where $\Omega_2 = \alpha^2 \Sigma_{11} + \alpha \Sigma_{12} + \alpha \Sigma_{21} + \Sigma_{22}$. For $j = 1, 2$, the (i, k) th element of Σ_{jj} is $2\eta_3 e^{-\eta_3 h_{ik}^2(j)} (1 - 2\eta_3 h_{ik}^2(j))$, and the (i, k) th element of $\Sigma_{12} = \Sigma'_{21}$ is $2\eta_3 e^{-\eta_3 \ell_{ik}^2(1,2)} (1 - 2\eta_3 \ell_{ik}^2(1,2))$. Now with the help of equations (39) and (40) we write down the conditional latent process model as

$$\begin{aligned} & \left[\mathbb{L} \middle| \mathbf{y}_0; \dots; \mathbf{y}_T; \mathbf{x}_0; \boldsymbol{\theta} \right] \\ & \propto [\mathbf{x}_1 | \mathbf{x}_0; \mathbf{y}_0; \mathbf{y}_1; \boldsymbol{\theta}] \dots [\mathbf{x}_T | \mathbf{x}_{T-1}; \dots; \mathbf{x}_0; \mathbf{y}_0; \dots; \mathbf{y}_T; \boldsymbol{\theta}] \\ & \propto \frac{(\sigma^2)^{-nT/2}}{T} e^{-\frac{2}{\sigma^2} \sum_{t=1}^T (\mathbf{x}_t - \alpha^2 \mathbf{x}_{t-1})^T \Omega_t^{-1} (\mathbf{x}_t - \alpha^2 \mathbf{x}_{t-1})}, \\ & \quad \prod_{t=1}^T |\Omega_t|^{1/2} \end{aligned}$$

where, for $m \in \{1, 2, \dots, T\}$, $\Omega_t = \alpha^2 \Sigma_{t-1, t-1} + \alpha \Sigma_{t-1, t} + \alpha \Sigma_{t, t-1} + \Sigma_{t, t}$, where the (i, k) th element of Σ_{jj} , for $j = t-1, t$, is $2\eta_3 e^{-\eta_3 h_{ik}^2(j)} (1 - 2\eta_3 h_{ik}^2(j))$, and the (i, k) th element of $\Sigma_{t-1, t} = \Sigma'_{t, t-1}$ is $2\eta_3 e^{-\eta_3 \ell_{ik}^2(t-1, t)} (1 - 2\eta_3 \ell_{ik}^2(t-1, t))$.

G Calculation of full conditional distributions of the parameters and the latent variables, given the observed data

G.1 Full conditional distribution of β_*

Before finding the full conditional distribution of β (hence β_*), we note that the only term that depends on β in equation (9) is $\exp\left\{-\frac{2}{\sigma^2}\sum_{t=1}^T[\boldsymbol{\mu}_{t-1}^T\Sigma_{t-1}^{-1}\boldsymbol{\mu}_{t-1}-2\mathbf{y}_t^T\Sigma_{t-1}^{-1}\boldsymbol{\mu}_{t-1}]\right\}$. Further notice that $\boldsymbol{\mu}_t = \beta\mathbf{y}_{t-1} + \text{constant}$ (with respect to β). Therefore, the term which depends on β (hence on β_*) simplifies to $e^{-\frac{2\beta^2}{\sigma^2}\sum_{t=1}^T\mathbf{y}'_{t-1}\Sigma_{t-1}^{-1}\mathbf{y}_{t-1}} \times e^{\frac{4\beta}{\sigma^2}\sum_{t=1}^T\mathbf{y}'_{t-1}\Sigma_{t-1}^{-1}\mathbf{y}_{t-1}}$, where $\beta = -1 + \frac{2e^{\beta_*}}{1+2e^{\beta_*}}$. The full conditional density of β_* , therefore, is given by

$$\begin{aligned} [\beta_*|\dots] &\propto [\beta_*]e^{-\frac{2\beta^2}{\sigma^2}\sum_{t=1}^T\mathbf{y}'_{t-1}\Sigma_{t-1}^{-1}\mathbf{y}_{t-1}+\frac{4\beta}{\sigma^2}\sum_{t=1}^T\mathbf{y}'_{t-1}\Sigma_{t-1}^{-1}\mathbf{y}_{t-1}} \\ &\propto e^{-\frac{\beta_*^2}{2\sigma^2\beta_*}}e^{-\frac{2\beta^2}{\sigma^2}\sum_{t=1}^T\mathbf{y}'_{t-1}\Sigma_{t-1}^{-1}\mathbf{y}_{t-1}+\frac{4\beta}{\sigma^2}\sum_{t=1}^T\mathbf{y}'_{t-1}\Sigma_{t-1}^{-1}\mathbf{y}_{t-1}} \\ &= \pi(\beta_*)g_1(\beta_*), \end{aligned}$$

where $\pi(\beta_*) = e^{-\frac{\beta_*^2}{2\sigma^2\beta_*}}$ and $g_1(\beta_*) = e^{-\frac{2\beta^2}{\sigma^2}\sum_{t=1}^T\mathbf{y}'_{t-1}\Sigma_{t-1}^{-1}\mathbf{y}_{t-1}+\frac{4\beta}{\sigma^2}\sum_{t=1}^T\mathbf{y}'_{t-1}\Sigma_{t-1}^{-1}\mathbf{y}_{t-1}}$.

G.2 Full conditional distribution of α_*

The full conditional density of α_* will be given by $[\alpha_*] \times [\text{Data,Latent}|\boldsymbol{\theta}]$. Now the term that depends on α (hence on α_*) in $[\text{Data,Latent}|\boldsymbol{\theta}]$, that is, in equation (9), is given by

$$g_2(\alpha_*) = \frac{1}{\prod_{t=1}^T|\Omega_t|^{1/2}}e^{-\frac{2}{\sigma^2}\sum_{t=1}^T[(\mathbf{x}_t-\alpha^2\mathbf{x}_{t-1})^T\Omega_t^{-1}(\mathbf{x}_t-\alpha^2\mathbf{x}_{t-1})]} \times e^{-\frac{2\alpha}{\sigma^2}\sum_{t=1}^T[\alpha\mathbf{x}_{t-1}^TD\Sigma_{t-1}^{-1}D\mathbf{x}_{t-1}-2\mathbf{y}_t^T\Sigma_{t-1}^{-1}D\mathbf{x}_{t-1}]},$$

where D is the $n \times n$ diagonal matrix containing the diagonal elements $\frac{1}{M_{s_i}}, i = 1, \dots, n$. In the above calculation we use $\boldsymbol{\mu}_t = \beta\mathbf{y}_t + \alpha D\mathbf{x}_t$. Thus the full conditional density of α_* is given by

$$[\alpha_*|\dots] \propto e^{-\frac{\alpha_*^2}{2\sigma^2\alpha_*}}g_2(\alpha_*).$$

G.3 Full conditional distribution of σ_θ^2

The only term that depends on σ_θ^2 in equation (9) is $\left(\frac{1}{\sigma_\theta^2}\right)^{n/2} \exp\left\{-\frac{1}{2\sigma_\theta^2}\mathbf{y}'_0\Delta_0^{-1}\mathbf{y}_0\right\}$, and therefore, the full conditional distribution of σ_θ^2 is

$$\begin{aligned} [\sigma_\theta^2|\dots] &\propto [\sigma_\theta^2] \left(\frac{1}{\sigma_\theta^2}\right)^{n/2} \exp\left\{-\frac{1}{2\sigma_\theta^2}\mathbf{y}'_0\Delta_0^{-1}\mathbf{y}_0\right\} \\ &\propto \left(\frac{1}{\sigma_\theta^2}\right)^{\alpha_\theta+n/2+1} \exp\left\{-\frac{1}{\sigma_\theta^2}\left(\frac{\gamma_\theta + \mathbf{y}'_0\Delta_0^{-1}\mathbf{y}_0}{2}\right)\right\}. \end{aligned}$$

That is, the full conditional distribution of σ_θ^2 is $\text{IG}\left(\alpha_\theta + n/2, \frac{\gamma_\theta + \mathbf{y}'_0 \Delta_0^{-1} \mathbf{y}_0}{2}\right)$.

G.4 Full conditional distribution of σ_p^2

Since the only term that depends on σ_p^2 in equation (9) is $\left(\frac{1}{\sigma_p^2}\right)^{n/2} \exp\left\{-\frac{1}{2\sigma_p^2} \mathbf{x}'_0 \Omega_0^{-1} \mathbf{x}_0\right\}$ and we have assumed inverse gamma with parameters α_p and γ_p ,

$$[\sigma_p^2 | \dots] \propto \left(\frac{1}{\sigma_p^2}\right)^{\alpha_p+1} \left(\frac{1}{\sigma_p^2}\right)^{n/2} \exp\left\{-\frac{1}{\sigma_p^2} \left(\frac{\gamma_p + \mathbf{x}'_0 \Omega_0^{-1} \mathbf{x}_0}{2}\right)\right\}.$$

This implies that the full conditional distribution of σ_p^2 is $\text{IG}\left(\alpha_p + n/2, \frac{\gamma_p + \mathbf{x}'_0 \Omega_0^{-1} \mathbf{x}_0}{2}\right)$.

G.5 Full conditional distribution of σ^2

Note that $[\text{Data}|\text{Latent}, \mathbf{x}_0, \mathbf{y}_0, \boldsymbol{\theta}]$ and $[\text{Latent}|\text{Data}, \mathbf{x}_0, \mathbf{y}_0, \boldsymbol{\theta}]$ depend on σ^2 . Therefore, the full conditional distribution of σ^2 can be achieved as follows:

$$\begin{aligned} [\sigma^2 | \dots] &\propto [\sigma^2] \prod_{t=1}^T [\mathbf{y}_t | \mathbf{y}_{t-1}, \mathbf{x}_{t-1}, \boldsymbol{\theta}] [\mathbf{x}_t | \mathbf{y}_t, \mathbf{y}_{t-1}, \mathbf{x}_{t-1}, \boldsymbol{\theta}] \\ &\propto [\sigma^2] (\sigma^2)^{-Tn} \exp\left\{-\frac{2}{\sigma^2} \sum_{t=1}^T [(\mathbf{y}_t - \boldsymbol{\mu}_t)^T \Sigma_{t-1}^{-1} (\mathbf{y}_t - \boldsymbol{\mu}_t) + (\mathbf{x}_t - \alpha^2 \mathbf{x}_{t-1})^T \Omega_t^{-1} (\mathbf{x}_t - \alpha^2 \mathbf{x}_{t-1})]\right\} \\ &\propto \left(\frac{1}{\sigma^2}\right)^{\alpha_v + Tn+1} \exp\left\{-\frac{1}{\sigma^2} \left[\frac{\gamma_v}{2} + 2\zeta\right]\right\}, \end{aligned}$$

where $\zeta = \sum_{t=1}^T [(\mathbf{y}_t - \boldsymbol{\mu}_t)^T \Sigma_{t-1}^{-1} (\mathbf{y}_t - \boldsymbol{\mu}_t) + (\mathbf{x}_t - \alpha^2 \mathbf{x}_{t-1})^T \Omega_t^{-1} (\mathbf{x}_t - \alpha^2 \mathbf{x}_{t-1})]$. Hence the full conditional distribution of σ^2 is inverse-Gamma with parameters $\alpha_v + Tm$ and $\gamma_v/2 + 2\zeta$.

G.6 Full conditional distributions of η_1^* , η_2^* , and η_3^*

We observe that only $[\mathbf{x}_0 | \boldsymbol{\theta}]$ depends η_1 (hence on η_1^*) and $[\mathbf{Y}_0 | \boldsymbol{\theta}]$ depends on η_2 (hence on η_2^*). Therefore, the full conditional densities of η_1^* and η_2^* are given by

$$\begin{aligned} [\eta_1^* | \dots] &\propto [\eta_1^*] [\mathbf{x}_0 | \boldsymbol{\theta}] \\ &\propto e^{-\eta_1^{*2}/2} \frac{1}{|\Omega_0|^{1/2}} e^{-\frac{1}{2\sigma_p^2} \mathbf{x}_0^T \Omega_0^{-1} \mathbf{x}_0} \\ &= \pi(\eta_1^*) g_3(\eta_1^*) \end{aligned} \tag{41}$$

and

$$\begin{aligned} [\eta_2^* | \dots] &\propto [\eta_2^*] [\mathbf{y}_0 | \boldsymbol{\theta}] \\ &\propto e^{-\eta_2^{*2}/2} \frac{1}{|\Delta_0|^{1/2}} e^{-\frac{1}{2\sigma_\theta^2} \mathbf{y}_0^T \Delta_0^{-1} \mathbf{y}_0} \\ &= \pi(\eta_2^*) g_4(\eta_2^*), \end{aligned} \tag{42}$$

respectively, where $\eta_1 = e^{\eta_1^*}$, $\eta_2 = e^{\eta_2^*}$, $\pi(\eta_1^*) = e^{-\eta_1^{*2}/2}$, $\pi(\eta_2^*) = e^{-\eta_2^{*2}/2}$, $g_3(\eta_1^*) = \frac{1}{|\Omega_0|^{1/2}} e^{-\frac{1}{2\sigma_p^2} \mathbf{x}_0^T \Omega_0^{-1} \mathbf{x}_0}$ and $g_4(\eta_2^*) = \frac{1}{|\Delta_0|^{1/2}} e^{-\frac{1}{2\sigma_\theta^2} \mathbf{y}_0^T \Delta_0^{-1} \mathbf{y}_0}$.

On the other hand, the joint conditional distribution of (Data, Latent) given $\mathbf{x}_0, \mathbf{y}_0, \boldsymbol{\theta}$ depends on η_3 (hence on η_3^*). Thus, the full conditional distribution of η_3^* is given by

$$\begin{aligned} [\eta_3^*] &\propto [\eta_3^*] \prod_{t=1}^T [\mathbf{y}_t | \mathbf{y}_{t-1}, \mathbf{x}_{t-1}, \boldsymbol{\theta}] [\mathbf{x}_t | \mathbf{y}_t, \mathbf{y}_{t-1}, \mathbf{x}_{t-1}, \boldsymbol{\theta}] \\ &\propto e^{-\eta_3^{*2}/2} \frac{1}{\prod_{t=1}^T |\Sigma_{t-1}|^{1/2} |\Omega_t|^{1/2}} e^{-\frac{2}{\sigma^2} \sum_{t=1}^T [(\mathbf{y}_t - \boldsymbol{\mu}_t)^T \Sigma_{t-1}^{-1} (\mathbf{y}_t - \boldsymbol{\mu}_t) + (\mathbf{x}_t - \alpha^2 \mathbf{x}_{t-1})^T \Omega_t^{-1} (\mathbf{x}_t - \alpha^2 \mathbf{x}_{t-1})]} \\ &= \pi(\eta_3^*) g_5(\eta_3^*), \end{aligned} \tag{43}$$

where $\eta_3 = e^{\eta_3^*}$, $\pi(\eta_3^*) = e^{-\eta_3^{*2}/2}$ and

$$g_5(\eta_3^*) = \frac{1}{\prod_{t=1}^T |\Sigma_{t-1}|^{1/2} |\Omega_t|^{1/2}} e^{-\frac{2}{\sigma^2} \sum_{t=1}^T [(\mathbf{y}_t - \boldsymbol{\mu}_t)^T \Sigma_{t-1}^{-1} (\mathbf{y}_t - \boldsymbol{\mu}_t) + (\mathbf{x}_t - \alpha^2 \mathbf{x}_{t-1})^T \Omega_t^{-1} (\mathbf{x}_t - \alpha^2 \mathbf{x}_{t-1})]}.$$

G.7 Full conditional distribution of \mathbf{x}_0

Using the fact that only \mathbf{x}_1 and \mathbf{y}_1 depend on \mathbf{x}_0 and writing $\boldsymbol{\mu}_0 = \beta \mathbf{y}_0 + \alpha D \mathbf{x}_0$, we have

$$\begin{aligned} [\mathbf{x}_0 | \dots] &\propto [\mathbf{x}_0 | \boldsymbol{\theta}] [\mathbf{x}_1 | \mathbf{y}_1, \mathbf{y}_0, \mathbf{x}_0, \boldsymbol{\theta}] [\mathbf{y}_1 | \mathbf{y}_0, \mathbf{x}_0, \boldsymbol{\theta}] \\ &\propto e^{-\frac{1}{2\sigma_p^2} \mathbf{x}_0^T \Omega_0^{-1} \mathbf{x}_0} e^{-\frac{2}{\sigma^2} (\mathbf{x}_1 - \alpha^2 \mathbf{x}_0)^T \Omega_1^{-1} (\mathbf{x}_1 - \alpha^2 \mathbf{x}_0)} e^{-\frac{2}{\sigma^2} (\mathbf{y}_1 - \beta \mathbf{y}_0 - \alpha D \mathbf{x}_0)^T \Sigma_0^{-1} (\mathbf{y}_1 - \beta \mathbf{y}_0 - \alpha D \mathbf{x}_0)} \\ &\propto e^{-\frac{1}{2\sigma_p^2} \left[\mathbf{x}_0^T \Omega_0^{-1} \mathbf{x}_0 + \frac{4\sigma_p^2 \alpha^4}{\sigma^2} \mathbf{x}_0^T \Omega_1^{-1} \mathbf{x}_0 + \frac{4\sigma_p^2 \alpha^2}{\sigma^2} \mathbf{x}_0^T D \Sigma_0^{-1} D \mathbf{x}_0 - \frac{8\sigma_p^2 \alpha^2}{\sigma^2} \mathbf{x}_0^T \Omega_1^{-1} \mathbf{x}_1 - \frac{8\sigma_p^2 \alpha}{\sigma^2} \mathbf{x}_0^T D \Sigma_0^{-1} (\mathbf{y}_1 - \beta \mathbf{y}_0) \right]} \\ &\propto e^{-\frac{1}{2\sigma_p^2} [\mathbf{x}_0^T A \mathbf{x}_0 - 2 \mathbf{x}_0^T B \mathbf{x}_1 - 2 \mathbf{x}_0^T C (\mathbf{y}_1 - \beta \mathbf{y}_0)]} \\ &\propto e^{-\frac{1}{2\sigma_p^2} (\mathbf{x}_0 - A^{-1} B \mathbf{x}_1 - A^{-1} C (\mathbf{y}_1 - \beta \mathbf{y}_0))^T A (\mathbf{x}_0 - A^{-1} B \mathbf{x}_1 - A^{-1} C (\mathbf{y}_1 - \beta \mathbf{y}_0))}, \end{aligned} \tag{44}$$

where $A = \Omega_0^{-1} + \frac{4\sigma_p^2 \alpha^4}{\sigma^2} \Omega_1^{-1} + \frac{4\sigma_p^2 \alpha^2}{\sigma^2} D \Sigma_0^{-1} D$, $B = \frac{4\sigma_p^2 \alpha^2}{\sigma^2} \Omega_1^{-1}$, $C = \frac{4\sigma_p^2 \alpha}{\sigma^2} D \Sigma_0^{-1}$. We note here that $D (= \text{diag}(1/M_{s_i})_{i=1}^n)$ is a positive definite matrix as all the diagonal entries are strictly positive, A being a sum of three positive definite matrices is also positive definite and hence invertible. Thus, from equation (44), we get $[\mathbf{x}_0 | \dots] \sim N_n(A^{-1}(B \mathbf{x}_1 + C(\mathbf{y}_1 - \beta \mathbf{y}_0)), \sigma_p^2 A^{-1})$.

H Algorithm for temporal prediction

We provide the algorithms for simulating observations from the posterior predictive densities for single-time point and multiple-time point predictions. Let $\mathbf{Y}_{T+1} = (Y(s_1, T+1), \dots, Y(s_n, T+1))^T$ and $\mathbf{x}_{T+1} = (x(s_1, T+1), \dots, x(s_n, T+1))^T$ be the response and latent variable at time point $T+1$. The aim is to simulate observations from the predictive density of \mathbf{Y}_{T+L} , for $L = 1, 2, \dots$. For $k = 1, \dots, N$, where N is the number of iterations after the burn-in period B , do the following:

- S1. simulate from $[\mathbb{L}, \boldsymbol{\theta} | \mathbb{D}]$ using Gibbs, and Metropolis Hastings within Gibbs via the full conditionals as outlined in Section 5. Let the simulated value at the k th iteration be denoted by $\boldsymbol{\theta}^{(k)}$ and $\mathbb{L}^{(k)}$.

- S2. Given $\boldsymbol{\theta}^{(k)}$ and $\mathbb{L}^{(k)}$, simulate n -variate observation from normal distribution with the mean $\boldsymbol{\mu}_T$, where the i th element of $\boldsymbol{\mu}_T$ is as mentioned in Section 3 with m replaced with T , β replaced with $\beta^{(k)}$, α replaced with $\alpha^{(k)}$, and covariance matrix Σ_T . The elements of Σ_T is the same as given in Section 3.1 after equation 6, with η_3 , α and j replaced with $\eta_3^{(k)}$, $\alpha^{(k)}$ and $T + 1$, respectively. Let the simulated observations be denoted by $\mathbf{y}_{T+1}^{(k)}$.
- S4. Then simulate \mathbf{x}_{T+1} from the n -variate normal distribution with mean $\alpha^{(k)^2} \mathbf{x}_T$ and covariance matrix Ω_{T+1} . The elements of Ω_T is the same as described in Section 3.2 with t replaced by $T + 1$, α replaced by $\alpha^{(k)}$ and η_3 replaced by $\eta_3^{(k)}$.
- S5. Update the data \mathbb{D} to $\mathbb{D}_1^{(k)} = \mathbb{D} \cup \{\mathbf{y}_{T+1}^{(k)}\}$ and the latent $\mathbb{L}^{(k)}$ to $\mathbb{L}_1^{(k)} = \mathbb{L} \cup \{\mathbf{x}_{T+1}^{(k)}\}$.
- S6. Given $\mathbb{D}_1^{(k)}$, $\mathbb{L}_1^{(k)}$ and $\boldsymbol{\theta}^{(k)}$, simulate $\mathbf{y}_{T+2}^{(k)}$ from the n -variate normal with mean $\boldsymbol{\mu}_{T+1}$ and covariance matrix Σ_{T+1} , where the i th element of $\boldsymbol{\mu}_{T+1}$ is as mentioned in Section 3 with m , β and α replaced with $T + 1$, $\beta^{(k)}$ and $\alpha^{(k)}$, respectively, and covariance matrix Σ_{T+1} . The elements of Σ_{T+1} is the same as given in Section 3.1 after equation 6, with η_3 , α and j replaced with $\eta_3^{(k)}$, $\alpha^{(k)}$ and $T + 2$, respectively. Let the simulated observations be denoted by $\mathbf{y}_{T+2}^{(k)}$.
- S7. Then simulate \mathbf{x}_{T+2} from the n -variate normal distribution with mean $\alpha^{(k)^2} \mathbf{x}_{T+1}^{(k)}$ and covariance matrix Ω_{T+1} . The elements of Ω_{T+1} are the same as described in Section 3.2 with t replaced by $T + 2$, α replaced by $\alpha^{(k)}$ and η_3 replaced by $\eta_3^{(k)}$.
- S8. Continue the procedure to get a simulated value $\mathbf{y}_{T+L}^{(k)}$.

I Algorithm for prediction of time series at a spatial point

Let s^* be a spatial location at which we want to obtain prediction for the time points t_1, \dots, t_T . Therefore, it is required to obtain observations from the distribution given by $[y(s^*, t), t = 1, \dots, T, |\mathbb{D}]$. Let us denote $(y(s^*, t), t = 1, \dots, T)$ by \mathbf{y}^* and $(x(s^*, t), t = 1, \dots, T)$ by \mathbf{x}^* . Notice that $(y(s_1, t), \dots, y(s_n, t), y(s^*, t))$ given \mathbb{L} , \mathbf{x}^* , $\boldsymbol{\theta}$ and $(y(s_1, t - 1), \dots, y(s_n, t - 1), y(s^*, t - 1))$ is a $(n + 1)$ -variate normal with mean $\boldsymbol{\mu}_{t-1}^* = \left(\beta y(s_1, t - 1) + \frac{\alpha x(s_1, t-1)}{M_{s_1}}, \dots, \beta y(s_n, t - 1) + \frac{\alpha x(s_n, t-1)}{M_{s_n}}, \beta y(s^*, t - 1) + \frac{\alpha x(s^*, t-1)}{M_{s^*}} \right)^T$, and covariance matrix Σ_{t-1}^* of order $n + 1 \times n + 1$. The elements of Σ_{t-1}^* are the same as given in Section 3.1. Let Σ_{t-1}^* be partitioned as $\Sigma_{t-1}^* = \begin{pmatrix} \Sigma_{t-1} & \mathbf{S}_{1,t-1} \\ \mathbf{S}_{1,t-1}^T & s_{n+1,n+1} \end{pmatrix}$, where Σ_{t-1} is a $n \times n$ matrix, $\mathbf{S}_{1,t-1}$ is a $n \times 1$ vector. Therefore, $[y(s^*, t) | \dots]$ follows a univariate normal with mean $\beta y(s^*, t - 1) + \frac{\alpha x(s^*, t-1)}{M_{s^*}} - \mathbf{S}_{1,t-1}^T \Sigma_{t-1}^{-1} (\mathbf{y}_t - \boldsymbol{\mu}_t)$ and variance $s_{n+1,n+1} - \mathbf{S}_{1,t-1}^T \Sigma_{t-1}^{-1} \mathbf{S}_{1,t-1}$. We use this fact to simulate $y(s^*, t)$, for $t = 1, \dots, T$, sequentially.

Initialize \mathbf{y}^* and \mathbf{x}^* by $\mathbf{y}^{*(0)}$ and $\mathbf{x}^{*(0)}$, and all the other unknowns. For $k = 1, \dots, N + B$, do the following.

- S1. For $t = 1, \dots, T$,
- S2. Define $\mathbb{D}^{(k-1)} = [\mathbb{D}, \mathbf{y}^{*(k-1)}]$ and $\mathbb{L}^{(k-1)} = [\mathbb{L}, \mathbf{x}^{*(k-1)}]$.
- S3. Simulate $\boldsymbol{\theta}^{(k)}$ from $[\boldsymbol{\theta} | \mathbb{D}^{(k-1)}, \mathbb{L}^{(k-1)}]$ using Gibbs and MH within Gibbs via full conditionals as given in Section 5. Let the simulated value be $\boldsymbol{\theta}^{(k)}$.

S4. Given, $\theta^{(k)}$ and $\mathbb{D}^{(k-1)}$, simulate the latent variables from their full conditionals as given in Section 5. Let the simulated value be $\mathbb{L}^{(k)}$.

S5. Given $\theta^{(k)}$ and $\mathbb{L}^{(k)}$, simulate $y(s^*, t)$ from $[y(s^*, t) | L^{(k)}, \theta^{(k)}, \mathbb{D}]$, say $y(s^*, t)^{(k)}$.

Store N observations after discarding B observations as burn-in.

J Modification for irregularly spaced data

Below we provide an idea how our model can be used in irregularly spaced time points. The detailed simulation and real data analysis will be taken up in a separate work. To deal with the irregularly spaced time points, we modify the equations (3) and (4) following the discretization of Ornstein-Uhlenbeck models.

Let observed times be $[0 = t_0 < t_1 < \dots < t_T, \Delta t_k = t_k - t_{k-1}]$. For each spatial location (s) and time interval $[t_{k-1}, t_k]$, the modified observation equation is given by

$$y(s, t_k) = \beta^{\Delta t_k} y(s, t_{k-1}) + \Delta t_k, M_s^{-1} \left(\alpha x(s, t_{k-1}) - \frac{\Delta t_k}{2} V'(y(s, t_{k-1})) \right)$$

and the modified latent equation is provided as

$$x(s, t_k) = \alpha^{2\Delta t_k} x(s, t_{k-1}) - \frac{\Delta t_k}{2} \left[\alpha V'(y(s, t_{k-1})) + V'(y(s, t_k)) \right].$$

The theoretical properties that we have proved in Section 2 remain valid. These can be argued as follows: Leap-frog algorithm is valid for variable step sizes; we already assume that the model has continuous paths in time; and, finally, the correlation decays to 0 as the time lags increases to infinity because $\prod_k \beta^{\Delta t_k} \rightarrow 0$ as $\sum_k \Delta t_k \rightarrow \infty$.

Moreover, the likelihoods in Section 3 can be modified easily with changed covariance matrices. They are described below. First we modify the conditional data likelihood, that is, for $k = 1, \dots, T$,

$$y_k | y_{k-1}, x_{k-1}, \Theta \sim \mathcal{N}_n \left(\mu_{k-1}, ; \sigma^2 \Sigma_{k-1}^{\Delta t_k} \right),$$

where

$$\mu_{k-1}(i) = \beta^{\Delta t_k} y(s_i, t_{k-1}) + \frac{\Delta t_k}{M_{s_i}} \left(\alpha x(s_i, t_{k-1}) - \frac{\Delta t_k}{2} V'(y(s_i, t_{k-1})) \right),$$

and

$$\Sigma_{k-1}^{\Delta t_k}(i, j) = \frac{\Delta t_k^2}{M_{s_i} M_{s_j}} \text{cov} (V'(y(s_i, t_{k-1})), V'(y(s_j, t_{k-1}))).$$

with

$$\text{cov}(V'(x), V'(x')) = 2\eta_3 \sigma^2 e^{-\eta_3 |x-x'|^2} (1 - 2\eta_3 |x-x'|^2).$$

as given in equation (5). Similarly, the likelihood of the latent variables can be written as

$$x_k | x_{k-1}, y_{k-1}, y_k \sim \mathcal{N}_n \left(\alpha^{2\Delta t_k} x_{k-1}, ; \frac{\sigma^2 \Delta t_k^2}{4} \Omega_k \right),$$

where the definition of Ω_k remains the same as in Section 3.2, with replacing the distances by

$$|y(s_i, t_{k-1}) - y(s_j, t_k)|.$$

K Supplementary plots for 3 component mixture of GPs

In this appendix, we provide the trace plots and the posterior densities of the complete time series of the latent variables for the simulated data used in Section 6.1.

K.1 Trace plots

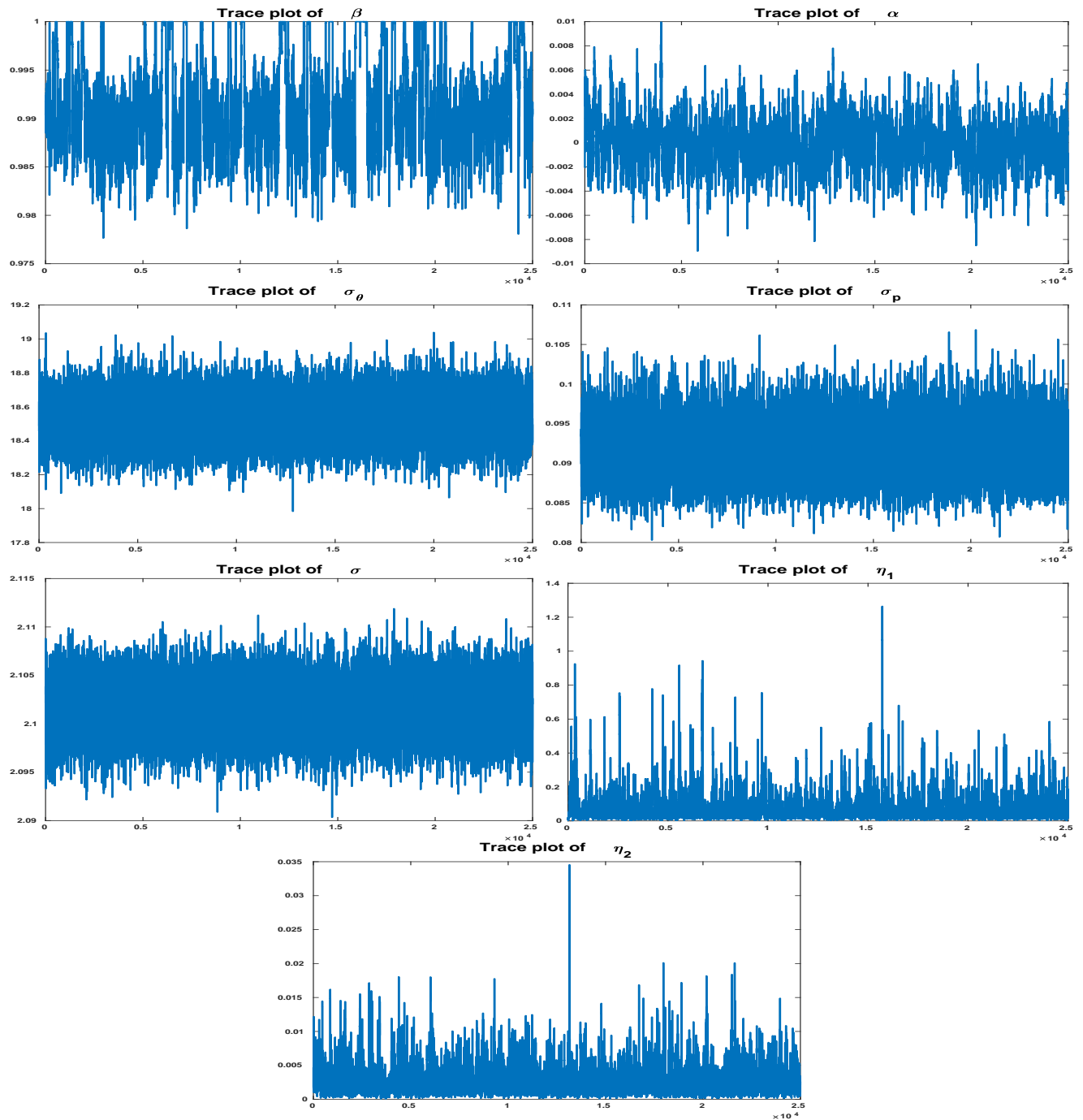


Figure 13: Trace plots for the parameters for data simulated from 3-component GP mixtures.

K.2 Posterior densities of the complete time series of latent variables

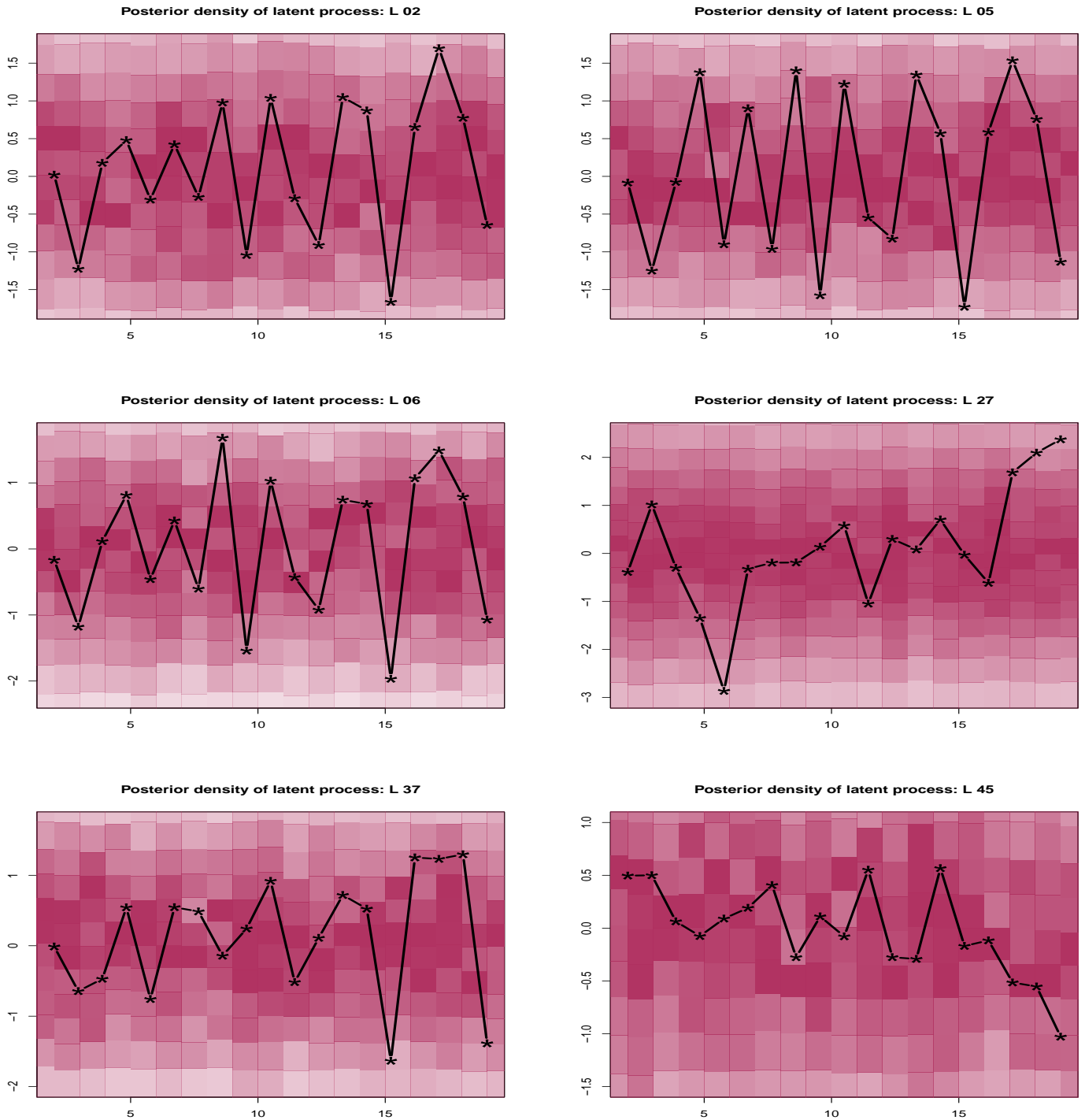


Figure 14: Posterior densities of latent variables for six locations for data simulated from 3-component mixture of GPs. Higher the intensity of the color, higher is the probability density. The black line represents the true values of the latent variables. L_i denote the locations.

L Supplementary plots for mixture of GQNs

Trace plots of the parameters and the posterior densities of the complete time series of the latent variables for two component mixture of GQNs are depicted below. The details of the data are given in Section 6.3.

L.1 Trace plots

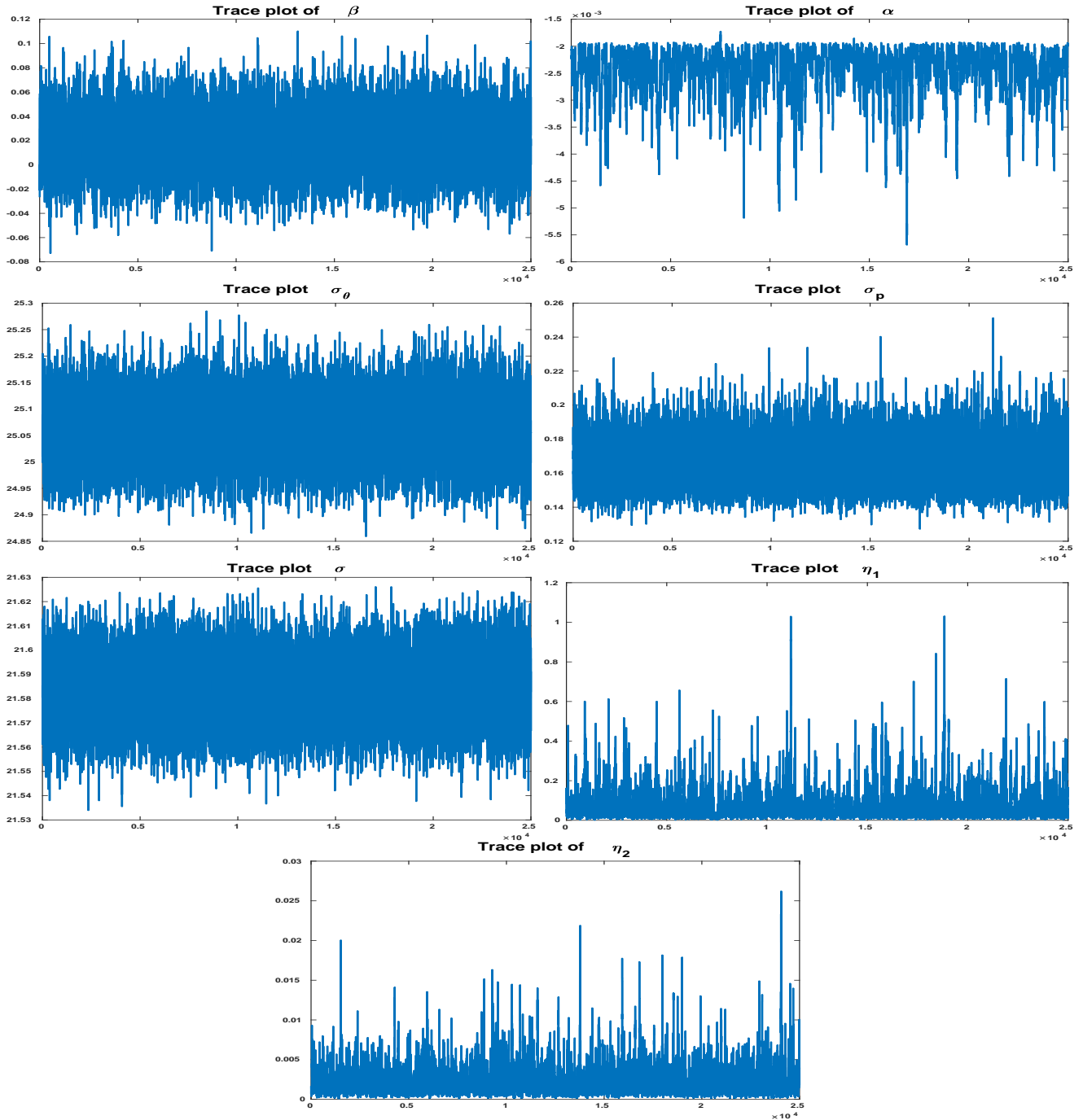


Figure 15: Trace plots for the parameters for data simulated from mixture of GQNs.

L.2 Posterior densities of the complete time series of the latent variables

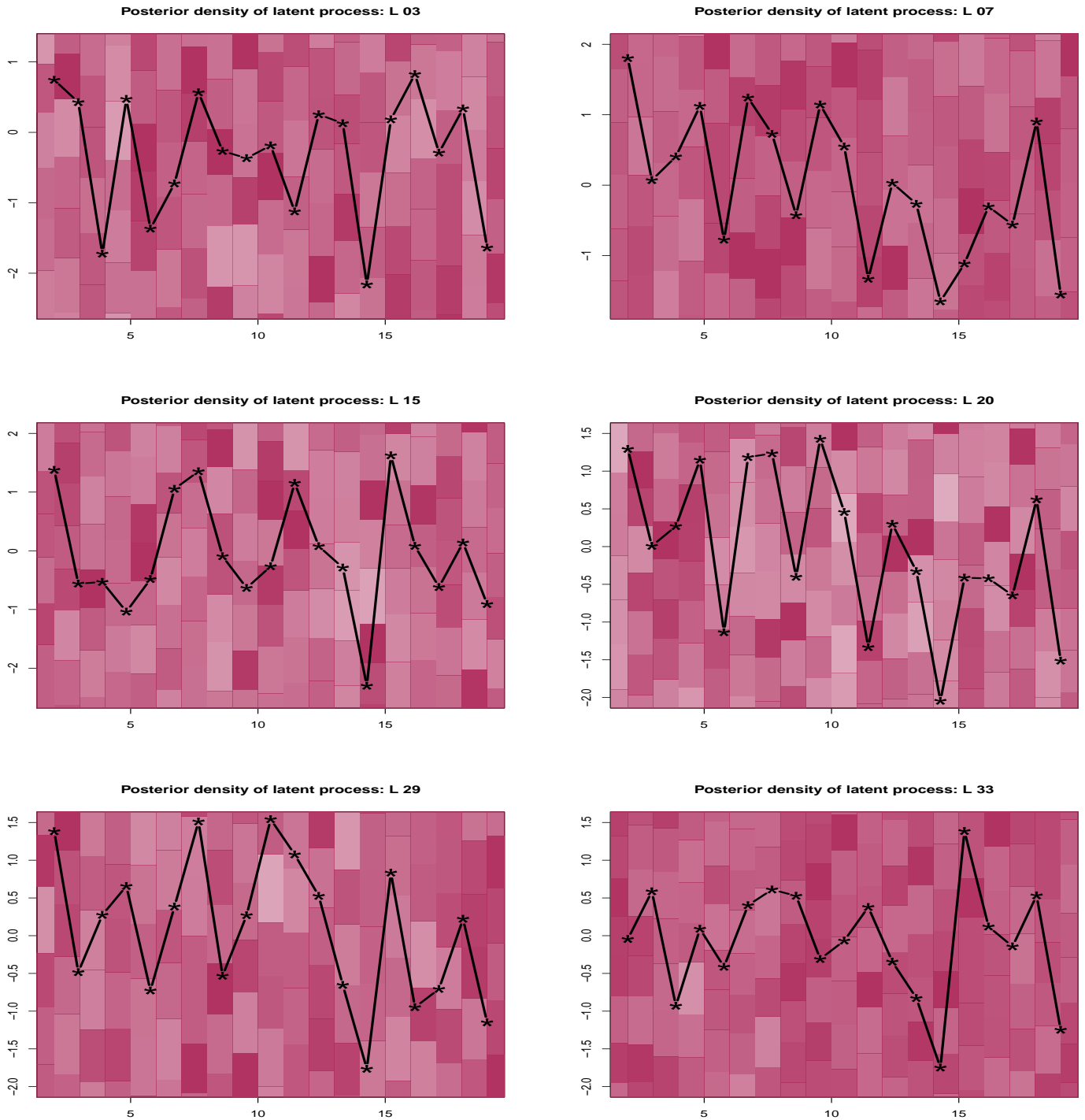


Figure 16: Posterior densities of latent variables for six locations for data simulated from mixture of two GQNs. Higher the intensity of the color, higher is the probability density. The black line represents the true values of the latent variables. L_i denote the locations.

M Supplementary plots for Alaska temperature data

M.1 Trace plots

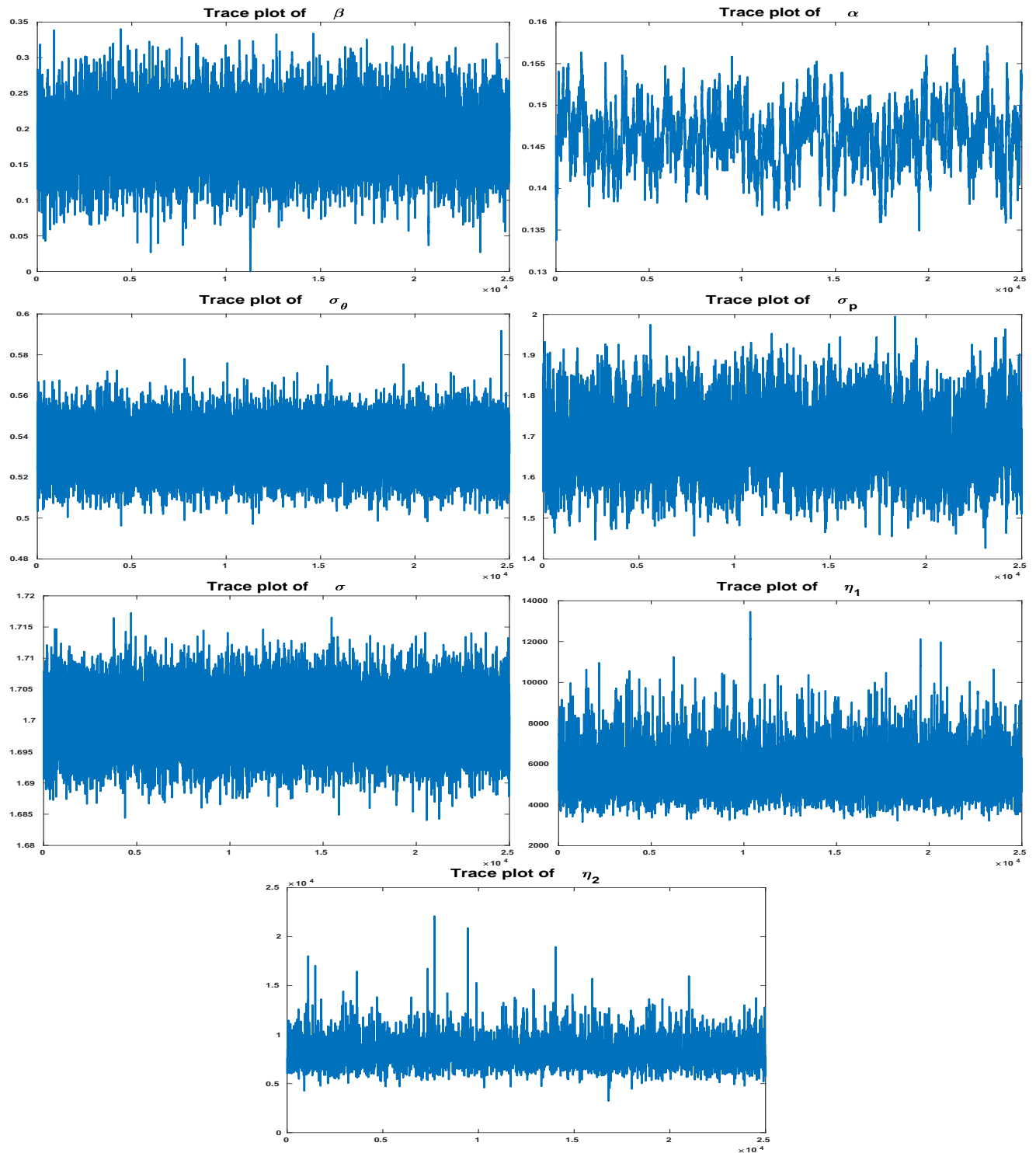


Figure 17: Trace plot for the parameters except for η_3 corresponding to the Alaska temperature data.

N Supplementary plots for sea temperature data

N.1 Trace plots

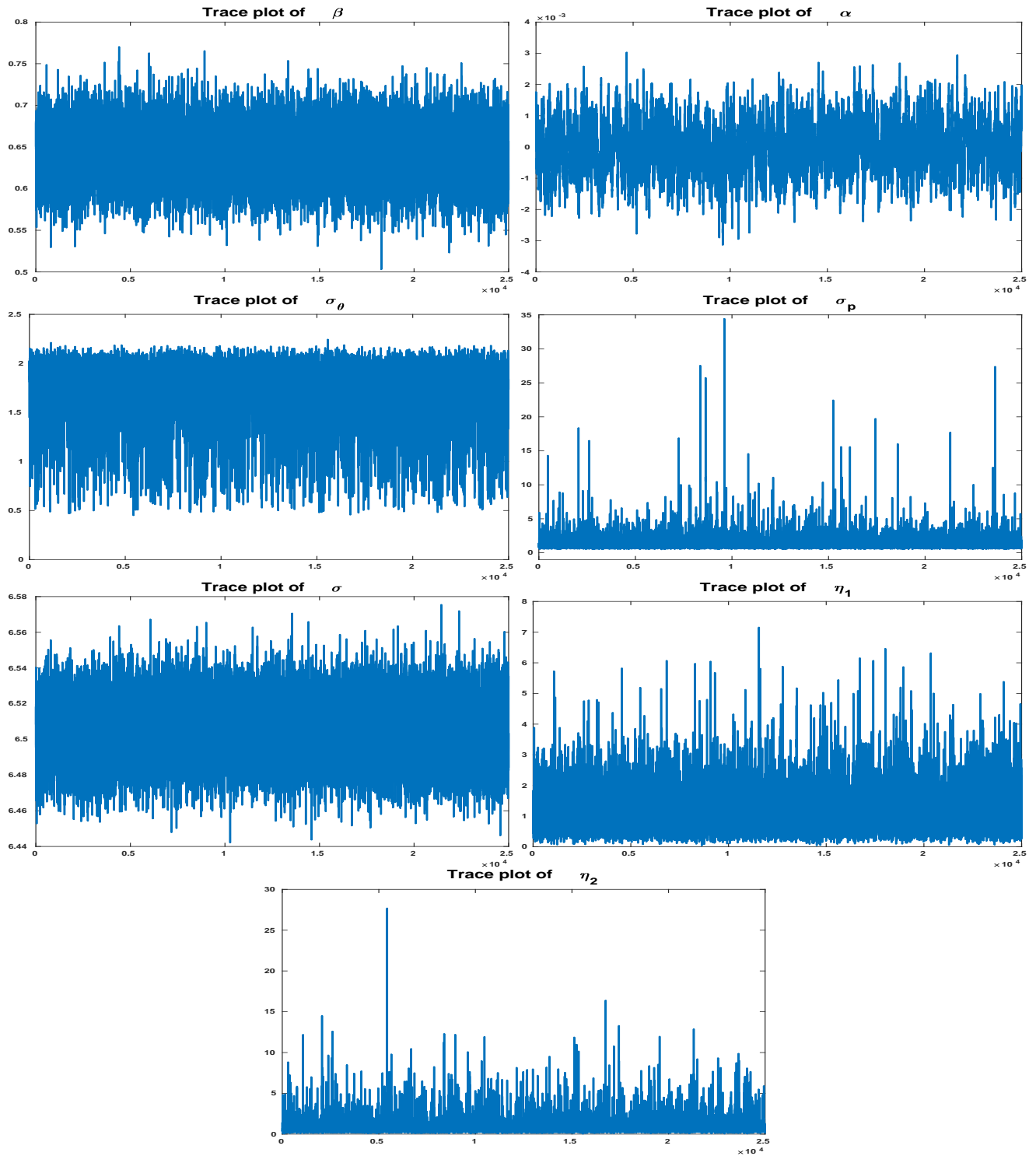


Figure 18: Trace plots of the parameters except for η_3 for the sea surface temperature data.

O Stationarity, convergence of lagged correlations to zero and non-Gaussianity of the detrended Alaska data process

This appendix demonstrates that the data set analyzed in Section 7.1 arises from a non-stationary and non-Gaussian process. Further, the analysis vindicates that the sample lagged correlation tends to 0 as the spatial and/or temporal lag tends to infinity.

O.1 Stationarity of the detrended Alaska data process

To check if the data arrived from a stationary or non-stationary process, we resorted to the recursive Bayesian theory and methods developed by Roy and Bhattacharya [2020]. In a nutshell, their key idea is to consider the Kolmogorov-Smirnov distance between distributions of data associated with local and global space-times. Associated with the j -th local space-time region is an unknown probability p_j of the event that the underlying process is stationary when the observed data corresponds to the j -th local region and the Kolmogorov-Smirnov distance falls below c_j , where c_j is any non-negative sequence tending to zero as j tends to infinity. With suitable priors for p_j , Roy and Bhattacharya [2020] constructed recursive posterior distributions for p_j and proved that the underlying process is stationary if and only if for sufficiently large number of observations in the j -th region, the posterior of p_j converges to one as $j \rightarrow \infty$. Nonstationarity is the case if and only if the posterior of p_j converges to zero as $j \rightarrow \infty$.

In our implementation of the ideas of Roy and Bhattacharya [2020], we set the j -th local region to be the entire time series for the spatial location \mathbf{s}_j , for $j = 1, \dots, 29$. Thus, the size of each local region is 65. We choose c_j to be of the same nonparametric, dynamic and adaptive form as detailed in Roy and Bhattacharya [2020]. The dynamic form requires an initial value for the sequence. In practice, the choice of the initial value usually has significant effect on the convergence of the posteriors of p_j , and so, the choice must be carefully made. However, in our case, for all initial values that we experimented with, lying between 0.05 and 1, the recursive Bayesian procedure led to the conclusion of stationarity of the underlying spatio-temporal process.

We implemented the idea with our parallelised C code on 29 parallel processors of a VMWare of Indian Statistical Institute; the time taken is less than a second. For the initial value 0.05, Figure 19 displays the means of the posteriors of p_j ; $j = 1, \dots, 29$, showing convergence to 1. The respective posterior variances are negligibly small and hence not shown. Thus, the detrended spatio-temporal process that generated the Alaska data, can be safely regarded as stationary.

O.2 Convergence of lagged spatio-temporal correlations to zero for the Alaska data

Recall that one major purpose of our Hamiltonian spatio-temporal model is to emulate the property of most real datasets that the lagged spatio-temporal correlations tend to zero as the spatio-temporal lag tends to infinity, irrespective of stationarity or nonstationarity. Here we compute the lagged correlations on 30 parallel processors on our VMWare, each processor computing the correlation for a partitioned interval of lag $\|\mathbf{h}\|$ such that the interval is associated with sufficient data, making the correlation well-defined. The time taken for this exercise are a few seconds. Figure 20 demonstrates convergence of the lagged spatio-temporal correlations to zero; with larger amount of data such demonstration would have been more convincing.

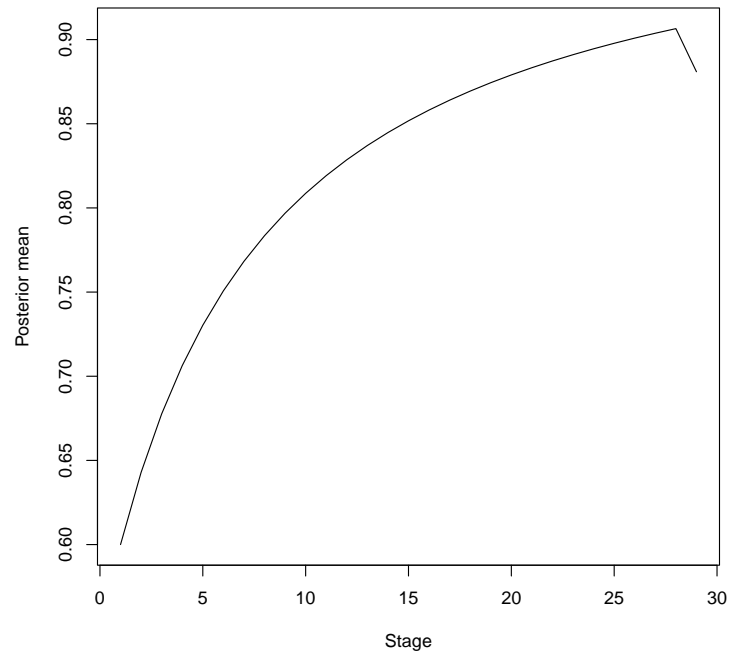


Figure 19: Alaska data analysis: detection of strict stationarity.

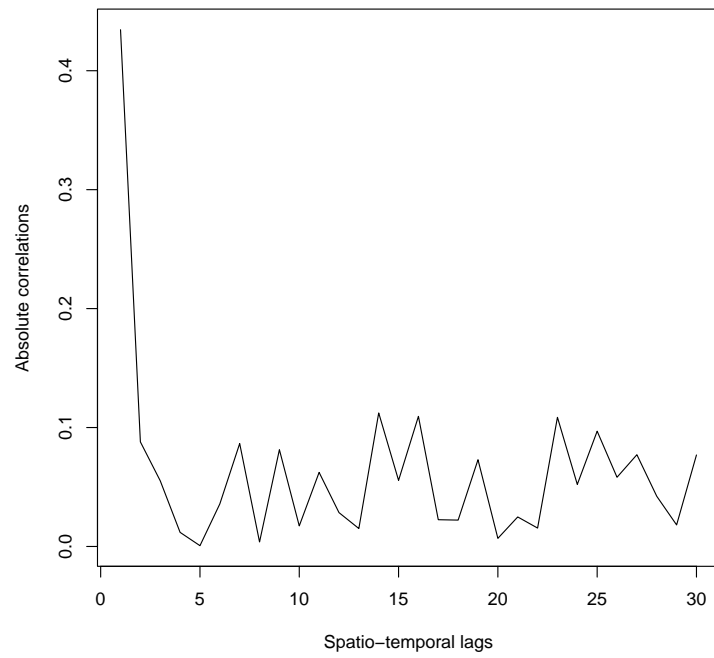


Figure 20: Alaska data analysis: lagged spatio-temporal correlations converging to zero.

O.3 Non-Gaussianity of the Alaska data

Simple quantile-quantile plots (not shown for brevity) revealed that the distributions of the time series data at the spatial locations, distributions of the spatial data at the time points, and the overall distribution of the entire data set, are far from normal. Thus, traditional Gaussian process based models of the underlying spatio-temporal process are ruled out. Since the temporal distributions at the spatial locations and the spatial distributions at different time points are also much different, it does not appear feasible to consider parametric stochastic process models for the data. These seem to make the importance of our nonparametric Hamiltonian process more pronounced.

References

- Mikyong Jun, Reto Knutti, and Douglas W Nychka. Spatial Analysis to Quantify Numerical Model Bias and Dependence: How Many Climate Models Are There? *Journal of the American Statistical Association*, 103(483):934–947, 2008.
- Reinhard Furrer and Stephan R Sain. Spatial Model Fitting for Large Datasets with Applications to Climate and Microarray Problems. *Statistics and Computing*, 19(2):113–128, 2009.
- Claudia Tebaldi and Bruno Sansó. Joint Projections of Temperature and Precipitation Change from Multiple Climate Models: a Hierarchical Bayesian Approach. *Journal of the Royal Statistical Society: Series A (Statistics in Society)*, 172(1):83–106, 2009.
- Stephan R Sain, Reinhard Furrer, and Noel Cressie. A Spatial Analysis of Multivariate Output from Regional Climate Models. *The Annals of Applied Statistics*, pages 150–175, 2011.
- Richard L Smith, Claudia Tebaldi, Doug Nychka, and Linda O Mearns. Bayesian Modeling of Uncertainty in Ensembles of Climate Models. *Journal of the American Statistical Association*, 104(485):97–116, 2009.
- Huiyan Sang, Mikyong Jun, and Jianhua Z Huang. Covariance Approximation for Large Multivariate Spatial Data Sets with an Application to Multiple Climate Model Errors. *The Annals of Applied Statistics*, pages 2519–2548, 2011.
- David Roxbee Cox and Valerie Isham. A Simple Spatial-Temporal Model of Rainfall. *Proceedings of the Royal Society of London. A. Mathematical and Physical Sciences*, 415(1849):317–328, 1988.
- Bruno Sanso and Lelys Guenni. Venezuelan Rainfall Data Analysed by Using a Bayesian Space–Time Model. *Journal of the Royal Statistical Society: Series C (Applied Statistics)*, 48(3):345–362, 1999.
- Sujit K Sahu, Alan E Gelfand, and David M Holland. Fusing Point and Areal Level Space–Time Data with Application to Wet Deposition. *Journal of the Royal Statistical Society: Series C (Applied Statistics)*, 59(1):77–103, 2010.
- Peter Guttorp, Wendy Meiring, and Paul D Sampson. A Space-Time Analysis of Ground-Level Ozone Data. *Environmetrics*, 5(3):241–254, 1994.
- Gabriel Huerta, Bruno Sansó, and Jonathan R Stroud. A Spatiotemporal Model for Mexico City Ozone Levels. *Journal of the Royal Statistical Society: Series C (Applied Statistics)*, 53(2):231–248, 2004.

- Francesca Bruno, Peter Guttorp, Paul D Sampson, and Daniela Cocchi. A Simple Non-Separable, Non-Stationary Spatiotemporal Model for Ozone. *Environmental and Ecological Statistics*, 16(4):515–529, 2009.
- Yiping Dou, Nhu D Le, and James V Zidek. Modeling Hourly Ozone Concentration Fields. *The Annals of Applied Statistics*, 4(3):1183–1213, 2010.
- Christopher J Paciorek, Jeff D Yanosky, Robin C Puett, Francine Laden, and Helen H Suh. Practical Large-Scale Spatio-Temporal Modeling of Particulate Matter Concentrations. *The Annals of Applied Statistics*, pages 370–397, 2009.
- David M Holland, Oliveira Victor De, Lawrence H Cox, and Richard L Smith. Estimation of Regional Trends in Sulfur Dioxide over the Eastern United States. *Environmetrics: The Official Journal of the International Environmetrics Society*, 11(4):373–393, 2000.
- Marco Giannitrapani, Adrian Bowman, Marian Scott, and Ron Smith. Sulphur Dioxide in Europe: Statistical Relationships Between Emissions and Measured Concentrations. *Atmospheric Environment*, 40(14):2524–2532, 2006.
- Rob Beelen, Gerard Hoek, Danielle Vienneau, Marloes Eeftens, Konstantina Dimakopoulou, Xanthi Pedeli, Ming-Yi Tsai, Nino Künzli, Tamara Schikowski, Alessandro Marcon, T. Kirsten Eriksen, et al. Development of NO₂ and NO_x Land Use Regression Models for Estimating Air Pollution Exposure in 36 Study Areas in Europe—The ESCAPE Project. *Atmospheric Environment*, 72:10–23, 2013.
- Heresh Amini, Seyed-Mahmood Taghavi-Shahri, Sarah B Henderson, Vahid Hosseini, Hossein Hassankhany, Maryam Naderi, Solmaz Ahadi, Christian Schindler, Nino Künzli, and Masud Yunesian. Annual and Seasonal Spatial Models for Nitrogen Oxides in Tehran, Iran. *Scientific Reports*, 6(1):1–11, 2016.
- Jin S Deng, Ke Wang, Yang Hong, and Jia G Qi. Spatio-Temporal Dynamics and Evolution of Land Use Change and Landscape Pattern in Response to Rapid Urbanization. *Landscape and Urban Planning*, 92(3-4):187–198, 2009.
- Avishek Chakraborty, Alan E Gelfand, Adam M Wilson, Andrew M Latimer, and John A Silander Jr. Modeling Large Scale Species Abundance with Latent Spatial Processes. *The Annals of Applied Statistics*, 4(3):1403–1429, 2010.
- Sudipto Banerjee, Bradley P Carlin, and Alan E Gelfand. *Hierarchical Modeling and Analysis for Spatial Data*. CRC press, 2014.
- Paul D Sampson and Peter Guttorp. Nonparametric Estimation of Nonstationary Spatial Covariance Structure. *Journal of the American Statistical Association*, 87(417):108–119, 1992.
- Moumita Das and Sourabh Bhattacharya. A Kernel-Enriched Order-Dependent Nonparametric Spatio-Temporal Process. *Spatial Statistics*, 55:100751, 2023.
- Sucharita Roy and Sourabh Bhattacharya. Bayesian Characterizations of Properties of Stochastic Processes with Applications. *arXiv preprint arXiv:2005.00035*, 2020.
- Sourabh Bhattacharya. Bayesian Lévy-Dynamic Spatio-Temporal Process: Towards Big Data Analysis. *Journal of the Indian Statistical Association*, 59(2):145–195, 2021. Special Issue on Spatio Temporal Modelling.

- Christopher Joseph Paciorek. *Nonstationary Gaussian Processes for Regression and Spatial Modelling*. PhD thesis, Carnegie Mellon University, 2003.
- Alan E Gelfand, Peter Diggle, Peter Guttorp, andMontserrat Fuentes. *Handbook of Spatial Statistics*. CRC press, 2010.
- Doris Damian, Paul D Sampson, and Peter Guttorp. Bayesian Estimation of Semi-Parametric Non-Stationary Spatial Covariance Structures. *Environmetrics: The Official Journal of the International Environmetrics Society*, 12(2):161–178, 2001.
- Alexandra M Schmidt and Anthony O’Hagan. Bayesian Inference for Non-Stationary Spatial Covariance Structure via Spatial Deformations. *Journal of the Royal Statistical Society: Series B (Statistical Methodology)*, 65(3):743–758, 2003.
- David Higdon. A Process-Convolution Approach to Modelling Temperatures in the North Atlantic Ocean. *Environmental and Ecological Statistics*, 5(2):173–190, 1998.
- D Higdon, J Swall, and J Kern. Non-Stationary Spatial Modeling. In J Bernardo, J Berger, A Dawid, and A Smith, editors, *Bayesian Statistics 6*, pages 761–768. Oxford University Press, Oxford, U.K., 1999.
- M. Fuentes and R.L. Smith. A New Class of Nonstationary Spatial Model. Technical report, North Carolina State University, 2001.
- Dave Higdon. Space and Space-Time Modeling Using Process Convolutions. In W. Anderson Clive, Barnett Vic, C. Chatwin Philip, and Abdel H. El-Shaarawi, editors, *Quantitative Methods for Current Environmental Issues*, pages 37–56. Springer, 2002.
- Montserrat Fuentes. Spectral Methods for Nonstationary Spatial Processes. *Biometrika*, 89(1):197–210, 2002.
- Christopher J Paciorek and Mark J Schervish. Spatial Modelling Using a New Class of Nonstationary Covariance Functions. *Environmetrics: The Official Journal of the International Environmetrics Society*, 17(5):483–506, 2006.
- Christopher K Wikle and Mevin B Hooten. A General Science-Based Framework for Dynamical Spatio-Temporal Models. *Test*, 19(3):417–451, 2010.
- Finn Lindgren, Håvard Rue, and Johan Lindström. An Explicit Link Between Gaussian Fields and Gaussian Markov Random Fields: the Stochastic Partial Differential Equation Approach. *Journal of the Royal Statistical Society Series B: Statistical Methodology*, 73(4):423–498, 2011.
- Marta Blangiardo and Michela Cameletti. *Spatial and Spatio-Temporal Bayesian Models with R-INLA*. John Wiley & Sons, 2015.
- David Bolin and Finn Lindgren. Spatial Models Generated by Nested Stochastic Partial Differential Equations, with an Application to Global Ozone Mapping. *The Annals of Applied Statistics*, pages 523–550, 2011.
- Rikke Ingebrigtsen, Finn Lindgren, and Ingelin Steinsland. Spatial Models with Explanatory Variables in the Dependence Structure. *Spatial Statistics*, 8:20–38, 2014.

- Finn Lindgren, David Bolin, and Håvard Rue. The SPDE Approach for Gaussian and Non-Gaussian Fields: 10 Years and Still Running. *Spatial Statistics*, 50:100599, 2022.
- Finn Lindgren and Håvard Rue. Bayesian Spatial Modelling with R-INLA. *Journal of Statistical Software*, 63(19), 2015.
- Virgilio Gómez-Rubio. *Bayesian Inference with INLA*. CRC Press, 2020.
- Alan E Gelfand, Athanasios Kottas, and Steven N MacEachern. Bayesian Nonparametric Spatial Modeling with Dirichlet Process Mixing. *Journal of the American Statistical Association*, 100(471):1021–1035, 2005.
- Montserrat Fuentes and Brian Reich. Multivariate Spatial Nonparametric Modelling via Kernel Processes Mixing. *Statistica Sinica*, 23(1), 2013.
- Jason A Duan, Alan E Gelfand, and CF Sirmans. Modeling Space-Time Data Using Stochastic Differential Equations. *Bayesian Analysis*, 4(4):733–758, 2009.
- Charles C Driver and Manuel C Voelkle. Hierarchical Bayesian Continuous Time Dynamic Modeling. *Psychological Methods*, 23(4):774, 2018.
- Noel Cressie and Christopher K Wikle. *Statistics for Spatio-Temporal Data*. John Wiley & Sons, 2015.
- Suman Guha. *Some Theoretical and Methodological Contributions to the Dynamic Modeling of Discrete-Time Spatial Time Series Data*. PhD thesis, Indian Statistical Institute, Kolkata, 2017.
- Michael Betancourt. A Conceptual Introduction to Hamiltonian Monte Carlo. *arXiv preprint arXiv:1701.02434*, 2017.
- Sai Hung Cheung and James L Beck. Bayesian Model Updating Using Hybrid Monte Carlo Simulation with Application to Structural Dynamic Models with Many Uncertain Parameters. *Journal of Engineering Mechanics*, 135(4):243–255, 2009.
- Joan-Andreu Lázaro-Camí and Juan-Pablo Ortega. Stochastic Hamiltonian Dynamical Systems. *arXiv preprint math/0702787*, 2007.
- Jialin Hong, Baohui Hou, Qiang Li, and Liying Sun. Three Kinds of Novel Multi-Symplectic Methods for Stochastic Hamiltonian Partial Differential Equations. *Journal of Computational Physics*, 467:111453, 2022.
- Peter Young. Everything You Wanted to Know about the Leapfrog Algorithm but Were Afraid to Ask. *American Journal of Physics*, 82(10):991–997, 2014. doi: 10.1119/1.4885396.
- Anurag Ghosh, Soumalya Mukhopadhyay, Sandipan Roy, and Sourabh Bhattacharya. Bayesian Inference in Nonparametric Dynamic State-Space Models. *Statistical Methodology*, 21:35–48, 2014.
- Satyaki Mazumder and Sourabh Bhattacharya. Bayesian Nonparametric Dynamic State Space Modeling with Circular Latent States. *Journal of Statistical Theory and Practice*, 10(1):154–178, 2016.
- Satyaki Mazumder and Sourabh Bhattacharya. Nonparametric Dynamic State Space Modeling of Observed Circular Time Series with Circular Latent States: a Bayesian Perspective. *Journal of Statistical Theory and Practice*, 11(4):693–718, 2017.

- Roger W. Hockney. The Potential Calculation and Some Applications. *Methods in Computational Physics*, 9:135–211, 1970.
- Loup Verlet. Computer "Experiments" on Classical Fluids. I. Thermodynamical Properties of Lennard-Jones Molecules. *Physical Review*, 159(1):98–103, 1967.
- M. L. Stein. *Interpolation of Spatial Data: Some Theory for Kriging*. Springer-Verlag, New York, Inc, 1999a.
- CE Rasmussen and CKI Williams. *Gaussian Process for Machine Learning*. the MIT Press, 2006.
- Michael L. Stein. *Interpolation of Spatial Data*. Springer, New York, 1999b.
- S. Bhattacharya. Mean-Square Convergence of a New Parameterized Leapfrog Scheme for Hamiltonian Systems Driven by Gaussian Process Potentials, 2026a. ArXiv preprint.
- S. Bhattacharya. MPL-HMC: A Tunable Parameterized Leapfrog Framework for Robust Hamiltonian Monte Carlo, 2026b. ArXiv preprint.
- Hao Zhang. Inconsistent Estimation and Asymptotically Equal Interpolations in Model-Based Geostatistics. *Journal of the American Statistical Association*, 99(465):250–261, 2004.
- Sudipto Banerjee. Modeling Massive Spatial Datasets Using a Conjugate Bayesian Linear Modeling Framework. *Spatial Statistics*, 37:100417, 2020.
- Moumita Das and Sourabh Bhattacharya. Transdimensional Transformation Based Markov Chain Monte Carlo. *Brazilian Journal of Probability and Statistics*, 33(1):87–138, 2019.
- Sudipto Banerjee, Bradley P Carlin, and Alan E Gelfand. *Hierarchical Modeling and Analysis for Spatial Data*. CRC press, Boca Raton, Florida, 2nd edition, 2015.